This is to certify that the
dissertation entitled

HEMODYNAMIC MONITORING VIA IMPULSE RESPONSE ESTIMATION

presented by

Da Xu

has been accepted towards fulfillment
of the requirements for the

Doctoral degree in Electrical Engineering

Major Professor's Signature

5/27/10

Date

HEMODYNAMIC MONITORING VIA IMPULSE RESPONSE ESTIMATION

By

Da Xu

A DISSERTATION

Submitted to
Michigan State University
in partial fulfillment of the requirements
for the degree of

DOCTOR OF PHILOSOPHY

Electrical Engineering

2010

ABSTRACT

HEMODYNAMIC MONITORING VIA IMPULSE RESPONSE ESTIMATION

By

Da Xu

Hemodynamic monitoring is a highly valuable guidance during observation, diagnosis, and treatment of cardiovascular diseases. While most hemodynamic monitoring systems today entail routine measurement and display of blood pressure or other arterial waveforms, more effective systems are demanded by a fast growth in the proportion of the elderly population and a major shortage of clinical staff projected over the next decade. To this end, novel techniques based on impulse response estimation are presented in this dissertation to continuously monitor cardinal hemodynamic variables by mathematical analysis of cardiovascular waveforms measured with instrumentation already in use or available.

Techniques based on the Windkessel model were proposed to continuously estimate cardiac output and left atrial pressure from peripheral arterial blood pressure, pulmonary artery pressure, and right ventricular pressure waveforms respectively. Long time interval analysis was applied in these techniques to circumvent the wave reflections and inertial effects in the blood pressure waveforms. The techniques were evaluated with animal/human experiments and showed application potential in clinical practice. Efforts were further made to extend the long time interval analysis

technique to the photoplethysmography waveform and pilot results confirmed the feasibility.

Techniques for robust estimation of the pulse wave velocity were developed in order to achieve accurate arterial stiffness and cuff-less blood pressure monitoring. System identification methods using both physiologic-based and black-box models were employed to improve the robustness of the techniques. Preliminary results obtained from animal/human experiments demonstrated potential clinical values of the techniques.

With further evaluation, these techniques may ultimately be employed conjunctively to arrive at continuous and effective hemodynamic monitoring systems in various clinical settings.

To my wife

ACKNOWLEDGEMENTS

It is a pleasure to thank those who made this dissertation possible. First of all, I would like to express my deepest gratitude to my advisor Dr. Ramakrishna Mukkamala for his professional guidance and persistent support to my research work. His technical genius and continuous spirit of adventure in regard to research have been motivating me throughout my Ph.D. study and will continuously benefit me in my future research career.

I would like to address my sincere appreciation to my committee members Dr. Bari Olivier, Dr. Selin Aviyente, and Dr. Shantanu Chakrabartty for their valuable advices and guidance on my work. Dr. Bari Olivier is meanwhile my collaborator, without whom none of the animal experiments in this dissertation would have been completed.

My gratitude also extends to my other collaborators: Dr. Andrew Reisner in Massachusetts General Hospital, Dr. Victor Convertino and Dr. Kathy Ryan in the United States Army Institute of Surgical Research, and Dr. Caroline Richards in University of Texas for their instructive opinions and suggestions regarding my research projects. In addition, my special thanks to Mr. Gary Muniz, Mr. Joseph Prinsen and Mr. Thoralf Hoelzer-Maddox for their great technical contributions to the experimental data collection.

I would like to take this opportunity to thank my former advisor Dr. Yuanyuan Wang in Fudan University, who introduced me into this exciting research area.

I am indebted to my colleagues for their generous help and the wonderful experiences enjoyed with them: Xiaoxiao Chen, Gokul Swamy, Guanqun Zhang, Federico Aletti, Soroor Soltani, Anton Khomyakov, Zhenwei Lu, Kabi Padhi, and Mohsen Moslehpour.

Finally, I owe my greatest thanks to my family, especially my wife Fang Sun, to whom I dedicate this dissertation. Without their unconditional support and encouragement, I would never have accomplished anything on this way.

TABLE OF CONTENTS

LIST OF TABLES

LIST OF FIGURES

ABBREVIATIONS

ABP	Arterial Blood Pressure
AC	Arterial Compliance
ARX	Autoregressive Exogenous Input
AUC	Area Under Curve
BCG	Ballistocardiography
BP	Blood Pressure
CO	Cardiac Output
DP	Diastolic Pressure
ECG	Electrocardiography
FDA	Food and Drug Administration
HR	Heart Rate
ICG	Impedance Cardiography
ICU	Intensive Care Unit
LAP	Left Atrial Pressure
LBNP	Lower Body Negative Pressure
LTIA	Long Time Interval Analysis
LVFP	Left Ventricular Filling Pressure
MAP	Mean Arterial Pressure
MDL	Minimum Description Length
OE	Output Error
PAC	Pulmonary Arterial Compliance

PAP	Pulmonary Artery Pressure
PAR	Pulmonary Arterial Resistance
PCWP	Pulmonary Capillary Wedge Pressure
PP	Pulse Pressure
PPG	Photoplethysmography
PWV	Pulse Wave Velocity
RMSE	Root-Mean-Squared-Error
RMSNE	Root-Mean-Squared-Normalized-Error
ROC	Receiver Operating Characteristic
RVP	Right Ventricular Pressure
SNR	Signal-to-Noise Ratio
SP	Systolic Pressure
SV	Stroke Volume
TPR	Total Peripheral Resistance

CHAPTER 1

INTRODUCTION

1.1 Background

The function of the cardiovascular circulation is to serve the needs of body tissues by transporting essential substances to the tissues, removing waste products of metabolism, conducting hormones from one part of the body to another, and maintaining an appropriate environment in the tissue fluids of the body (52). The cardiovascular circulation is divided into the systemic circulation and the pulmonary circulation. Systemic circulation transports oxygenated blood from the heart to the body tissues and returns oxygen-deprived blood back to the heart, while pulmonary circulation propels oxygen-depleted blood into the lung for exchange of oxygen and carbon dioxide and circulates the now oxygen-rich blood to the heart. Each of the circulation systems contains a pump (the heart), a series of tubes for transportation (arteries or veins), and thin tubes for exchanging substances between the blood and the interstitial fluid (capillaries).

Physical quantities can be measured inside or outside the cardiovascular circulation to record electrical activity of the heart (e.g., electrocardiography (ECG)), pressure in the heart or blood vessel (e.g., blood pressure (BP)), volume change in blood vessel (e.g., photoplethysmography (PPG)), flow rate in blood vessel, body resistance change induced by the circulation (e.g., impedance cardiography (ICG)),

and recoil to the force generated by the pumping heart (e.g., ballistocardiography (BCG)). Continuous measurements of these quantities result in hemodynamic waveforms.

1.2 Motivation and Objective

Hemodynamic monitoring is extremely useful in diagnosis and therapy guidance of cardiovascular disease, which is one of the leading causes of mortality in the United States. In addition, the growth in the proportion of elderly population and shortage of clinical staff (8, 145) imply the urgent need for continuous (i.e., automated) and effective hemodynamic monitoring systems. The objective of this dissertation is to investigate new techniques based on impulse response estimation in an attempt to ultimately build continuous, less invasive, and more effective hemodynamic monitoring systems.

1.3 Limitation of Convention Methods

Today, hemodynamic monitoring in clinical settings mostly involves continuous measurement and display of BP waveforms. Minimally invasive catheters are employed at intensive care unit (ICU) to measure a peripheral arterial BP (ABP) waveform from typically the radial artery (2, 74). Moreover, non-invasive systems for measurement of a peripheral BP waveform are now commercially available (1, 5). Invasive catheters are also used in critically ill patients to measure BP waveforms from the pulmonary artery and right heart (95, 115). Recently, a well-tested and safe implantable device has also been developed for chronic ambulatory monitoring of the

right ventricular pressure (RVP) waveform for congestive heart failure patients (92, 111, 112). In addition to BP monitoring, the PPG technique, which measures blood volume change in the microvascular bed of tissue, also has widespread applications in clinical hemodynamic monitoring (12, 24).

Although these waveform monitoring systems are used in clinical settings, critical information in the waveforms has not been fully revealed yet. The PPG waveform is not fully understood and issues such as calibration and motion artifact during measurement also hinder its clinical applications. Perhaps, as a result, successful applications of PPG technique today are limited (i.e., the monitoring of the blood oxygen saturation, rather than the waveform itself, through pulse oximeter (12, 14)). Furthermore, although BP waveforms are more intensively studied and provide continuous and safe measurements for clinical use, they are not able to provide precise and sufficient information to indicate the circulatory status.

One limitation of BP monitoring is that BP does not provide an early indicator of changes in circulatory status because of the cardiovascular control system (e.g., the autonomic nervous system) which tends to maintain the BP levels within a narrow range (52). For example, as illustrated in Fig. 1.1a, BP is maintained in the early stage of hemorrhage while other hemodynamic variables (e.g., cardiac output (CO), the total blood flow rate in the circulation) change significantly (16). In the sense of hemodynamic monitoring, the maintained BP could be misleading and allow insufficient time for interventions before the frank hypotension eventually occurs (see Fig. 1.1a). On the other hand, CO provides an earlier indicator of circulatory changes and may permit adequate time for successful therapy.

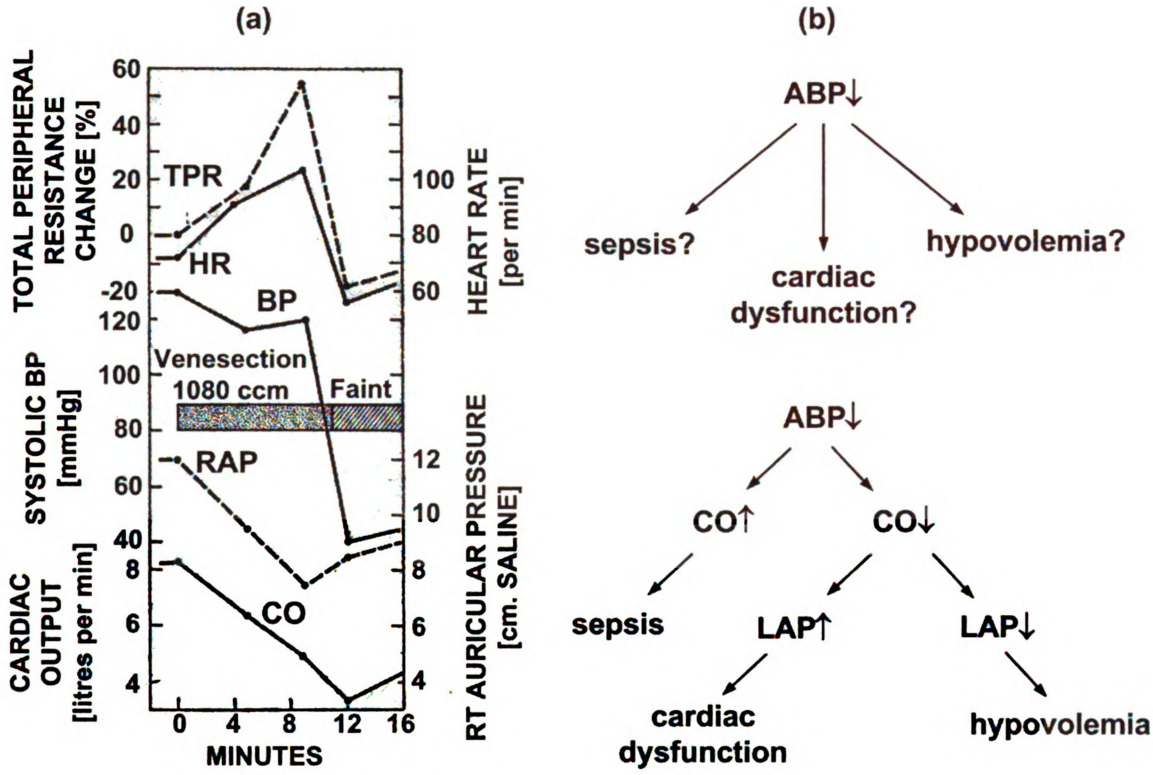

Figure 1.1 Limitations of conventional blood pressure (BP) monitoring. **(a)** In the early stages of hemorrhage, BP is maintained even while cardiac output (CO) is falling due to the cardiovascular control system. Thus, BP does not provide an early indicator of harmful changes in circulatory status and, as a result, may not provide enough time for effective therapy. (Adapted from (16).) **(b)** BP is not sufficiently specific to permit diagnosis and guide therapy. However, a differential diagnosis may be obtained by also monitoring CO and left atrial pressure (LAP).

Another limitation is that BP could be affected by multiple physiologic factors. Therefore, diagnosis and therapy are only possible when additional hemodynamic variables other than BP are available. For example, when decrease of BP is observed, CO and left atrial pressure (LAP, which indicates the filling pressure or preload of the left ventricle) or other measures of left ventricular filling pressure (LVFP) must also be monitored so as to distinguish different possible causes (sepsis, cardiac dysfunction, or hypovolemia) (72, 118) (see Fig. 1.1b).

As shown above, hemodynamic variables such as CO and LAP are more clinically valuable than BP. In addition, pulse wave velocity (PWV, which is the speed of energy wave propagation in the arteries) is another cardinal cardiovascular parameter. PWV increases with decreasing arterial compliance (AC) and is perhaps the most common index of arterial stiffness (15). Further, since AC varies inversely with BP, PWV and BP show strong, positive correlation. PWV may, in fact, represent the only viable means at present for achieving continuous, non-invasive, and cuff-less monitoring of BP. Several methods are currently available for measuring CO, LAP, and PWV (see Table 1.1).

Table 1.1 Conventional methods for measuring cardiac output (CO), left atrial pressure (LAP), and pulse wave velocity (PWV).

Hemodynamic Variable	Method	Advantages	Disadvantages
CO	aortic flow probe (43)	continuous (i.e., automated); accurate	thoracotomy
	bolus thermodilution (43)	relatively simple; inexpensive	pulmonary artery catheterization; operator
	continuous thermodilution (43)	continuous right ventricular ejection fraction (153, 163)	pulmonary artery catheterization; less accurate than bolus thermodilution (164)
	oxygen fick (43)	accurate; inexpensive	two catheterizations; operator
	impedance cardiography (43, 86)	continuous; non-invasive	inaccurate in the presence of lung fluids (35)
	ultrasound (e.g., Doppler (43, 86))	non-invasive	expert operator; expensive
LAP	left atrial catheter (133)	continuous; accurate	too invasive and risky
	pulmonary capillary wedge pressure (120, 143)	relatively simple; inexpensive	pulmonary artery catheterization; operator
PWV	foot-to-foot time delay (27)	relatively simple; non-invasive	susceptible to measurement artifact

The most accurate methods measuring CO and LAP involve placing an ultrasonic flow probe around the ascending aorta (43) and directly catheterizing the left atrium (133). While these methods afford continuous monitoring, they are rarely performed in clinical practice due to high level of invasiveness and associated risk of blood clot formation and embolization (e.g., stroke).

In clinical setting, the standard methods for monitoring CO and LAP both involve the use of the less risky pulmonary artery catheter (95, 143). CO is specifically estimated by the bolus thermodilution method. This method involves injecting a bolus of cold saline in the right atrium via a proximal catheter port, measuring temperature downstream in the pulmonary artery with a thermistor near the distal catheter end, and computing the average CO based on conservation laws. LAP is estimated through the pulmonary capillary wedge pressure (PCWP) method. This method involves advancing the catheter into a branch of the pulmonary artery, inflating a balloon at the catheter tip, and measuring the distal steady-state pressure. In theory, the resulting PCWP should approximately equal LAP, as flow has ceased through the branch.

Despite their use in critically ill patients, the thermodilution and PCWP methods have significant limitations. The main limitation is that these methods require an operator to make each individual measurement. Consequently, thermodilution and PCWP measurements are typically made infrequently. Indeed, in 775 critically ill patients instrumented with pulmonary artery catheters, only 0.83 thermodilution and 0.15 PCWP measurements were made on average per day (8). Another limitation is that several technical problems must be overcome in making valid PCWP

measurements. These problems include partial wedging and balloon over-inflation (82, 104), dependence of the measurement on the wedge catheter position (58, 68), and proper interpretation of phasic PCWP (49, 62). Even the developers of the PCWP method reported that they could properly measure PCWP only about 75% of the time in the cardiac catheterization laboratory (120). Similarly, technical problems are also encountered in making thermodilution measurements in which variations in injectate volume, rate, and temperature introduce significant error in the measurement (83, 102, 138). A third limitation is that the injection of fluid and balloon inflation poses risk (e.g., air emoblization) (43, 73, 88). Perhaps due in part to infrequent use (126, 146) and misuse (80, 118, 125, 146) of the PCWP and thermodilution methods, the potential benefit of CO and LAP monitoring in guiding clinical decision-making may not, in general, be sufficiently attained through the thermodilution and PCWP methods to exceed the upfront risk of using the invasive catheter.

CO is also non-invasively measured using ICG (36, 43, 77, 78, 86) technique. This technique is based on the resistance change in the thorax to a low-intensity, high-frequency alternating current applied to the thorax by two surface electrodes placed at the root of the neck and two surface electrodes placed at the xiphoid process at the midaxillary line. Stroke volume (SV) is computed according to the Kubicek equation (78) and CO is taken as the product of SV and heart rate (HR). Although this technique achieves non-invasive monitoring of CO, the measurement involves electrode placement on the neck and chest, which is sometimes precluded by surgical wounds. In addition, ICG may not perform as well in critically ill patients as healthy subjects (65) because of errors associated with abnormal thoracic anatomy (e.g., post-

pneumonectomy) or intra-thoracic fluid (e.g., pleural effusions, pulmonary edema, ARDS) (20, 35, 36).

PWV is conventionally measured through the time delay between the onsets of upstroke of proximal and distal arterial waveforms (i.e., foot-to-foot time delay) (27, 48). Sometimes, this parameter is more conveniently approximated through the time delay between the R-wave of an ECG waveform and the foot of a distal arterial waveform. But, this convenience comes at the significant price of confounding the time delay with the pre-ejection period (48, 113). Despite its simplicity, this conventional method to determine PWV is susceptible to measurement noise especially the motion artifact.

1.4 Scope and Organization of the Dissertation

This dissertation aims to bridge the readily available continuous measurements (e.g., BP, PPG, ICG, and BCG) to clinically more significant hemodynamic variables (e.g., CO, LAP, and PWV) via mathematical analysis techniques so as to make the hemodynamic monitoring both effective (i.e., tracking the key variables needed to direct therapy) and easy-to-use (i.e., continuous and less invasive or non-invasive). In each technique, an impulse response is identified from available measurements and the hemodynamic variable is estimated from the impulse response (i.e., impulse response estimation).

This dissertation is organized as follows: Chapter 1 includes a brief background of the cardiovascular circulation, the motivation of the work, and the limitations of current hemodynamic monitoring systems. Chapter 2 describes background

knowledge and concepts used in following chapters. Chapter 3 reviews a previously developed technique for monitoring CO from peripheral ABP waveform and evaluates the technique with new human data. In addition, the proof-of-concept of extending this technique to PPG waveform is demonstrated as well. Chapter 4 and Chapter 5 formulate two extended techniques for monitoring CO and LAP from pulmonary artery pressure (PAP) and RVP waveforms respectively. Chapter 6 introduces robust PWV estimation techniques by application of system identification to proximal and distal arterial waveforms. Chapter 7 summarizes major contributions of the dissertation and proposes future work.

CHAPTER 2

BACKGROUND

In this chapter, important background knowledge and concepts using in following chapters are briefly introduced.

2.1 System Identification and Impulse Response

2.1.1 System identification

The cardiovascular circulation or part of it can be considered as a dynamic system and the hemodynamic measurements are the input (i.e., stimulus) and output (i.e., response) of the system. The approach to identify the dynamic system from observed input and output signals is called system identification, which is the basis of signal processing techniques used in this dissertation (see Fig. 2.1) (89).

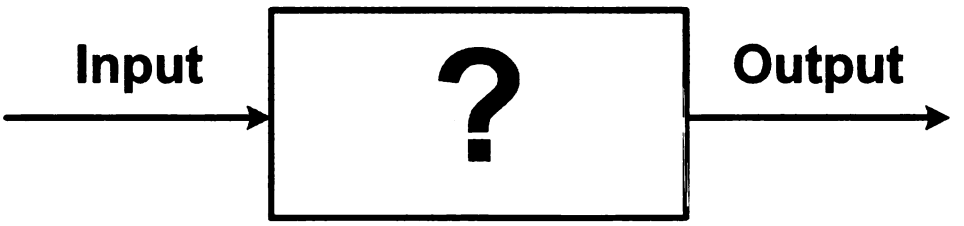

Figure 2.1 The concept of system identification.

The real-life complicated system is characterized by mathematical models in order to make the system identification applicable. These mathematical models are divided into gray-box and black-box models in terms of the availability of pre-

knowledge about the system. The gray-box model assumes that partial knowledge of the system is understood (e.g., the structure of the cardiovascular system can be obtained based on physical or physiological properties but the parameters in the model are unknown). Gray-box model identification is helpful to better understand the dynamic system as the model parameters generally have specific physical meanings. On the other hand, the black-box model assumes no prior knowledge about the system to be identified, that is, both the system structure and model parameters are unknown. Some standard model structures are used to represent the system in this case. While the black-box model provides less insight into the true system, the model structure is more flexible than that of the gray-box model. Both models are used in this dissertation.

2.1.2 Impulse response

Consider a system with input signal x(t) and output y(t) (t indicates discrete time here and hereafter in the dissertation). Intuitively, output y(t) is the response of the system to input x(t). For a linear, time-invariant system, when the input is a unit impulse function $\delta(t)$ (which has the value zero everywhere except at $t = 0$ where its value is infinitely large in such a way that its total integral is one), the corresponding output h(t) is called the impulse response (89). The impulse response is a complete characterization of the dynamic system and the system response y(t) to any input x(t) can be computed as follows:

$$y(t) = \sum_{k=-\infty}^{\infty} h(k)\,x(t-k) \tag{2.1}$$

Therefore, system identification can also be viewed as the identification of the system impulse response.

2.2 Black-Box Models and Least Squares Method

2.2.1 Autoregressive exogenous input model

One of the most widely used black-box models is the autoregressive exogenous input (ARX) model (89), which is also frequently employed in this dissertation. The basic relationship between input and output in this model is formulated by the following linear difference equation:

$$\begin{aligned} y(t) &= a_1\, y(t-1) + \ldots + a_m\, y(t-m) + b_1\, x(t-1) + \ldots + b_n\, x(t-n) + e(t) \\ &= \sum_{k=1}^{m} a_k\, y(t-k) + \sum_{k=1}^{n} b_k\, x(t-k) + e(t) \end{aligned} \tag{2.2}$$

where e(t) is an unobserved, white noise that is uncorrelated with x(t). Unknown parameters $\{a_k\}$ and $\{b_k\}$ are referred to as autoregressive and exogenous coefficients respectively. The constants m and n are called model orders. By introducing the vectors

$$\begin{aligned} \theta &= [a_1 \ldots a_m \quad b_1 \ldots b_n]^T \\ \varphi(t) &= [y(t-1) \ldots y(t-m) \quad x(t-1) \ldots x(t-n)]^T, \end{aligned} \tag{2.3}$$

Eq. 2.2 can be rewritten as

$$y(t) = \varphi^T(t)\,\theta + e(t) \tag{2.4}$$

where T indicates the transposition of the vector. The ARX model can be expressed in Z-domain as well by the following equation:

$$Y(z) = \frac{B(z)}{1 - A(z)} X(z) + \frac{1}{1 - A(z)} E(z) \tag{2.5}$$

where $A(z) = a_1 z^{-1} + a_2 z^{-2} + \ldots + a_m z^{-m}$, $B(z) = b_1 z^{-1} + b_2 z^{-2} + \ldots + b_n z^{-n}$, and E(z) is the Z transform of e(t).

2.2.2 Least squares method

In order to estimate the parameters in ARX model (i.e., θ), certain criterions are needed to define the optimal θ of the model. One of the most popular criterions is the least squares method, that is, θ is selected to minimize the mean square of the prediction error (i.e., e(t)) (89), which is denoted as follows:

$$\hat{\theta} = \arg \min_{\theta} V(\theta, t) \tag{2.6}$$

where

$$V(\theta, t) = \frac{1}{N} \sum_{t=1}^{N} [y(t) - \hat{y}(t)]^2 = \frac{1}{N} \sum_{t=1}^{N} [y(t) - \varphi^T(t)\,\theta]^2 = \frac{1}{N} \sum_{t=1}^{N} e^2(t) \tag{2.7}$$

In Eq. 2.7, N is the number of samples of observed input and output and hat indicates estimated values.

Since V(θ,t) is quadratic in θ, the minimum value can be found by setting the derivative to zero:

$$0 = \frac{d}{d\theta} V(\theta, t) = \frac{2}{N} \sum_{t=1}^{N} \varphi(t)[y(t) - \varphi^T(t)\theta]$$

which gives the optimal θ in the least squares sense

$$\hat{\theta} = \left[\sum_{t=1}^{N} \varphi(t)\,\varphi^{T}(t)\right]^{-1} \sum_{t=1}^{N} \varphi(t)\,y(t) \tag{2.8}$$

2.2.3 Output error model

Another commonly employed black-box model is the output error (OE) model with the Z-domain form as follows:

$$Y(z) = \frac{B(z)}{1 - A(z)} X(z) + E(z) \tag{2.9}$$

While the ARX model minimizes the one-step prediction error, the OE model tries to minimize the full prediction error. However, the OE model can not be implemented linearly as the ARX model. Instead, nonlinear optimization methods such as numerical search are employed to identify the OE model.

2.3 Receiver Operating Characteristic Curve

Receiver operating characteristic (ROC) curve (60, 103) is remarkably useful in medical decision-making. To demonstrate the basic concept of the ROC curve, a specific illustration is helpful. In a binary decision-making scheme (e.g., to decide whether a patient has a certain cardiovascular disease), generally a discrimination metric is measured from the patient and compared to a threshold. For example, a resulting metric greater than the threshold indicates the presence of the disease (i.e., positive outcome), otherwise, the outcome is negative. The test outcome is then compared to the gold standard that indicates whether the patient really has the disease in order to evaluate the metric. If the test outcome is positive and the patient does

have the disease, it is defined as a true positive. Similarly, false positive means that positive outcome appears on patient without disease. Further, true negative and false negative can likewise be introduced.

The ROC curve is a graphical plot of the true positive rate versus false positive rate as the threshold is varied. In this example, the true positive rate is the number of true positives divide by the number of ill patients, while the false positive rate is computed by dividing the number of false positives with the number of patients without the disease. Fig. 2.2 shows examples of the ROC curves.

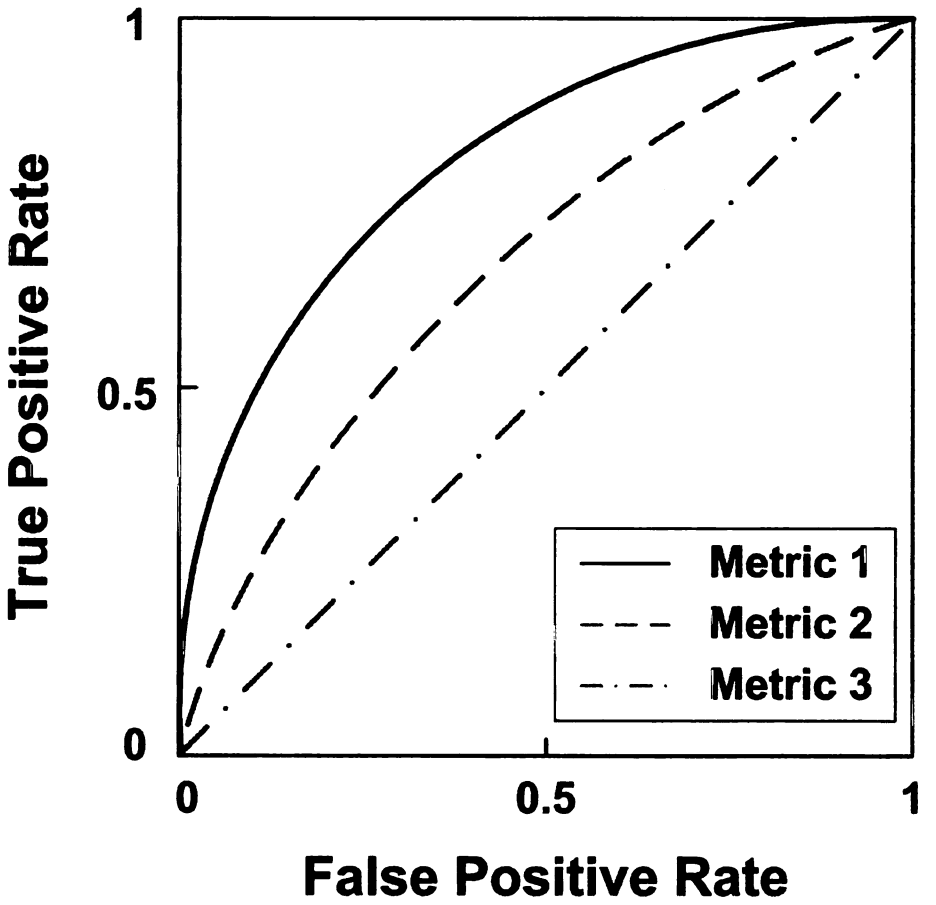

Figure 2.2 Examples of receiver operating characteristic (ROC) curves for three discrimination metrics.

According to the definition of true positive rate and false positive rate, metric 1 is the best discriminator and metric 3 is the poorest one in Fig. 2.2. Indeed, metric 3 shows no capability of discrimination at all.

Intuitively, the area under ROC curve (ROC AUC) could be used to assess the discrimination metric quantitatively. More details about the meaning and applications of the ROC AUC are described in (54, 55).

CHAPTER 3

CARDIAC OUTPUT MONITORING BY PERIPHERAL ARTERIAL BLOOD PRESSURE WAVEFORM ANALYSIS

3.1 Introduction

Numerous investigators have proposed analysis techniques to monitor CO from ABP waveforms over the last century. Frank first suggested that CO could be estimated from ABP waveforms (47). Erlanger et al. proposed the first such technique in 1904 (46). Their technique involved detecting pulse pressure (PP) from the central ABP waveform, which was observed to be positively correlated to SV (i.e., SV-PP), and multiplying it by HR to determine CO for each beat within constant scale factors (i.e., CO-PP·HR). In this way, the technique is able to track the relative changes of CO or the absolute CO values after calibration with an absolute CO measurement. (Note that, in the context of continuous monitoring in the acute setting to direct therapy or detect a hemodynamic event, changes would be most relevant.) However, this technique assumes that cardiac ejection occurs instantaneously when, in actuality, it occurs over finite time in which a portion of the ejected blood passes through the aorta.

Bourgeois et al. proposed one of the most compelling techniques (21, 22) among the numerous ensuing studies of Erlanger et al.'s work (87, 98, 121, 136, 147, 149). Their technique represents the arterial tree with a Windkessel model accounting for

the lumped compliance of the large arteries (arterial compliance, AC) and the total peripheral resistance (TPR) of the small arteries (108) (see Fig. 3.1a).

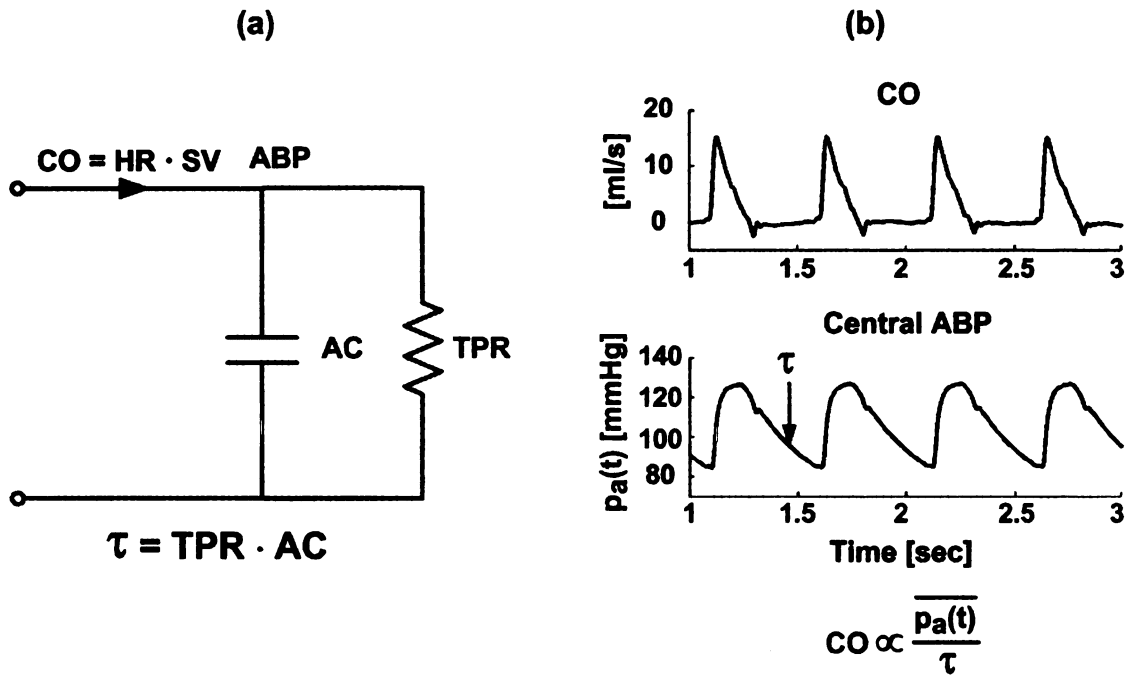

Figure 3.1 Previous technique for CO monitoring by analysis of the central arterial blood pressure (ABP) waveform based on Windkessel model (22). **(a)** Electrical analog of the Windkessel model of the arterial tree. This model predicts that ABP should decay like a pure exponential during each diastolic interval with a time constant (τ) equal to the total peripheral resistance (TPR) times the nearly constant arterial compliance (AC). **(b)** Based on this model, an exponential is fitted to each diastolic interval of the ABP waveform to estimate τ and then proportional CO is computed via Ohm's law.

According to this model, ABP should decay like a pure exponential during each diastolic interval with a time constant (τ) equal to the product of TPR and AC. Since AC is relatively constant over a wide pressure range and on the time scale of months to years (53), CO could then be estimated to within a constant scale factor by dividing the time-average of ABP with τ (i.e., similar to invoking Ohm's law) (see Fig. 3.1b).

Thus, their technique involved fitting an exponential to each diastolic interval of the ABP waveform in order to estimate τ. Wesseling et al. proposed a more intricate "Modelflow" technique by representing the arterial system with a nonlinear three-element Windkessel model (150).

Bourgeois et al. were able to validate their technique when applied to central ABP waveforms, whose diastolic intervals can resemble pure exponential decays following incisura (see Fig. 3.1b). However, central ABP waveforms are rarely measured for routine monitoring due to its high level of invasiveness carrying the risks of thrombo-embolism (e.g., stroke). Furthermore, in readily available peripheral ABP waveforms, exponential diastolic decays are usually not apparent due to the high-frequency arterial wave reflections. That is, when the heart ejects blood, pressure and flow waves are initiated and propagate through the arterial tree. Whenever the waves reach a site of impedance mismatch, especially the high resistance arterial termination points (99, 108, 152), they are in part reflected back towards the heart. The long and varying distances between the aorta and arterial termination points result in forward and backward waves in the aorta with large phasic differences (108). So, waves with relatively short wavelengths (i.e., high frequency), which constructively add in the peripheral ABP waveforms because of the close proximity to the reflection sites, destructively interfere in the aorta and mitigate their cumulative effects on the central ABP waveform. On the other hand, waves with longer wavelengths (i.e., low frequency) constructively add and are felt by the aorta (108). As a result, the ABP waveform becomes progressively distorted with

increasing distance from the heart (see Fig. 3.2) (99, 109). Most notably, PP and systolic pressure (SP) become increasingly amplified, while exponential diastolic decays become less apparent.

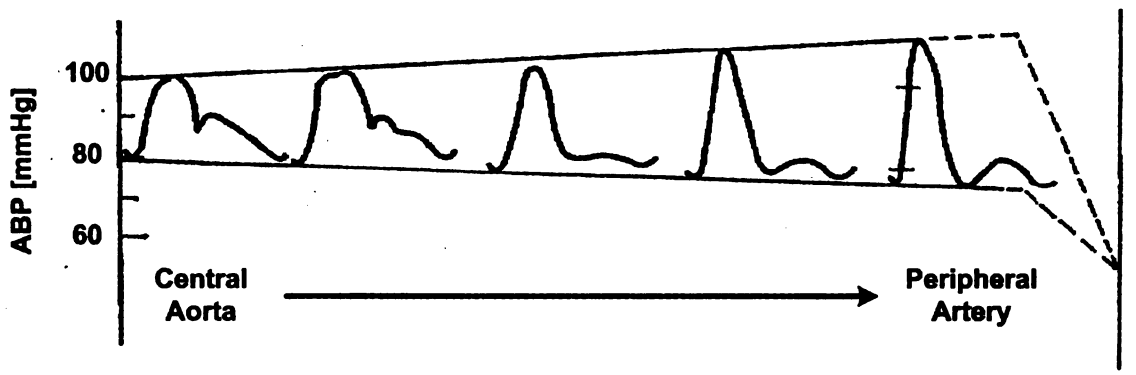

Figure 3.2 The ABP waveform becomes progressively distorted from the central aorta to the peripheral arteries due to wave reflections in the arterial tree. (Adapted from (99).)

Thus, the peripheral ABP generally cannot be adequately represented with the Windkessel model. As a result, the technique of Bourgeois et al. is not successful when applied to peripheral ABP waveforms. Indeed, the confounding (i.e., high frequency) arterial wave reflection has been an obstacle of all previous techniques for monitoring CO from peripheral ABP waveforms (33, 39, 117). One important reason is that these techniques are applied over short time scales within a cardiac cycle, where the confounding wave reflections dominate. Even so, two PP-based techniques and a Windkessel-type technique are now commercially available for continuous and minimally invasive CO monitoring (39). While these techniques have shown overall accuracies good enough for the Food and Drug Administration (FDA), they can markedly overestimate CO during strong vasoconstriction states such as hypovolemia

(33, 39, 117). This overestimation may at least be partly attributed to the augmentation of wave reflections, which buffers the decrease in peripheral PP via SV.

Fortunately, the corruptive effects of these high frequency reflections diminish and would not complicate the waveform with increasing time scale (108). This important concept is demonstrated in Fig. 3.3, which illustrates two ABP waveforms measured at the same time but at different sites in the arterial tree. The short time scale (within one beat) variations are different because the complex wave reflections at the two measurement sites differ from each other. However, the slow (beat-to-beat) variations are much more similar as the confounding effects of the wave reflections diminish over long time scale. The key point is that, as the wavelengths of the propagating waves increase, the pressures at the various arterial sites converge to the same level such that the arterial tree behaves more like a single reservoir. Therefore, the Windkessel model becomes a more valid representation of the arterial tree over longer time scales. For example, if pulsatile activity abruptly ceased, then peripheral ABP would eventually decay like a pure exponential once the faster wave reflections vanish. Based on this fact, a new technique was introduced for continuously monitoring changes in CO by analyzing a peripheral ABP waveform over long time intervals so as to circumvent the confounding wave reflections and was evaluated on animal and human data sets (57, 90, 105, 106).

As discussed in Chapter 1, CO could be a more precise indicator of progressive hemorrhage, which is a serious cause of hypotension and shock, causing morbidity and mortality in diverse patient populations (including trauma casualties, surgical patients, and patients treated with anticoagulation). Indeed, the earlier hypovolemia is

detected, the greater the opportunity exists for caregivers to administer volume replacement or perform a hemostatic intervention. Moreover, it is important to assess the efficacy of volume resuscitation, for example, to discriminate between patients with successful volume therapy and may even be at risk for over-resuscitation and those who may need operative as a result of failed volume therapy (50).

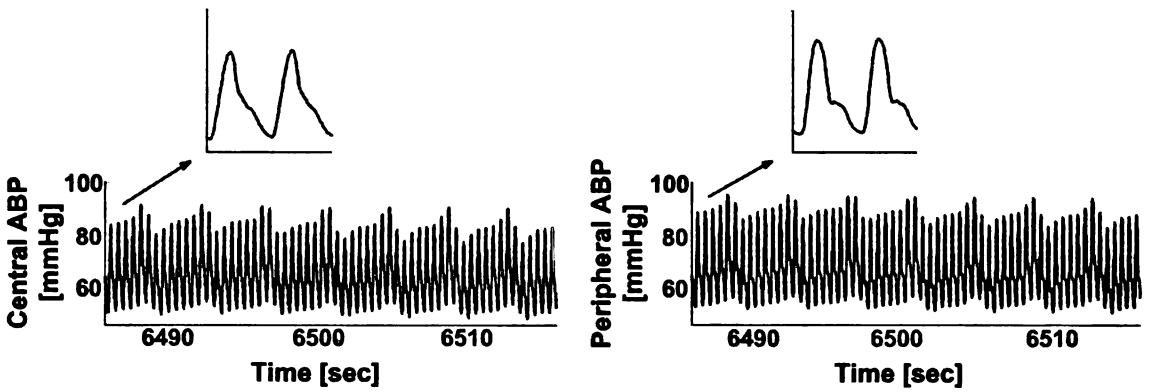

Figure 3.3 Two ABP waveforms simultaneously measured from the central aorta and the radial artery. (Adapted from (106).)

In this chapter, the aforementioned long time interval analysis (LTIA) technique was reviewed and evaluated in 21 healthy humans subjected to lower body negative pressure (LBNP), which is a safe human hemorrhage model. The technique was then compared with other available techniques in terms of the ability to 1) detect progressive hypovolemia; 2) discriminate between hypovolemia and its resuscitation; 3) discriminate between high-tolerant and low-tolerant subjects (122). Further, the LTIA technique was investigated through a pilot study where the technique was applied to the PPG waveform to monitor CO change in two canine experiments in which controlled progressive hemorrhage was induced and followed by resuscitation.

3.2 The Technique

The technique analyzes the peripheral ABP waveform over long time intervals (seconds to minutes) in order to determine the pure exponential decay which would eventually result if pulsatile activity abruptly ceased. More specifically, the ABP response to a single, solitary cardiac contraction is estimated by optimal fitting of a segment of ABP waveform (see impulse response h(t) in Fig. 3.4). Then the Windkessel time constant τ is measured by fitting an exponential to the tail end of h(t) once the faster wave reflections have vanished (see Fig. 3.4). Finally, proportional CO is computed via Ohm's law. (Thus, the technique accounts for the faster wave effects in the ABP waveform through the estimated impulse response but does not attempt to physically model them, as there is no need in the context of estimating average proportional CO). The technique, as is illustrated in Fig. 3.4, is specifically implemented in four mathematical steps as follows.

First, a cardiac contractions signal (x(t)) is derived from the measured ABP waveform segment (y(t)) based on the well-known impulse ejection model (46, 96). That is, as indicated in Fig. 3.4, x(t) is formed as an impulse train in which each impulse is located at the onset of upstroke of an ABP pulse (R) and has an area equal to the ensuing pulse pressure (PP).

Second, the relationship between x(t) and y(t) is characterized by estimating an impulse response (h(t)) which when convolved with x(t) best fits y(t) in the least squares sense. The estimated h(t) represents the ABP response to a single cardiac contraction. The impulse response h(t) is specifically estimated with the following

ARX structure (also see Section 2.2):

$$y(t) = \sum_{k=1}^{m} a_k\, y(t-k) + \sum_{k=1}^{n} b_k\, x(t-k) + e(t) \tag{3.1}$$

where e(t) is the unmeasured residual error, $\{a_k, b_k\}$ are sets of unknown parameters, and m and n represent the unknown model order limiting the number of parameters (89). For a fixed model order, the parameters are estimated from x(t) and y(t) in closed-form through the least squares minimization of e(t) (89). The model order is determined by minimizing the minimum description length (MDL) criterion (89).

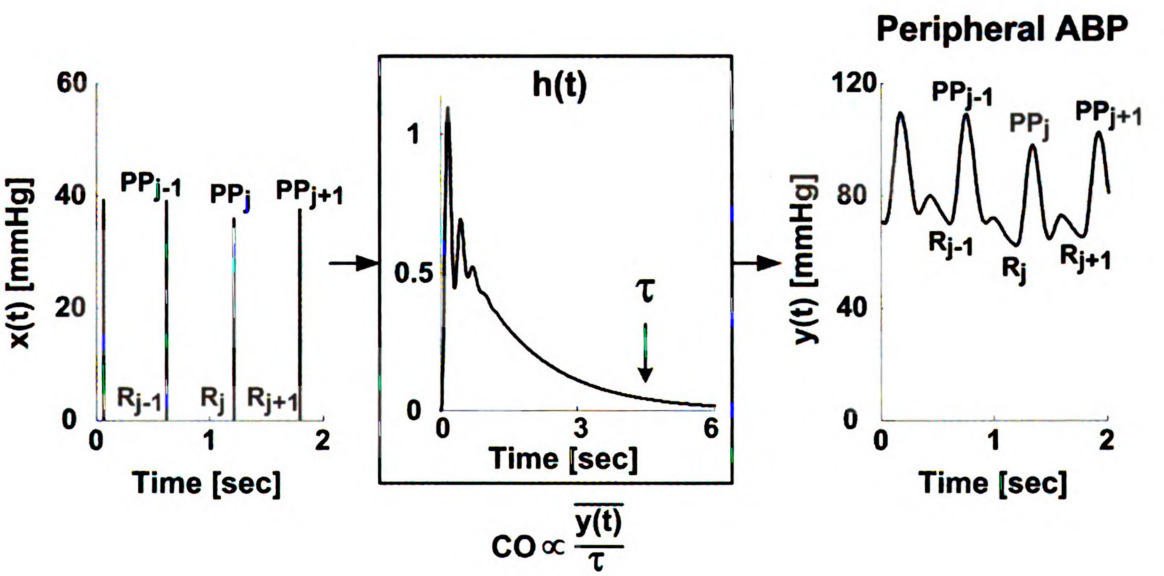

Figure 3.4 Long time interval analysis (LTIA) technique for monitoring relative CO change from a peripheral ABP waveform (90, 106). First, a cardiac contractions signal (x(t)) is constructed from a peripheral ABP waveform segment (y(t)). Second, the ABP response (impulse response) to a single cardiac contraction (h(t)) is estimated so as to optimally fit y(t) when convolved with x(t). Then, the Windkessel time constant τ is determined by fitting an exponential to the tail end of h(t) once the faster wave reflections vanish. Finally, proportional CO is computed via Ohm's law so as to monitor the relative change in CO.

With the estimated parameters, h(t) is computed as follows:

$$h(t) = \sum_{k=1}^{\hat{m}} \hat{a}_k h(t-k) + \sum_{k=1}^{\hat{n}} \hat{b}_k \delta(t-k) \tag{3.2}$$

where hat indicates estimated parameters, and $\delta(t)$ is the unit impulse function.

Third, τ is determined over the interval of h(t) ranging from two to four seconds after the time of its maximum value based on the following exponential equation:

$$h(t) = A e^{-t/\tau} + w(t) \tag{3.3}$$

The unknown parameters A and τ here are estimated through least squares minimization of the unmeasured residual error w(t). This optimization is achieved in closed-form using linear least squares estimation after log transformation of h(t) (89). In principle, reliable determination of τ is achieved by virtue of accurately fitting the long time scale variations in the ABP waveform segment y(t).

Finally, average proportional CO is computed to within a constant scale factor equal to 1/AC as follows:

$$CO \propto \frac{\overline{y(t)}}{\tau} \tag{3.4}$$

where overbar indicates time average. This technique represents the first attempt to monitor CO by circumventing the wave reflections in a peripheral ABP waveform.

Note that AC is assumed to be constant here. Indeed, AC is mainly due to the aorta, which is relatively sparse in smooth muscle (23, 100). So, changes in vasomotor tone should only have a small effect on AC. Further, AC is not very sensitive to ABP changes, as wave propagation delay time, which is inversely related

to AC, varies only modestly with large ABP changes (119). Thus, the well-known inverse relationship between AC and ABP (53) may only become a major factor during extreme ABP perturbations. Consequently, and more precisely, AC is approximately constant over a wide ABP range and on the time scale of months to years. On the other hand, small variations in AC do represent a source of the CO error. Therefore, further investigation of the LTIA technique accounting for AC changes (e.g. via estimation of PWV (see Chapter 6)) is warranted.

3.3 Methods

3.3.1 Experimental procedures

The study was approved by the Institutional Review Board for the use of human subjects at the Brooke Army Medical Center at Fort Sam Houston, Texas. 21 healthy, normotensive subjects aged 27-52 years with no chronic cardiopulmonary medical condition underwent the investigational protocol. In addition, female subjects underwent an initial urine test prior to experimentation to ensure that they were not pregnant. Subjects maintained their normal sleep pattern, refrained from exercise, and abstained from caffeine and other autonomic stimulants. During an orientation session that preceded each experiment, all subjects received a verbal briefing and a written description of all procedures and risks associated with the experiments, and were made familiar with the laboratory, the protocol, and procedures. Subjects gave written informed voluntary consent to participate in the experiments.

LBNP was applied in the present investigation, which is a highly-reproducible experimental tool to simulate loss of central blood volume (e.g., hemorrhage) in

humans (30, 32). Subjects were placed in the supine position and secured in the LBNP chamber using a neoprene skirt designed to form an airtight seal between the subject and the chamber. The application of negative pressure to the lower body (below the iliac crest) results in a redistribution of blood away from the upper body to the lower extremities and abdomen. Subjects underwent an LBNP protocol consisting of a 5-min baseline period, followed by sequential exposure to -15, -30, -45, -60, -70, -80, -90 and -100 mmHg decompression for 5 minutes each. Not all subjects were exposed to all levels of LBNP. Termination of LBNP was based on a precipitous fall in SP of more than 15 mmHg coincident with presyncopal symptoms such as nausea, dizziness, or lightheadedness. Upon the presence of these signs and symptoms (i.e., hemodynamic decompensation), LBNP was released and the pressure within the chamber immediately returned to atmospheric pressure (0 mmHg). After cessation of LBNP and a 5-min transition interval (to allow for a return of fluid sequestered in the lower body), data were collected for an additional 5 minutes ("recovery"), which simulated complete volume resuscitation of hypovolemic patients.

Continuous HR was measured with a four-lead ECG with lead II configuration. Beat-to-beat SV was measured non-invasively using ICG technique (HIC-2000 Bio-Electric Impedance Cardiograph, Bio-impedance Technology, Chapel Hill, NC). SV was computed according to the Kubicek equation (78) (SV-ICG) and CO was taken as the product of SV and HR (CO-ICG). CO-ICG and SV-ICG were taken as the reference in this study. Continuous non-invasive peripheral ABP was measured using the Finometer (Finapres Medical Systems, Amsterdam, the Netherlands) which employs the volume clamp method of Penaz (63). All continuous waveform data

were sampled at 500 Hz and were recorded directly to computer with commercial hardware and software (DataQ Instruments, Akron, OH). The Finometer also automatically outputs SV (SV-MF) and CO (CO-MF) estimated from the ABP waveform using the Modelflow technique (67, 150). These data were recorded directly to a data acquisition system on a beat-to-beat basis.

3.3.2 Data analysis

The technique was applied to up to 5-min (90 seconds at least) ABP waveforms in each level of decompression as well as the recovery stage to estimate CO changes (CO-LTIA). Proportional SV was also computed by dividing the estimated CO with HR (SV-LTIA). For comparison, beat-to-beat COs computed by Modelflow, ICG, and PP·HR methods were averaged over the same segments analyzed by the LTIA technique. Each of the four metrics (CO-ICG, CO-MF, CO-LTIA, CO-PP·HR) was normalized by its baseline value for each subject. The reported metrics therefore represent relative or percent (%) values with respect to baseline. Group means (%) were computed for each metric, using the average of all subjects' values, for each level of decompression, and the recovery. Pair-wise correlation coefficient analysis was performed for all the metrics in order to quantify the relationships between investigational measures of different techniques.

We compared how well the metrics could distinguish between any two levels of LBNP. Specifically, for every combination of LBNP levels for which there were data for all subjects (i.e., -15 mmHg, -30 mmHg, -45 mmHg, -60 mmHg, and recovery), ROC curve (60, 103) (see Section 2.3) was computed and the ROC AUC with

standard error was calculated (54). The AUC quantifies how well two different LBNP levels were distinguished by an investigational metric. For example, if all the CO measurements at -30 mmHg, across all subjects, were lower than those from -15 mmHg, then that hypothetical metric would yield an AUC of 1.0 (indicating a perfect ability to discriminate between the two levels). Conversely, if the distribution of CO measurements from -30 mmHg LBNP was perfectly overlapped with that from -15 mmHg LBNP, then that metric would yield an AUC of 0.5 (indicating no utility for discrimination). The level of statistical significance of the difference between two AUCs was determined by the Hanley-McNeil method for paired data (55).

All subjects tolerated LBNP to -60 mmHg for at least 90 seconds. 13 out of 21 subjects were able to withstand LBNP of -70 mmHg for at least 90 seconds and were termed the "high-tolerant" subjects. The remaining eight subjects were termed the "low-tolerant" subjects. We tested if the investigational metrics, as measured at -60 mmHg, would discriminate between high-tolerant and low-tolerant subjects. ROC AUCs with standard errors were likewise calculated and tested for statistical differences using the Hanley-McNeil method (54, 55).

The SV metrics (SV-ICG, SV-MF, SV-LTIA, SV-PP) were similarly analyzed.

3.4 Results

3.4.1 Detection of progressive hypovolemia

The group means of CO-ICG, CO-MF, CO-LTIA, and CO-PP·HR are shown in Fig. 3.5. CO-PP·HR did not decline with increasing LBNP. Indeed, on average, CO-PP·HR increased even as LBNP progressed to -60 mmHg. Because CO-PP·HR failed

to provide the most rudimentary indication of progressive central hypovolemia, this metric is excluded in further results. CO-ICG, CO-MF, and CO-LTIA tracked LBNP during progressive decompression. These methods were statistically similar in distinguishing between levels of -15, -30, -45, and -60 mmHg, as determined by ROC AUC analysis (see Table 3.1).

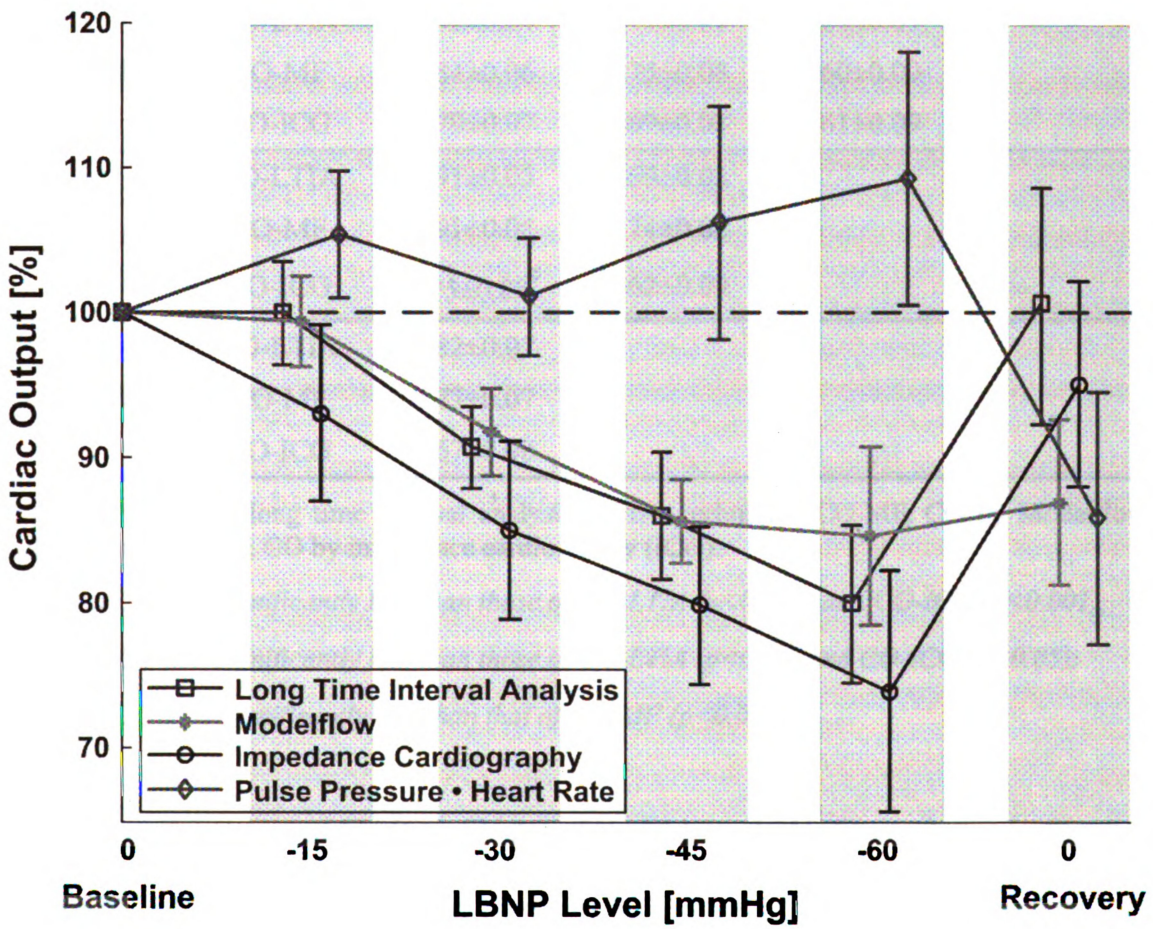

Figure 3.5 Group means of subjects (n = 21) for the investigational CO metrics through progressive levels of lower body negative pressure (LBNP) decompression, expressed as % of baseline measurement. Vertical positions of data points were staggered to display non-overlapping 95% confidence intervals.

Table 3.1 Area under receiver operating characteristic curves (ROC AUCs) with standard errors for discrimination between different levels of lower body negative pressure (LBNP), using investigational CO metrics.

		-15 mmHg	-30 mmHg	-45 mmHg	-60 mmHg
Recovery	CO-LTIA	0.46±0.09	0.66±0.08	0.76±0.07	0.80±0.07
	CO-MF	0.22±0.07[a]	0.41±0.09[a]	0.57±0.09[b]	0.61±0.09[b]
	CO-ICG	0.49±0.09	0.67±0.08	0.75±0.08	0.79±0.07
-60 mmHg	CO-LTIA	0.92±0.04	0.77±0.07	0.64±0.09	
	CO-MF	0.84±0.06	0.75±0.08	0.60±0.09	
	CO-ICG	0.79±0.07	0.69±0.08	0.61±0.09	
-45 mmHg	CO-LTIA	0.91±0.05	0.69±0.08		
	CO-MF	0.91±0.05	0.74±0.08		
	CO-ICG	0.75±0.08[c]	0.62±0.09		
-30 mmHg	CO-LTIA	0.82±0.07			
	CO-MF	0.77±0.07			
	CO-ICG	0.67±0.08			

CO-LTIA is CO by long time interval analysis (LTIA) technique; CO-MF, CO by Modelflow method; and CO-ICG, CO by impedance cardiography (ICG).

[a] *AUC of CO-MF significantly less than those of CO-LTIA ($p<0.001$) and CO-ICG ($p<0.001$);*

[b] *AUC of CO-MF significantly less than those of CO-LTIA ($p<0.01$) and CO-ICG ($p<0.05$);*

[c] *AUC of CO-ICG significantly less than that of CO-MF ($p<0.05$).*

The group means of SV-ICG, SV-MF, SV-LTIA, and SV-PP are shown in Fig. 3.6. SV-ICG, SV-MF, and SV-LTIA also tracked LBNP during progressive decompression. These methods were statistically similar in distinguishing between decompression levels of -15, -30, -45, and -60 mmHg, as determined by ROC AUC analysis (see Table 3.2). SV-PP also declined, but not as reliably, and it yielded less AUCs than the other metrics.

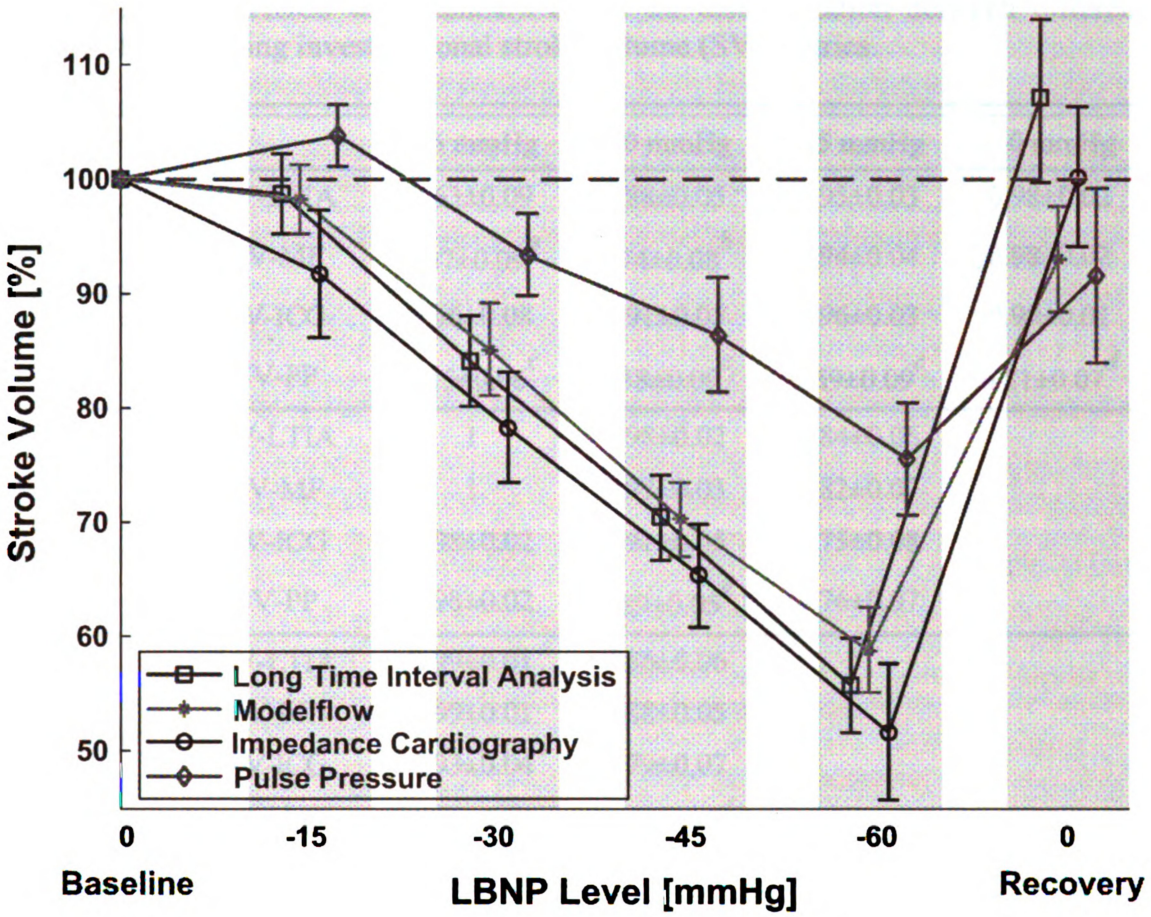

Figure 3.6 Group means of subjects (n = 21) for the investigational stroke volume (SV) metrics through progressive levels of LBNP decompression, expressed as % of baseline measurement. Vertical positions of data points were staggered to display non-overlapping 95% confidence intervals.

The correlation coefficients (with 95% confidence intervals) between investigational techniques and the reference ICG technique for CO metrics were 0.64 (0.51-0.74) (LTIA:ICG) and 0.52 (0.36-0.65) (MF:ICG). The correlation coefficients (with 95% confidence intervals) for SV metrics were 0.83 (0.76-0.88) (LTIA:ICG), 0.77 (0.69-0.85) (MF:ICG), and 0.60 (0.46-0.71) (PP:ICG). (Note that a greater range of SV metrics was observed than the range in CO, as seen in Fig. 3.5 and 3.6. Accordingly, correlations between SV metrics tended to be greater than CO metrics.)

Table 3.2 ROC AUCs with standard errors for discrimination between different levels of LBNP, using investigational stroke volume (SV) metrics.

		-15 mmHg	-30 mmHg	-45 mmHg	-60 mmHg
Recovery	SV-LTIA	0.63±0.09	0.88±0.05	0.95±0.03	0.98±0.02
	SV-MF	0.37±0.09[a]	0.74±0.08[b]	0.94±0.04	0.98±0.02
	SV-ICG	0.66±0.08	0.91±0.05	0.96±0.03	0.99±0.01
	SV-PP	0.15±0.06[c]	0.38±0.09[c]	0.59±0.09[c]	0.81±0.07[d]
-60 mmHg	SV-LTIA	1	0.98±0.02	0.84±0.06	
	SV-MF	1	0.97±0.03	0.82±0.07	
	SV-ICG	0.98±0.02	0.91±0.05	0.75±0.08	
	SV-PP	0.98±0.02	0.89±0.05[e]	0.76±0.07	
-45 mmHg	SV-LTIA	0.99±0.01	0.86±0.06		
	SV-MF	0.99±0.01	0.88±0.05		
	SV-ICG	0.93±0.04	0.79±0.07		
	SV-PP	0.92±0.04	0.71±0.08[f]		
-30 mmHg	SV-LTIA	0.86±0.06			
	SV-MF	0.87±0.06			
	SV-ICG	0.78±0.07			
	SV-PP	0.83±0.06			

SV-LTIA is SV by LTIA technique; SV-MF, SV by Modelflow method; SV-ICG, SV by ICG technique; and SV-PP, SV estimated from pulse pressure (PP).

[a] *AUC of SV-MF significantly less than those of SV-LTIA ($p<0.0001$) and SV-ICG ($p<0.01$);*

[b] *AUC of SV-MF significantly less than those of SV-LTIA ($p<0.01$) and SV-ICG ($p<0.05$);*

[c] *AUC of SV-PP significantly less than those of SV-LTIA ($p<0.0001$), SV-MF ($p<0.01$), and SV-ICG ($p<0.0001$);*

[d] *AUC of SV-PP significantly less than those of SV-LTIA ($p<0.01$), SV-MF ($p<0.01$), and SV-ICG ($p<0.01$);*

[e] *AUC of SV-PP significantly less than that of SV-LTIA ($p<0.05$);*

[f] *AUC of SV-PP significantly less than those of SV-LTIA ($p<0.05$) and SV-MF ($p<0.05$).*

3.4.2 Discrimination between hypovolemia and its resuscitation

CO-LTIA and CO-ICG tracked decompression and returned to a near baseline level during recovery (see Fig. 3.5). CO-MF tracked decompression but, during recovery, returned to only 87% of baseline, which was comparable to the average CO-MF measured between -30 and -45 mmHg of LBNP.

For discrimination between LBNP and recovery, CO-LTIA was quite similar to CO-ICG in terms of AUCs (see Table 3.1). Both CO-LTIA and CO-ICG were superior to CO-MF for discriminating between hypovolemia and euvolemia (i.e., termination of LBNP, which was our simulation of complete resuscitation). The difference was statistically significant for any level of LBNP (see Table 3.1).

The SV metric was more discriminatory (i.e., higher AUC) than the corresponding CO metric in all comparisons. SV-LTIA and SV-ICG were similar in terms of AUCs (see Table 3.2) and both superior to SV-MF for discriminating between hypovolemia and euvolemia (see Table 3.2). SV-LTIA and SV-ICG were superior to SV-PP at almost any two LBNP levels.

3.4.3 Discrimination between high-tolerant and low-tolerant subjects

By assessing which subjects had the largest reductions in CO (or SV) at -60 mmHg, it was possible to discriminate, to some degree, between high-tolerant and low-tolerant subjects (i.e., which subjects were most at-risk of cardiovascular collapse with any additional LBNP). ROC analysis of CO-LTIA yielded an AUC of 0.66 (where preservation of CO-LTIA was associated with high-tolerant subjects and reduced CO-LTIA was associated with low-tolerant subjects), and was significantly

greater than CO-MF (see Table 3.3). CO-MF yielded a ROC AUC of 0.40 which means that preservation of CO-MF was paradoxically associated with low-tolerant subjects. SV metrics yield higher AUCs than corresponding CO metrics and the best discriminator between high-tolerant and low-tolerant subjects was SV-LTIA with AUC of 0.86, which was significantly greater than SV-ICG and SV-MF, though non-significantly better than SV-PP (see Table 3.3).

Table 3.3 ROC AUCs with standard errors for discrimination between high-tolerant and low-tolerant subjects using CO and SV metrics at -60 mmHg LBNP.

	LTIA	MF	ICG	PP(·HR)
CO	0.66±0.13	0.40±0.13[a]	0.49±0.13	0.55±0.13
SV	0.86±0.09	0.54±0.13[b]	0.61±0.13[c]	0.79±0.11

[a] *AUC of CO-MF significantly less than that of CO-LTIA ($p<0.05$);*

[b] *AUC of SV-MF significantly less than that of SV-LTIA ($p<0.01$);*

[c] *AUC of SV-ICG significantly less than that of SV-LTIA ($p<0.05$).*

3.5 Discussion

In this study, we evaluated the LTIA technique for monitoring CO and SV from a peripheral ABP waveform on 21 healthy humans subjected to LBNP, which is a carefully-controlled laboratory procedure to induce, then resolve, a standardized circulatory disturbance. The technique was compared with other three non-invasive CO and SV measurement modalities (i.e., Modelflow, ICG, and PP(·HR)) in term of the diagnostic capabilities. The ICG technique was taken as the reference.

LTIA and ICG methods, based on waveform analysis and thoracic bioimpedance,

respectively, yielded similar ROC AUCs for both CO and SV metrics. Throughout progressive hypovolemia, Modelflow was diagnostically similar to both LTIA and ICG. SV-PP also declined, but not as reliably, during progressive hypovolemia and it trended towards lower AUCs than the other SV metrics. The reduction in PP underestimated the actual reduction of SV, which was evidenced by the finding that CO-PP·HR paradoxically increased during progressive LBNP. With simulated resuscitation, (i.e., termination of LBNP), CO-MF, SV-MF, and SV-PP remained reduced, with inferior ability to discriminate between hypovolemia and euvolemia (see Table 3.1 and Table 3.2).

It appears that both ICG and LTIA methods would be preferable for monitoring subjects who receive resuscitation for their hypovolemia. In terms of practical requirements, ICG technique suffers from several problems as discussed in Chapter 1. The LTIA technique, on the other hand, requires a peripheral ABP waveform, which can be measured via an indwelling arterial catheter or a non-invasive finger-cuff apparatus, e.g., the Finometer used in this study.

Clinically, it would be most useful to monitor a circulatory metric that is an accurate indicator of impending cardiovascular collapse. Therefore, all the metrics were assessed in terms of the ability to indicate which subjects would prove unable to tolerate additional LBNP. The results showed that protection of SV-LTIA at -60 mmHg LBNP was a strong predictor (AUC 0.86) of high tolerance to the deepest levels of LBNP. The AUC of SV-LTIA was significantly greater than SV-ICG (AUC 0.61) and SV-MF (AUC 0.54). In general, SV metrics were more predictive of tolerance than CO metrics. Paradoxically, CO-MF yielded an AUC less than 0.50,

meaning that the biggest reductions in CO-MF at -60 mmHg LBNP were associated with the most tolerant subjects, which is counter-intuitive and also inconsistent with prior findings (31, 130). Overall, the superior ability of SV-LTIA to identify between high-tolerant and low-tolerant subjects suggests it may be a more valid assessment of circulatory status compared with the alternatives.

While the Modelflow technique performed similarly to both LTIA and ICG methods during progressive hypovolemia, it showed inferior ability to discriminate between hypovolemia and its resolution. Although the Modelflow technique employs an intricate three-element Windkessel model, it analyzes the waveform over short time scale (single cardiac cycle) and is expected to suffer from the confounding wave reflections as discussed above. Remaining reduced CO-MF and SV-MF during recovery implied that the technique may not be reliable when CO and SV were restored. During different levels of decompression, TPR is significantly changed in order to maintain the BP level. Therefore, the contour of ABP waveforms at different LBNP levels exhibited large differences even at the same measurement site due to varying wave reflections (see Fig. 3.7). We speculate that perhaps the Modelflow method was not flexible enough to account for these contour changes caused by fast waves, which was not a dominant factor in the LTIA technique (108). (In Fig. 3.7, the waveform shape during recovery is notably different from that from baseline, which may explain why the estimates from recovery by Modelflow technique failed to return to the baseline level.)

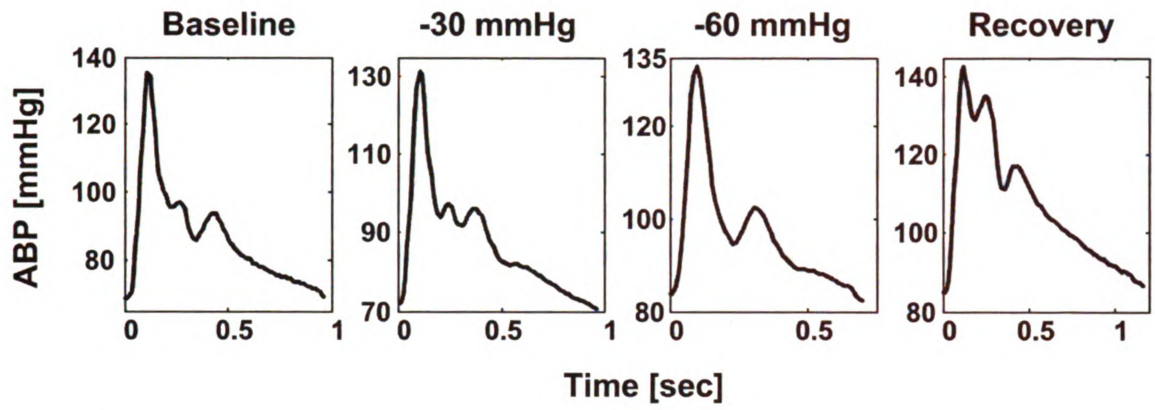

Figure 3.7 Excerpts of ABP waveforms from one subject during different levels of decompression.

PP has value in the diagnosis of progressive hypovolemia (see Table 3.2), though it was consistently less diagnostic than SV-LTIA and SV-ICG. PP and SV were found to be correlated, which has been previously noted in other reports (e.g., high correlation of variability of PP and SV during major abdominal surgery (42).) At the same time, it is important to appreciate that the magnitude of reduction in SV was underestimated by PP. This is highlighted by the fact that CO-PP·HR paradoxically increased throughout progressive LBNP. These results suggest that any algorithm that assumes PP is a quantitative surrogate for SV (e.g., the FloTrac method (4)) will need to offer substantial compensation, and these findings may also explain why certain PP-based algorithms have shown inconsistent reliability in some clinical reports (44). A variation of CO-PP·HR proposed by Liljestrand and Zander, in which PP·HR was scaled by (SP+diastolic pressure (DP)) to adjust for arterial compliance (85), was reported by Sun et al. to be well performed in an ICU population consisting of older patients with relatively less dynamic changes in TPR (140). However, in our dataset, PP·HR/(SP+DP) failed to decline with progressive LBNP.

In terms of the validity of the experimental model, the results (see Fig. 3.5) were consistent, on average, with prior reports involving LBNP to reduce CO. Using echocardiography, Kimmerly et al. found that CO had fallen to 79% at -40 mmHg of LBNP (75), while Chang et al. reported that CO had fallen to 65% at -45mmHg of LBNP using CO_2 rebreathing (25). We found that subjects returned to near their baseline circulatory state (e.g., CO-ICG values were 95±7% of their baseline values) 5-10 minutes after cessation of LBNP, which is consistent with a prior finding that intravascular fluid sequestered by LBNP is immediately returned upon cessation of LBNP, and most edema is resorbed within minutes after cessation of LBNP (91). In light of our trends for CO-ICG and CO-LTIA, and in light of the LBNP literature, we conclude that CO in this study declined as a function of LBNP as expected, and that the recovery interval was physiologically similar to euvolemia.

There are several limitations to this study. First, the study of healthy subjects in laboratory conditions may not be strictly equivalent to clinical use. For instance, there may be more measurement error in actual clinical use, or other confounding factors, such as vasopressor infusion. However, this study design provided unambiguous outcomes impossible to accomplish through clinical trials, so such controlled laboratory studies may be quite complimentary to clinical "real world" investigations. Second, the peripheral ABP was measured using the Finometer. It is possible that ABP waveform analysis using an indwelling arterial catheter might yield different results. Therefore, these results may not necessarily generalize to subjects with an indwelling ABP measurement. On the other hand, the Finometer has been shown to provide a valid measurement of ABP (51). Moreover, a non-invasive

method of CO monitoring could be useful in the management of the majority of hospitalized patients without invasive arterial lines.

In conclusion, we found that CO and SV estimated by LTIA, ICG, and Modelflow techniques, all tracked progressive hypovolemia. SV-PP also declined, but CO-PP·HR was not a suitable quantitative surrogate for CO, as it erroneously increased during progressive LBNP. After restoration of circulating volume, CO and SV by LTIA and ICG were able to distinguish between ongoing hypovolemia and resuscitation, while the metrics by Modelflow and PP(·HR) were significantly less discriminatory. Protection of SV-LTIA was the strongest predictor of high tolerance to the deepest levels of LBNP. In all instances, SV metrics were more discriminatory than CO metrics. These results have implications for the utility of non-invasive CO and SV measurements to track progressive bleeding and effective fluid resuscitation.

3.6 Technique Extension

As discussed in Chapter 1, despite the simplicity and low cost of PPG technique, the PPG waveform is not fully understood and its clinical applications are limited. On the other hand, monitoring of critical hemodynamic variables such as CO based on the PPG waveform would be valuable for developing non-invasive, low-cost, and easy-to-use hemodynamic monitoring systems. To this end, we conducted a pilot study to investigate the feasibility of CO monitoring from the PPG waveform by the LTIA technique.

3.6.1 CO monitoring by PPG waveform analysis

The peripheral ABP waveform represents the pulsatile BP in peripheral vascular bed while the PPG waveform indicates corresponding blood volume change. The "pressure-to-volume" relationship may be characterized by a low pass filter (13), according to which most low frequency components of the peripheral ABP waveform would be preserved in the PPG waveform. As discussed above, in the LTIA technique, the low frequency information in the waveform is much more crucial than the high frequency components to determine CO. Therefore, the LTIA technique, in principle, should be applicable to the PPG waveform as well. However, in order to estimate the correct impulse response and time constant τ, the PPG waveform has to be first calibrated to BP levels (i.e., DP, SP, and mean arterial pressure (MAP)) during the period of measurement. The oscillometry (i.e., the cuff) measurements or other BP monitoring techniques (e.g. non-invasive and cuff-less BP monitoring via PWV estimation (see Chapter 6)) could be employed for the calibration.

3.6.2 Methods

To evaluate this extension of the technique, we performed canine experiments with protocol inducing controlled progressive hemorrhage and followed volume resuscitation, which is approved by the MSU All-University Committee on Animal Use and Care.

Experiments were performed in two normal adult beagles (9.6-10.4 kg). Briefly, general anesthesia was induced and mechanical ventilation was instituted. A micromanometer-tipped catheter was positioned at the pulmonary artery for reference

thermodilution CO measurement. A fluid-filled catheter was placed at ascending aorta via a femoral artery for aortic pressure waveform and another fluid-filled catheter at carpal or dorsal pedal artery for peripheral ABP waveform. Surface electrodes were placed for standard ECG waveform. The measurements were then recorded at a sampling rate of 1000 Hz. The PPG waveform was collected with a separate device by placing a PPG sensor at the tongue. ECG waveform was also measured by the device and the measurements were recorded at a sampling rate of 250 Hz. Synchronization between the two sets of measurements was achieved by aligning marks in two ECG waveforms induced by electrical muscle stimulation during the experiments.

All measurements were recorded during a 10-min baseline period followed by five 20-min fixed-volume hemorrhage and a 25-min retransfusion period. During each hemorrhage, 60 ml blood was removed over 5-min followed by 5-min equilibration and 10-min steady period. All shed blood was then retransfused over 10-min followed by 5-min equilibration and 10-min steady period. During the 10-min steady period of each of the seven conditions, the following measurements were made: three cuff measurements (each of which included DP, SP, and MAP values) at 0-min, 5-min, and 10-min marks respectively and two thermodilution CO measurements right after the second cuff record (one or two more thermodilution if initial two measurements did not agree).

Clean 1-min segments were selected from the 10-min steady records during each of the seven conditions for analysis. Cuff BP measurements, which were intended to be used to calibrate the PPG waveform, did not agree well with BP measured by

fluid-filled catheters. Therefore, to prove the concept, BP levels averaged from the peripheral ABP waveforms during the same 1-min segments of analysis were utilized to calibrate the PPG waveform. The LTIA technique was then applied to the calibrated PPG waveforms and the estimated CO values were normalized by the baseline value for each dog and compared with the likewise normalized reference thermodilution CO. (Note that the reference CO of each condition was averaged over the thermodilution measurements made during that condition.)

3.6.3 Pilot results and discussion

Fig. 3.8 shows the results of applying the LTIA technique to calibrated PPG waveforms as well as the reference thermodilution measurements for each dog. The estimated CO by LTIA technique corresponded well to the reference measurements during progressive hemorrhage and retransfusion.

The preliminary results demonstrate the feasibility of extending the LTIA technique to the calibrated PPG waveform. However, there are two limitations in the study.

First, the anesthesia in the first experiment blunted the cardiovascular reflexes in the dog. Hence, BP decreased and HR barely changed during hemorrhage (results not shown) while, in reality, BP is maintained and HR increases before the cardiovascular control system eventually collapses (see Fig. 1.1). Nevertheless, BP decreased not as much as both reference and estimated CO during progressive hemorrhage and did not return to the reference CO during retransfusion, which, to some degree, reveals the advantage of the new technique. A different anesthesia procedure was used in the

second experiment in an attempt to maintain BP during the bleed. The BP was maintained effectively until the middle stages of the bleed (120 and 180 ml blood loss), when serious problems occurred with the experimental preparation due to the anesthesia. These problems caused 1) the isolated time point reference CO measurement to be unreliable during 120 ml; 2) the reference CO measurement to actually increase during 180 ml; and 3) a reduced ability to maintain BP towards the end stages of the hemorrhage. Therefore, the unreliable data at 120 ml blood loss and the counter-intuitive data at 180 ml blood loss were excluded in dog 2 of Fig. 3.8.

Another limitation is that invasive peripheral ABP was used to calibrate the PPG waveforms instead of cuff measurements, which is not applicable in practice where ABP waveform is not available. Therefore, if further investigation confirms that the cuff measurement is not accurate enough for calibration, alternative cuff-less and non-invasive BP estimation techniques are required.

In summary, the feasibility of the new LTIA technique based on the calibrated PPG waveform is demonstrated. However, to complete this study, proper anesthesia procedure without compromising the cardiovascular control system is needed and accurate BP estimation techniques should be developed (e.g., via PWV estimation (see Chapter 6)).

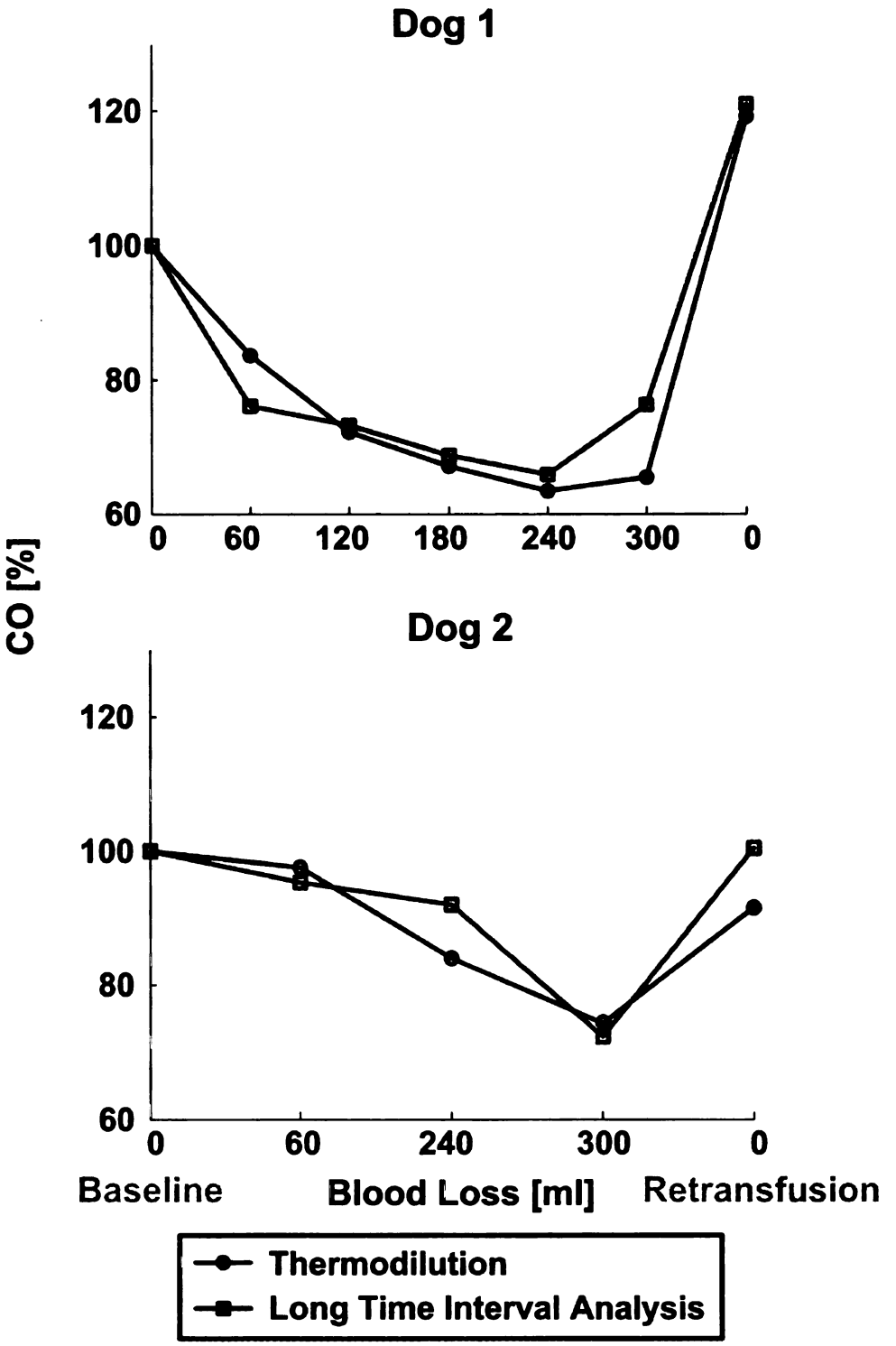

Figure 3.8 Normalized CO values estimated by the LTIA technique applied to calibrated photoplethysmography (PPG) waveforms compared with reference thermodilution measurements.

CHAPTER 4

CARDIAC OUTPUT AND LEFT ATRIAL PRESSURE MONITORING BY PULMONARY ARTERY PRESSURE WAVEFORM ANALYSIS

4.1 Introduction

As discussed in Chapter 1, both CO and LAP are critical variables as they can facilitate the diagnosis, monitoring, and treatment of various disease processes such as left ventricular failure, mitral valve disease, and shock of any cause. For example, a decrease in CO while LAP is rising would indicate an insult to the heart, whereas a decrease in CO while LAP is falling would indicate a vascular anomaly or a reduction in effective circulating blood volume.

In critically ill patients, the standard methods for monitoring CO and LAP (i.e., thermodilution and PCWP, respectively) both involve the use of the pulmonary artery catheter. While these techniques suffer from major limitations (see details in Chapter 1), the pulmonary artery catheter, on the other hand, also permits continuous monitoring of the PAP waveform. Since CO and LAP are both significant determinants of PAP, we considered that it could be possible to continuously monitor these two critical hemodynamic variables by mathematical analysis of the PAP waveform.

A few investigative teams have proposed techniques for monitoring CO by PAP waveform analysis (29, 40, 144, 161, 162). This set of papers describes a total of five

different techniques that analyzed each individual beat of the PAP waveform to compute CO to within a proportionality constant. However, similar to the peripheral ABP waveform, confounding waves as well as inertial effects in the low-resistance pulmonary circulation are prominent in the PAP waveform over the short time scales within a beat (108). Perhaps, as a result, the success of the techniques was, in general, shown to be limited.

Far fewer techniques have been introduced for estimating LAP from even general BP waveforms. Over half a century ago, Cournand helped establish the classic technique of monitoring LAP through the end-diastolic PAP (34, 56) that is sometimes used in clinical practice (95). However, end-diastolic PAP is not as accurate as PCWP (61) and is contraindicated for following LAP during pulmonary hypertension (59, 95). Within the past two decades, some investigators have proposed techniques to predict LAP from a BP waveform through formula derived from a training dataset of LVFP measures and BP waveforms. In particular, McIntyre led the development of a technique to monitor left ventricular end-diastolic pressure from the peripheral ABP response to a Valsalva maneuver (101, 133). This technique is now available on the market with FDA clearance (3). Marik and others formulated a technique to monitor PCWP from peripheral SP variations induced by mechanical ventilation (94, 157). Most recently, deBoisblanc et al. conceived a technique to predict PCWP from the PAP waveform specifically using a neural network (38). The former two techniques, which extract LVFP information from the induced intrathoracic pressure variations, provide an attractive minimally invasive or non-invasive means to sensitively monitor LAP but do require a hemodynamic

perturbation. On the other hand, the latter, more invasive technique is continuous and may be more specific, as PAP is directly determined by LAP whereas ABP is not. For all of these techniques, accuracy is dependent on the availability of comprehensive training datasets.

In short, there is a paucity of techniques in the literature for monitoring CO or LAP from the PAP waveform. Moreover, amongst the few previous techniques, none simultaneously estimate both CO and LAP. In this chapter, we developed a new technique to continuously monitor both CO and LAP by mathematical analysis of the PAP waveform (156). The technique is notable in that it 1) analyzes inter-beat (i.e., long time scale) variations in the PAP waveform in which confounding waves and inertial effects cease to be major factors (108); 2) is not based on training data and may therefore be generally applicable; and 3) jointly estimates CO and LAP. We then performed experiments in five dogs in order to evaluate the technique with respect to the most accurate available reference methods during commonly employed hemodynamic interventions.

4.2 The Technique

The technique for continuous CO and LAP monitoring by PAP waveform analysis represents an extension of the LTIA technique introduced in Chapter 3 for monitoring CO by analysis of a peripheral ABP waveform (90, 106).

The technique arises from the Windkessel model of the pulmonary circulation shown in Fig. 4.1a. This model predicts that PAP should decay like a pure exponential function during each diastolic interval with a time constant (τ) equal to

the product of the pulmonary arterial resistance (PAR) and the pulmonary arterial compliance (PAC). The model further predicts that the exponential pressure decay should equilibrate towards LAP rather than zero pressure.

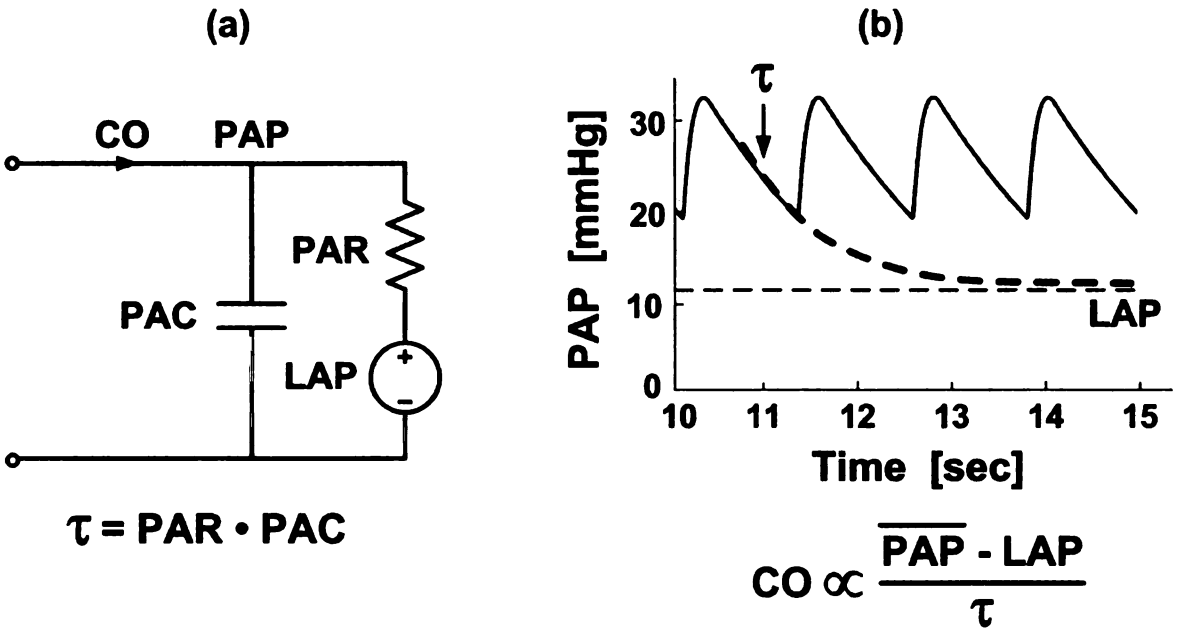

Figure 4.1 A potential technique for continuous CO and LAP monitoring by intra-beat analysis of the pulmonary artery pressure (PAP) waveform. **(a)** The Windkessel model of the pulmonary circulation. **(b)** The model suggests that a time constant τ, which is equal to the product of the pulmonary arterial resistance (PAR) and the pulmonary arterial compliance (PAC), and average LAP may be determined from the PAP waveform by fitting an exponential plus a constant term to each of its diastolic intervals. Moreover, assuming PAC is relatively constant, proportional CO may then be determined similar to invoking Ohm's law.

Thus, as illustrated in Fig. 4.1b, the Windkessel model suggests that both τ and average LAP may be determined from the PAP waveform by fitting a single exponential function plus a constant term to each of its diastolic intervals. Moreover, assuming PAC is relatively constant over a monitoring period, proportional CO may then be determined by subtracting LAP from the time average of PAP and dividing

this difference by τ (i.e., similar to invoking Ohm's law).

However, pure exponential diastolic decays are generally not apparent in experimental PAP waveforms (144) (see Fig. 4.3) due to complex wave reflections and inertial effects in the pulmonary circulation (108). On the other hand, as we and other researchers have previously noted, such phenomena may only complicate the PAP waveform over short time scales (i.e., high frequencies) (90, 106, 108). For example, as the time scale increases (i.e., the frequency decreases), the wavelengths of the propagating waves become larger with respect to the dimension of the pulmonary circulation such that the circulation appears more lumped, and inertial effects, which are proportional to the time derivative of the flow rate, become more attenuated. Thus, the Windkessel model of Fig. 4.1a may be a more valid representation of the long time scale or beat-to-beat (i.e., low frequency) dynamics of the PAP waveform. So, for example, if pulsatile activity abruptly ceased, then PAP may eventually decay like a pure exponential function and equilibrate to LAP once the faster confounding dynamics vanish.

Similar to the previous LTIA technique (see Chapter 3), this technique analyzes the PAP waveform over long time intervals in order to determine the pure exponential decay and equilibrium pressure that would eventually result once pulsatile activity suddenly ceased. More specifically, average LAP and the PAP-LAP response to a single, solitary cardiac contraction (see impulse response h(t) in Fig. 4.2) are simultaneously estimated by optimal prediction of a 6-min segment of the PAP waveform. Then, τ is determined by fitting a single exponential function to the tail

end of h(t) once the faster wave and inertial effects have vanished (see Fig. 4.2). Finally, average proportional CO is computed similar to invoking Ohm's law and calibrated with a single absolute CO measurement. The technique is likewise implemented in four steps as follows.

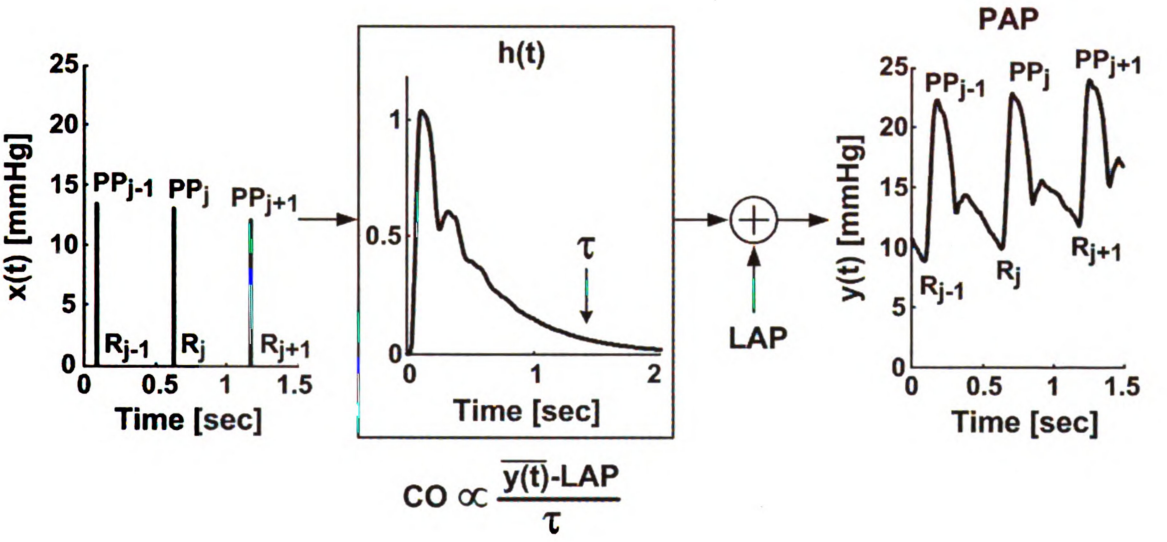

Figure 4.2 LTIA technique for monitoring relative CO change and LAP from a PAP waveform. First, a cardiac contractions signal (x(t)) is constructed from a PAP waveform segment (y(t)). Second, y(t) is fitted according to the sum of a constant term with the convolution between x(t) and an impulse response (h(t)). That is, the constant term and h(t) are estimated so as to optimally fit y(t). Next, the time constant τ of the Windkessel model of Fig. 4.1 is determined by fitting an exponential to the tail end of h(t) once the faster wave and inertial effects vanish. Finally, average proportional CO is determined similar to invoking Ohm's law.

First, a cardiac contractions signal (x(t)) is constructed through the formation of an impulse train in which each impulse is located at the time of end-diastolic PAP (R) and has an area equal to the subsequent pulse pressure (PP) (46, 96).

Second, y(t) is fitted according to the sum of an unknown constant term with the convolution between the known x(t) and an unknown impulse response (h(t)). That is,

the constant term and h(t) are estimated so as to permit the best fit or prediction of y(t) in the least squares sense. The estimated constant term represents the average LAP, while, by mathematical definition, the estimated h(t) represents the PAP-LAP response to a single cardiac contraction. The impulse response h(t) and average LAP are specifically estimated with the following ARX structure with constant term a_0:

$$y(t) = a_0 + \sum_{k=1}^{m} a_k\, y(t-k) + \sum_{k=1}^{n} b_k\, x(t-k) + e(t) \tag{4.1}$$

where e(t) is the unmeasured residual error; $\{a_k, b_k\}$, sets of unknown parameters; m and n, unknown model order (89). For a fixed model order, the parameters are estimated from x(t) and y(t) through regularized least squares minimization of e(t). This optimization is achieved in closed-form using linear least squares estimation with Tikonov regularization (89). The model order is determined by minimizing the MDL criterion (89) over a range of $1 \leq m, n \leq 15$. With the estimated parameters, average LAP and h(t) are computed as follows:

$$LAP = \hat{a}_0 \Big/ \left(1 - \sum_{k=1}^{\hat{m}} \hat{a}_k \right) \tag{4.2}$$

$$h(t) = \sum_{k=1}^{\hat{m}} \hat{a}_k\, h(t-k) + \sum_{k=1}^{\hat{n}} \hat{b}_k\, \delta(t-k) \tag{4.3}$$

where hat indicates estimated parameters, and $\delta(t)$ is the unit impulse function.

Third, τ is determined, based on Eq. 3.3, over the interval of h(t) ranging from one to two seconds following the time of its maximum value. In theory, accurate determination of τ as well as average LAP is achieved by virtue of h(t) coupling the

long time scale or beat-to-beat variations in x(t) to y(t).

Finally, average proportional CO is computed to within a constant scale factor equal to 1/PAC as follows:

$$CO \propto \frac{\overline{y(t)} - LAP}{\tau} \tag{4.4}$$

where overbar indicates time average. The proportional CO estimate may then be conveniently calibrated to absolute CO with a readily available thermodilution measurement.

4.3 Methods

We conducted canine experiments to evaluate the PAP waveform LTIA technique and to compare it to competing intra-beat analysis techniques. We outline our methods for experimental procedures and data analysis below.

4.3.1 Experimental procedures

Experiments were performed in five normal adult dogs (10-26 kg), either beagles or mongrels. Each dog was studied on two separate experimental days under a protocol approved by the MSU All-University Committee on Animal Use and Care.

On the first experimental day, chronic instrumentation was installed in the dog for data recording using a sterile procedure as follows. General anesthesia was induced with an intravenous injection of propofol (2.2-6.6 mg/kg) and maintained with inhaled isoflorane (1.5-2.5%), and mechanical ventilation was instituted. A left lateral thorocotomy was performed. An ultrasonic flow probe was placed around the ascending aorta for reference CO (A-series, Transonic Systems, Ithaca, NY). (After

chronic implantation of this flow probe to ensure acoustic coupling, the error in measuring relative CO changes, which is all that is needed to evaluate the technique for estimating proportional CO, is reported to be 2% (6, 11). One source of this error is changes to coronary blood flow (4-5% of the CO (52)), which is not captured by the flow probe.) A tygon catheter was placed in the left atrial appendage for reference LAP (Norton, Akron, OH). The chest was evacuated and closed in layers, with the cable and catheter tunneled subcutaneously and exteriorized between the scapulae. The dog was then allowed 10-14 days for recovery during which the catheter was irrigated daily with a heparinized saline solution.

On the second experimental day, additional transient instrumentation was achieved as follows. General anesthesia was induced and maintained as previously described. Mechanical ventilation was instituted at a rate of 12 breaths/min and a tidal volume of 20-25 ml/kg (in three of the dogs). A micromanometer-tipped catheter was inserted into a jugular vein and positioned under fluoroscopic guidance in the main pulmonary artery for the PAP waveform (Millar Instruments, Houston, TX). Another micromanometer-tipped catheter was similarly inserted and positioned for the RVP waveform (in four of the dogs). A third micromanometer-tipped catheter was placed in the descending thoracic aorta via femoral artery access in conjunction with fluoroscopic guidance for an ABP waveform (in three of the dogs). A catheter was inserted into a cephalic vein for drug and isotonic fluid administration, and surface electrodes were positioned for two frontal ECG leads. All of the analog transducer outputs were interfaced to a personal computer through an A/D conversion system (DataQ Instruments, Akron, OH). The cardiovascular measurements were

then recorded in each dog at a sampling rate of 500-1000 Hz over the course of 100-230 minutes during a subset of the following common hemodynamic interventions: infusions of dobutamine, isoproterenol, esmolol, phenylephrine, nitroglycerin, and volume as well as hemorrhage. Various infusion rates were employed followed by recovery periods.

4.3.2 Data analysis

The technique was applied off-line to 6-min non-overlapping segments of the PAP waveforms resampled to 90 Hz so as to estimate proportional CO and absolute LAP trends for each dog. (When the 6-min segment included a step PAP change due to bolus drug infusion, the technique was applied to the longest steady interval of the waveform within the segment.) The corresponding absolute reference CO and LAP trends were established by averaging the aortic flow probe and LAP catheter measurements over the identical time segments. To compare an estimated proportional CO trend with the absolute reference CO trend, the former trend was first scaled to have the same mean value as the latter trend in each dog. The estimated, calibrated CO and absolute LAP trends were then evaluated against their corresponding reference trends through 1) classic regression analysis to comprehensively illustrate the estimated values versus the reference values and provide the correlation coefficient (ρ) between these values; 2) Bland-Altman analysis (19) (which has become the standard for comparing two clinical measurement methods) to comprehensively illustrate the estimation errors versus the highly accurate reference values (rather than the average of the estimated and

reference values) and indicate the bias μ and precision σ of the estimation errors; and 3) the root-mean-square of the estimation errors (RMSE = $\sqrt{(\mu^2+\sigma^2)}$) to succinctly indicate the overall error size. Both absolute and relative estimation errors were assessed, with relative CO estimation errors in units of percent and absolute LAP estimation errors in units of mmHg emphasized for congruence with previous, related studies (e.g., (37)). (Note that the CO RMSE here, when expressed in percent, is equivalent to the CO root-mean-squared-normalized-error (RMSNE) that we have reported in previous studies (90, 106, 141).) In addition, the changes in the estimated, calibrated CO and absolute LAP trends with respect to their mean values in each dog were evaluated against the corresponding changes in the reference trends for some of the hemodynamic interventions through Bland-Altman analysis.

For comparison, three competing intra-beat analysis techniques were also applied to the measured PAP waveforms. The first technique was the classic end-diastolic PAP estimate of LAP. The second technique, which is illustrated in Fig. 4.1, involved fitting a single exponential and constant term to each diastolic interval (approximated as the downstroke from peak systolic pressure to end-diastolic pressure) of the PAP waveform so as to estimate τ and LAP, and then computing proportional CO by subtracting LAP from the time average of PAP and dividing this difference by τ. The third technique involved 1) fitting multiple complex exponentials and a constant term to each diastolic interval of the PAP waveform (via a numerical search) to account for confounding wave reflections and inertial effects in addition to τ and LAP; 2) extrapolating the exponentials to low pressure and fitting a single exponential to the

extrapolated values so as to determine τ; and 3) likewise computing proportional CO with the estimated LAP and τ. These single and multiple exponential fitting techniques may have neither been tested nor proposed before. However, the two techniques do represent adaptations to a technique previously proposed by Engelberg et al. in which τ is estimated by directly fitting a single exponential to each diastolic interval of the PAP waveform minus the LAP waveform (45).

To make a fair comparison, the beat-to-beat τ and LAP estimated by the intra-beat analysis techniques were averaged over the same 6-min time segments analyzed by the LTIA technique so as to compute analogous proportional CO and absolute LAP trends. The LAP trends estimated by the classic end-diastolic PAP technique were then comprehensively evaluated as described for the LTIA technique, whereas the proportional CO and absolute LAP trends estimated by the two new exponential fitting techniques were assessed only through the RMSE for the sake of brevity.

4.4 Results

Fig. 4.3 illustrates sample segments of the PAP waveform as well as the measured aortic flow (CO) and LAP waveforms from one of the dogs during baseline, phenylephrine, and hemorrhage interventions. Relative to baseline, CO decreased and LAP increased during phenylephrine due to enhanced cardiac afterload, while CO and LAP both decreased during hemorrhage due to diminished venous return. As exemplified in Fig. 4.3, pure exponential diastolic decays were generally not apparent in the measured PAP waveforms throughout the experiments.

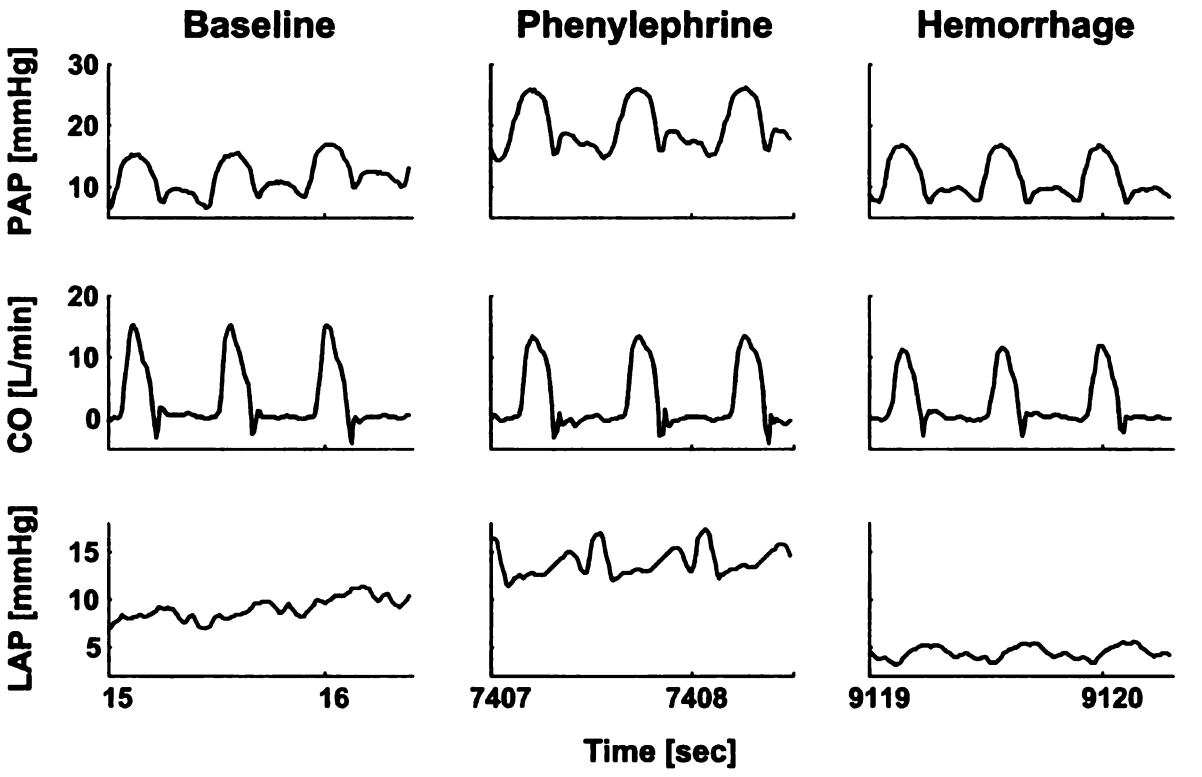

Figure 4.3 Sample segments of the PAP waveform and the measured aortic flow (CO) and LAP waveform from dog 5 during baseline, phenylephrine, and hemorrhage conditions. Note that pure exponential diastolic decays are not apparent in the PAP waveform segments.

Table 4.1 and Figs. 4.4-4.6 show the results of applying the new LTIA technique as well as the classic end-diastolic PAP technique to the measured PAP waveforms. In particular, Table 4.1 lists the hemodynamic range and calibrated CO and absolute LAP RMSEs for each dog. Fig. 4.4 illustrates regression plots of the calibrated CO and absolute LAP estimates for each dog, while Fig. 4.5 shows Bland-Altman plots of these estimates pooled over all five dogs. Fig. 4.6 illustrates Bland-Altman plots of the changes in the calibrated CO and absolute LAP estimates (with respect to their mean values in each dog) for the dobutamine, esmolol, phenylephrine, and nitroglycerin interventions pooled over all five dogs. (Note that similar plots for the

other employed interventions included significantly fewer data points and therefore did not provide as interesting of an assessment.)

Table 4.1 Summary of hemodynamic range and results of the LTIA technique as well as the classic end-diastolic pulmonary artery pressure (PAP) technique for each dog.

Dog	CO Range [L/min]	LAP Range [mmHg]	Mean PAP Range [mmHg]	Mean ABP Range [mmHg]	HR Range [bpm]	CO RMSE [%] ([L/min])	LAP RMSE [mmHg] ([%])	LAP via EDPAP RMSE [mmHg] ([%])
1	0.9–2.4	6.6–16.4	17.4–26.1	N/A	101–139	5.6 (0.09)	1.5 (12.2)	2.0 (23.8)
2	2.2–3.8	5.0–18.3	12.7–32.9	N/A	131–168	21.6 (0.58)	1.7 (15.4)	7.5 (83.7)
3	2.0–6.5	8.2–31.5	15.1–36.3	75–170	115–155	18.7 (0.40)	2.4 (18.2)	7.3 (80.1)
4	3.1–6.0	4.5–11.2	10.2–15.6	67–95	129–148	13.0 (0.53)	0.9 (13.7)	2.0 (34.6)
5	1.9–7.4	5.1–29.7	11.3–30.9	58–165	117–164	13.5 (0.50)	2.2 (27.3)	3.2 (48.3)
TOTAL	**0.9–7.4**	**4.5–31.5**	**10.2–36.3**	**58–170**	**101–168**	**15.2 (0.47)**	**1.7 (18.3)**	**4.7 (56.0)**

ABP is arterial blood pressure; HR, heart rate; EDPAP, end-diastolic PAP, and RMSE, root-mean-squared-error.

CO ranged from about 75% to 200% of its baseline value on average in each dog, whereas LAP generally ranged from about 4.5 to 17 mmHg in the dogs and briefly reached higher values up to 31.5 mmHg. Mean PAP varied by 15 mmHg on average in each dog, while mean ABP changed over a much larger range of up to 106 mmHg in one dog. HR varied over a range of about 70 bpm over all the dogs but did not reach values below 100 bpm.

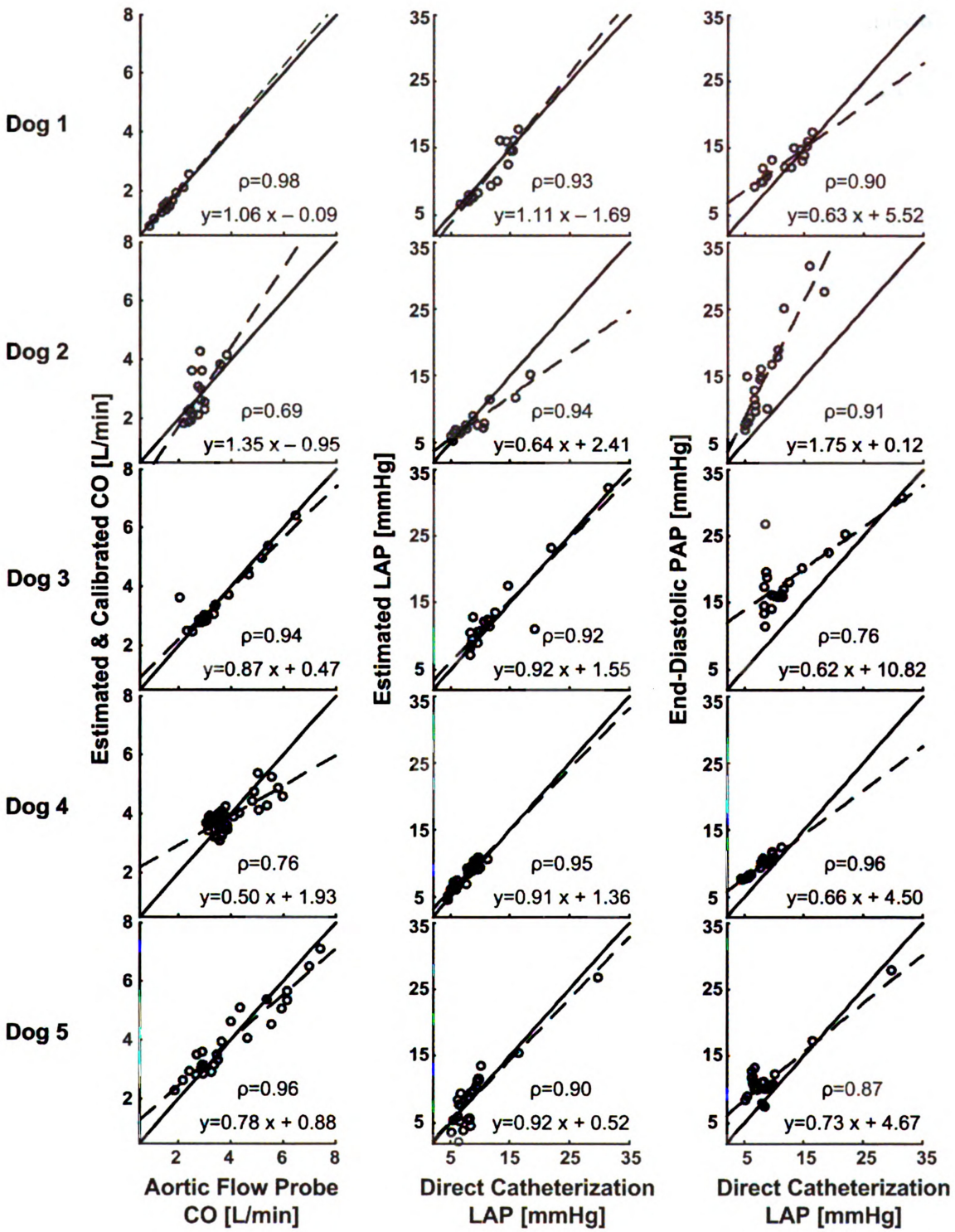

Figure 4.4 Results of the LTIA technique and the classic end-diastolic PAP technique in terms of regression plots of the calibrated CO and absolute LAP estimates versus their corresponding reference aortic flow probe CO and LAP catheter values for each dog. ρ is the correlation coefficient between the estimated and reference values.

The correlation coefficient ρ between the estimated and reference CO values was 0.87±0.06 (mean±SE) over all the dogs and ranged from 0.69 to 0.98 for each dog, while the calibrated CO RMSE was 15.2% (0.47 L/min) over all the dogs and ranged from 5.6% (0.09 L/min) to 21.6% (0.58 L/min) for each dog. Amongst the three large calibrated CO error outliers (> 40%; see Fig. 4.5), two were obtained between interventions (recovery period) from dog 2 and the other was obtained during the phenylephrine intervention in dog 3. If these outliers were ignored, the overall calibrated CO RMSE would reduce to 11.8%. The calibrated CO RMSE was almost entirely due to precision error merely as a result of the manner in which the proportional CO estimates were calibrated. The calibrated CO errors showed a mild, negative correlation with the reference CO values ($\rho = -0.26$), with the calibrated CO estimates being systematically underestimated at high reference CO values (> 4.5 L/min). This underestimation occurred only when HR and SV were both high (results not shown). However, the absolute value of the calibrated CO errors was virtually uncorrelated with the reference CO values ($\rho = -0.07$). The errors in the changes in the calibrated CO estimates appeared roughly of the same magnitude for the four illustrated interventions (if the single large positive outlier in the phenylephrine intervention were ignored).

The correlation coefficient ρ between the LAP values estimated by the new technique and the reference LAP values was 0.93±0.01 over all the dogs and ranged from 0.90 to 0.95 for each dog, while the LAP RMSE was 1.7 mmHg (18.3%) over all the dogs and ranged from 0.9 mmHg (12.2%) to 2.4 mmHg (27.3%) for each dog.

The overall RMSE of the estimated LAP, which was un-calibrated, had essentially no bias error component. The LAP errors and their absolute values were likewise only modestly related to the reference LAP values (ρ = -0.22 and 0.31), with no obvious systematic overestimation or underestimation over any reference LAP range. Similarly, the errors in the changes in the LAP estimates appeared approximately of the same magnitude for the four illustrated interventions (if the single large negative outlier in the phenylephrine intervention were ignored).

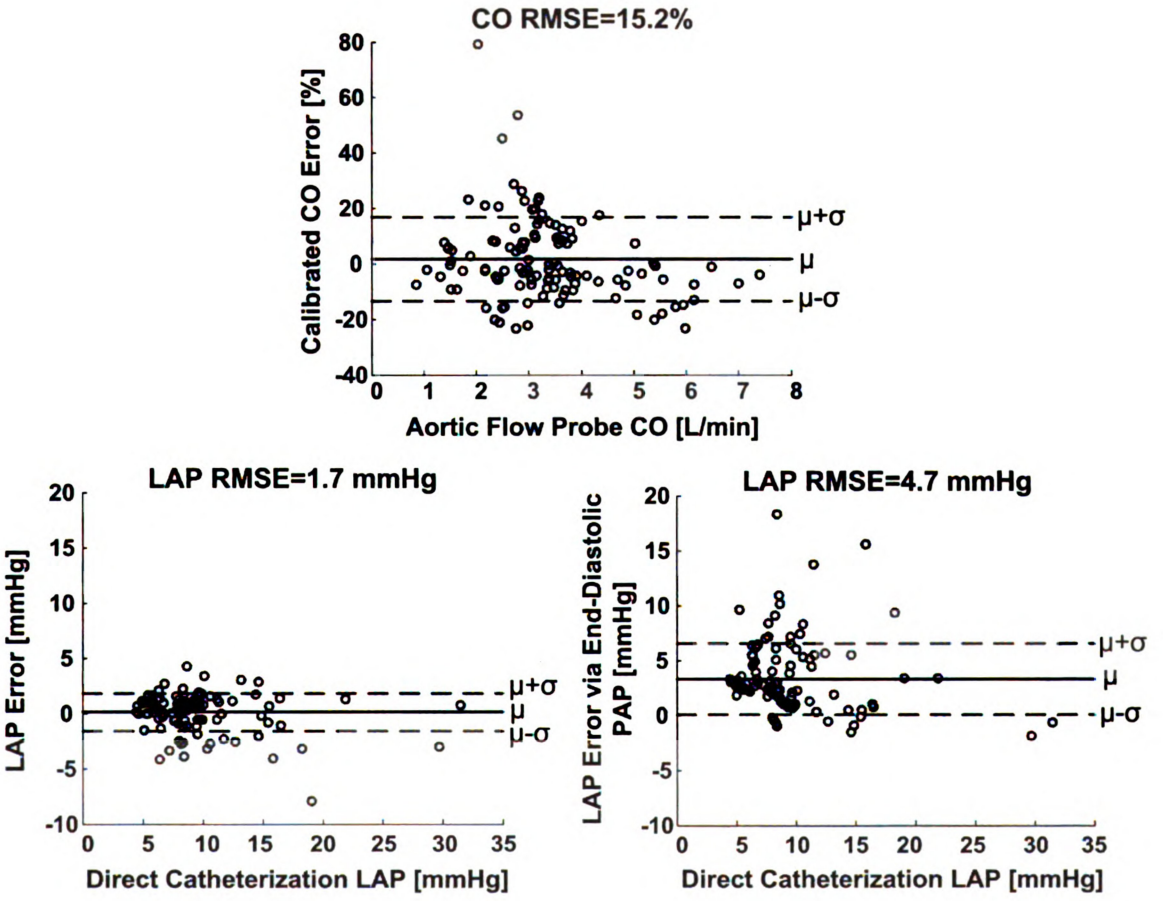

Figure 4.5 Results of the LTIA technique and the classic end-diastolic PAP technique in terms of Bland-Altman plots of the calibrated CO and absolute LAP errors versus the reference aortic flow probe CO and LAP catheter values pooled over all five dogs. μ is the bias error; σ, the precision error; and RMSE the root-mean-squared-error (i.e., $\sqrt{(\mu^2+\sigma^2)}$).

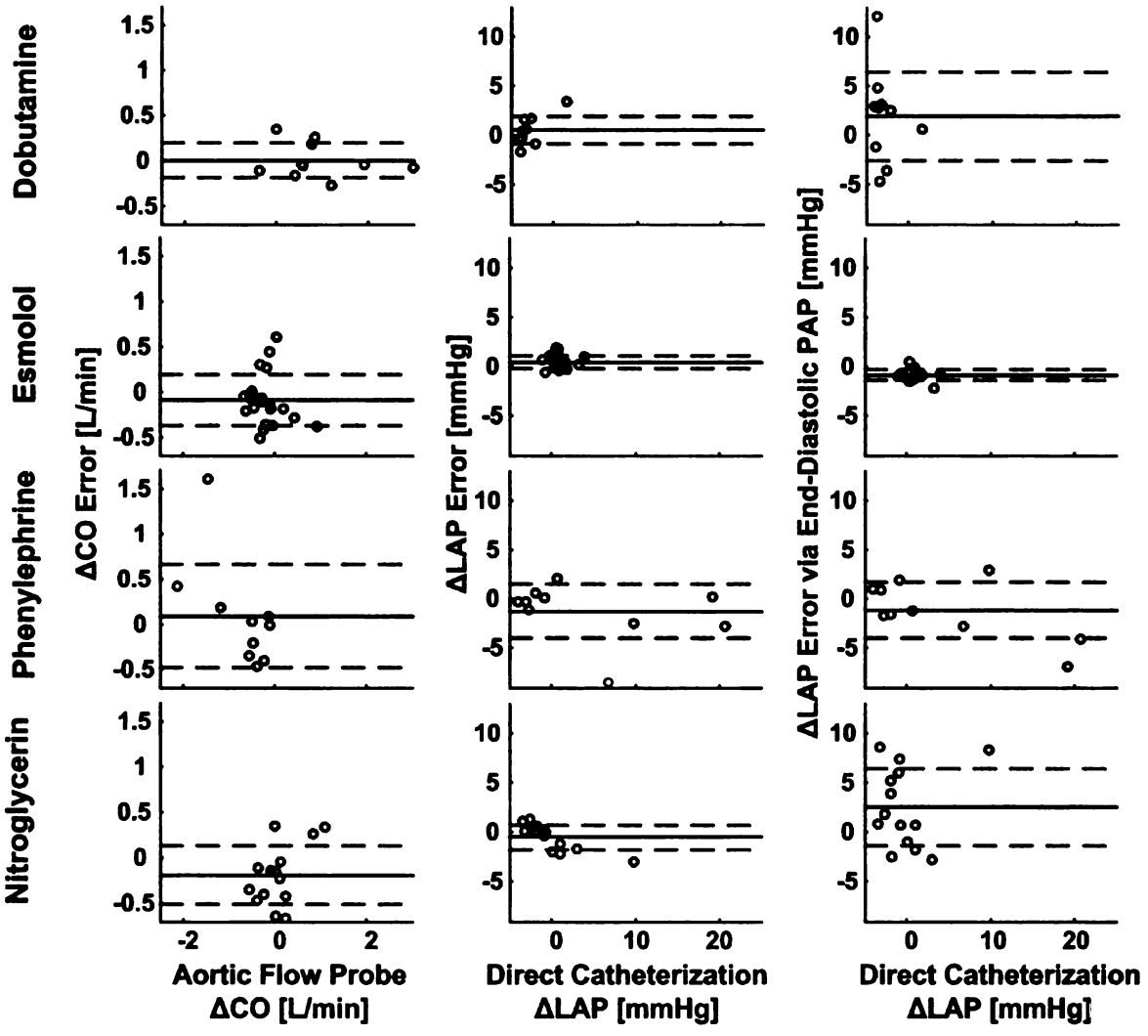

Figure 4.6 Results of the LTIA technique and the classic end-diastolic PAP technique in terms of Bland-Altman plots of the changes in the calibrated CO and absolute LAP estimates (with respect to their mean values in each dog) versus the corresponding changes in their reference values for the dobutamine, esmolol, phenylephrine, and nitroglycerin interventions pooled over all five dogs.

The correlation coefficient ρ between the LAP values estimated by the classic end-diastolic PAP technique and the reference LAP values was 0.88±0.03 over all the dogs and ranged from 0.76 to 0.96 for each dog, while the overall LAP RMSE was 4.7 mmHg (56.0%) over all the dogs and ranged from 2.0 mmHg (23.8%) to 7.5 mmHg (83.7%) for each dog. This overall LAP RMSE was due to a bias error of 3.3

mmHg and a precision error of 3.5 mmHg. The LAP errors and their absolute values were also hardly correlated to the reference LAP values (ρ = -0.12 and -0.04). Finally, the errors in the changes in these LAP estimates were about the same as the changes in the LAP values estimated by the new technique for the esmolol and phenyleprhine interventions but much larger for the dobutamine and nitroglycerin interventions.

As further comparison, the overall calibrated CO and absolute LAP RMSEs were 20.2% (0.58 L/min) and 4.5 mmHg (53.7%) for the single exponential fitting technique and 18.0% (0.58 L/min) and 2.8 mmHg (31.9%) for the multiple exponential fitting technique employing three complex exponentials (detailed results not shown in the table or figures). Note that we were unable to reduce the latter RMSEs by using more exponentials or performing the fit over the actual diastolic intervals as established with the simultaneously measured RVP waveforms.

4.5 Discussion

Previously, we developed and validated a LTIA technique to monitor relative changes in CO by analyzing a peripheral ABP waveform (57, 90, 105, 106, 122), which effectively fits a Windkessel model of the systemic arterial tree to the ABP variations occurring over time scales greater than a cardiac cycle wherein confounding wave reflections cease to be a major factor (see Chapter 3). Here, we extended the LTIA technique to the PAP waveform so as to monitor LAP in addition to CO. The extension amounts to the inclusion of a constant term in the analysis to account for average LAP (see Figs. 4.1, Fig. 4.2, and Eq. 4.1). That is, an additive constant term is estimated along with the impulse response so as to optimally fit the

PAP waveform segment. Note that this extension is actually necessary for reliable fitting, as LAP is a major determinant of PAP due to the small PAR in pulmonary circulation. Then, the Windkessel time constant of the pulmonary arterial tree (τ = PAR·PAC) is similarly determined from the tail end of the impulse response, and average proportional CO is computed by subtracting average LAP from the time average of PAP and dividing this difference by τ (thereby implicitly assuming a linear PAR and constant PAC). In principle, this extension may likewise be applied to an ABP waveform so as to monitor venous pressure as well as proportional CO. However, venous pressure is usually much smaller than ABP due to the large TPR and may therefore be neglected or difficult to estimate. While the technique in Chapter 3 may permit continuous and minimally invasive or even non-invasive monitoring of relative changes in CO, the more invasive technique here should be preferred when LAP monitoring is also indicated. Furthermore, the proportional CO estimates may be conveniently calibrated to absolute CO with a thermodilution measurement.

The extended LTIA technique is unique to the few aforementioned, related PAP waveform analysis techniques in that 1) it analyzes PAP variations over time scales greater than a cardiac cycle in which wave reflections and inertial effects are attenuated; and 2) it jointly estimates both CO and LAP.

The results of this study indicate that the new technique agreed well with reference aortic flow probe CO and LAP catheter measurements from five dogs during commonly employed hemodynamics interventions (see Table 4.1 and Figs. 4.4-4.6). That is, the overall calibrated CO and absolute LAP RMSEs of the

technique were 15.2% and 1.7 mmHg, respectively. These RMSEs compare favorably to the 17% error reported for clinical thermodilution measurements (66, 138) and the 1-2 mmHg error found in valid PCWP measurements (61, 81). (Note that larger PCWP errors may be expected in clinical practice, as PCWP measurements are often made incorrectly as discussed in Chapter 1.) The calibrated CO RMSE here is also similar to that obtained with our original LTIA technique in six swine (106). The study results also show that the new technique was in better agreement with the reference methods than three competing intra-beat analysis techniques, namely the classic end-diastolic PAP technique and the two exponential fitting techniques proposed herein. In particular, the LTIA technique estimated LAP with hardly any bias, unlike the end-diastolic PAP technique, and less than half the precision error of this classic technique. The multiple exponential fitting technique did provide lower calibrated CO and absolute LAP RMSEs than the other two intra-beat analysis techniques by accounting for the wave reflections and inertial effects with complex exponentials. However, these RMSEs, especially pertaining to LAP, were still larger than those of the LTIA technique, which captured information embedded in the beat-to-beat PAP variations.

We were not able to achieve a HR lower than 100 bpm in our canine experiments with the employed interventions. Thus, our study is limited in that it does not address the validity of the technique over this lower HR range. However, theoretically, our technique should perform more accurately as HR decreases, because the Windkessel model of Fig. 4.1 becomes a more valid representation of the PAP waveform with decreasing frequency. For example, if the HR were sufficiently low, a pure

exponential decay may be visually apparent towards the end of the longer diastolic interval (i.e., the fast confounding dynamics will have had enough time to vanish).

An assumption of the new technique is that PAC is constant within a subject over a monitoring period. This assumption is specifically needed to be able to estimate relative changes in CO. (The estimation of absolute LAP is not at all reliant on this assumption.) However, some previous studies suggest that PAC may, on the contrary, decrease with increasing pressure (79, 123, 129, 132). If PAC varied widely within each of our dogs, then the estimation of proportional CO would be unreliable, with the CO error showing substantial, positive correlation to mean PAP. However, proportional CO was well estimated as we have discussed, and the CO error was only modestly correlated with mean PAP ($\rho = 0.20$). Thus, PAC may have been at least approximately constant over a mean PAP range of up to 21 mmHg within a dog here. The relative constancy of PAC that we observed here contradicts the aforesaid studies but is consistent with other studies (76, 134). The contrasting results could be due to differences in the technique for estimating PAC and the experimental conditions (e.g., mean PAP range). While larger changes in mean PAP within a given subject could certainly elicit more significant changes in PAC, in such circumstances, the proportional CO estimates could always be recalibrated to the new PAC value with a readily available thermodilution measurement. Note that the small changes in PAC that likely occurred in our experiments do represent a source of the CO error of the technique.

Another potential source of the errors is that the technique did not account for all

of the major mechanisms of respiratory variability in the PAP waveform. That is, the external reference pressure of the pulmonary circulation is in actuality intrathoracic pressure rather than the zero pressure indicated by the Windkessel model of Fig. 4.1. Thus, the technique cannot account for respiratory-induced changes in intrathoracic pressure that are directly transmitted to PAP. However, note that the technique is able to account for the respiratory-induced variations in intrathoracic pressure that modulate venous return to the right heart and the respiratory sinus arrhythmia phenomenon (131) through the cardiac contractions signal.

On the other hand, nonlinearity of PAR due to recruitment and distension phenomena probably did not represent a major source of the errors here. Since the dogs were in the supine posture and average LAP was never less than 4.5 mmHg (see Table 4.1), all of the collapsible pulmonary capillaries may have been open (i.e., zone 3 pulmonary blood flow) throughout the study (52, 114). Thus, PAR may have always been operating in its linear regime. However, note that even when some of the pulmonary capillaries are collapsed (i.e., zone 1 pulmonary blood flow) and some are exhibiting the vascular waterfall effect (i.e., zone 2 pulmonary blood flow) (52, 114), the linear PAR assumption may not be grossly violated as PAR is specifically assumed to be linear only over each 6-min segment of analysis (i.e., piece-wise linear).

Like intra-beat analysis techniques, the LTIA technique can be implemented in real time on a home personal computer. Its main disadvantage with respect to the conventional techniques is that it cannot identify very rapid CO and LAP changes. However, we believe that the temporal resolution afforded by our LTIA technique (on the order of a few minutes) will be sufficient to successfully guide many therapeutic

interventions as well as detect most deleterious hemodynamic events, with rapid catastrophic events (e.g., ventricular arrhythmias) being easily detected with standard modalities (e.g., surface ECG leads). Another disadvantage of the LTIA technique is that PAP waveform artifact observed in the critical care setting may be a more significant problem. That is, the new technique requires a contiguous segment of relatively artifact-free PAP waveform on order of minutes for analysis, while the conventional techniques require just a beat. However, note that PAP waveform artifact was a non-factor in the present controlled laboratory experiments.

It should be noted that the continuous thermodilution method, which was introduced sometime after the standard bolus thermodilution method and is gaining popularity (116, 158-160), is also able to provide continuous CO monitoring with a temporal resolution on order of minutes through use of the pulmonary artery catheter (with a thermal filament proximal to the catheter end for automatic heating of blood). However, the signal-to-noise ratio of this method is small compared to standard thermodilution (43), which may render the continuous method to be less accurate (164). Moreover, in contrast to the PAP waveform analysis technique here, the continuous thermodilution method is unable to provide continuous LAP monitoring.

There are several other methods currently available for measuring CO (43). Ultrasound methods are perhaps the most notable, as they are non-invasive and also provide measurements of left atrial dimensions. However, a major disadvantage of these methods is that they require a well-trained operator to make each measurement. Another important disadvantage is that left atrial dimensions, unlike LAP, do not permit tracking of pulmonary edema and differentiation between cardiac dysfunction

and hypovolemia (118). Our technique would therefore be preferred when the invasiveness of the pulmonary artery catheter is permissible.

Upon future successful testing in humans over a wide hemodynamic range (including a lower HR range than that studied herein), our new LTIA technique on PAP waveform may ultimately be employed for continuous CO and LAP monitoring in critically ill patients instrumented with pulmonary artery catheters. Such continuous monitoring capabilities would offer considerable advantages over the standard, operator-required thermodilution and PCWP methods. These advantages include: 1) circumventing the infrequent use, misuse, and added risk of the standard methods (see Chapter 1); 2) saving precious time in the busy critical care environment (43); 3) obtaining an early indication of deleterious hemodynamic events so as to provide enough time for successful therapy; 4) being able to assess in real-time the effects of fluid and drug interventions for optimal therapy (e.g., targeting diuretic dosage in heart failure patients to minimize LAP without significantly compromising CO); and 5) permitting remote critical care monitoring (127). We therefore believe that the new technique, in conjunction with specific pulmonary artery catheter management protocols as called for in recent editorials (26, 80, 118, 126), may ultimately allow the pulmonary artery catheter to reveal a clinical benefit in a wide variety of critically ill patient populations.

CHAPTER 5

CARDIAC OUTPUT AND LEFT ATRIAL PRESSURE MONITORING BY RIGHT VENTRICULAR PRESSURE WAVEFORM ANALYSIS

5.1 Introduction

In addition to hemodynamic monitoring systems based on invasive catheters or non-invasive commercial devices as discussed in Chapter 3 and Chapter 4, ambulatory hemodynamic monitoring systems are also being developed recently. For example, a fully implantable device for chronic measurement of the RVP waveform, with a configuration similar to a standard single lead pacemaker, has been developed and verified (92, 111, 112), which allows long-term hemodynamic monitoring of congestive heart failure patients and potentially permit optimal day-to-day care, reduce hospital admissions, and eliminate repeated central catheterizations. Although the RVP waveform provides relevant clinical information, it is well appreciated that CO and LAP are more useful for assessing cardiac function and managing volume status (see Chapter 1). If these two cardinal hemodynamic variables could be mathematically derived from the RVP waveform, then the potential of long-term hemodynamic monitoring may be fully realized with an established device.

A few techniques have been proposed to estimate CO or LAP by analysis of the RVP waveform. Bennett and co-workers were recently able to show that end-diastolic PAP may be well estimated from the value of RVP at the time of its maximal

positive derivative ("ePAD") over each beat (28, 110, 124) and may therefore be used to approximate LAP. However, as demonstrated by other investigators as well as our study (see Chapter 4), end-diastolic PAP is not as accurate as PCWP when estimating LAP (59, 61, 95, 156). More recently, Bennett and co-workers have also proposed a technique to track relative CO change through a portion of the systolic RVP area of each beat (70, 71). However, to our knowledge, techniques for deriving CO or LAP from the RVP waveform are otherwise lacking.

In this chapter, we developed a new technique based on impulse response estimation to monitor CO and LAP by RVP waveform analysis (155). In contrast to the two aforesaid intra-beat analysis techniques, our technique seeks to estimate LAP itself rather than the end-diastolic PAP, and jointly estimates relative CO change. Further, similar to the LTIA techniques introduced in Chapter 3 and Chapter 4, the new technique examines the slow beat-to-beat variations in the RVP waveform wherein simple Windkessel behavior dominates (108) in an attempt to augment the estimation accuracy of the average over the beats, while the previous techniques only analyze the fast changes in the waveform within an individual beat in which complicating wave reflections and inertial effects are known to be prominent. To demonstrate feasibility, we evaluated the new LTIA technique and compared it to the previously proposed intra-beat analysis techniques based on four chronic canine experiments in which the RVP waveform and accurate reference measurements were simultaneously recorded during common hemodynamic interventions.

5.2 The Technique

We previously developed and verified LTIA techniques to estimate the relative change in CO from a peripheral ABP waveform (90, 106) (see Chapter 3) and CO and LAP from a PAP waveform (156) (see Chapter 4). This new technique for estimating relative CO change and LAP from the RVP waveform directly arises from the latter technique by exploiting the fact that RVP is nearly equal to PAP during the ejection intervals provided that pulmonic valve stenosis is absent.

The technique is illustrated in Fig. 5.1. This technique is applied to continuous segments (on order of minutes) of a digitized RVP waveform in six steps.

First, the ejection intervals of the RVP waveform segment (y(t)) are identified so as to establish an "incomplete" PAP waveform segment that is specifically missing diastolic intervals. In particular, the ejection interval for each beat is detected from the time of the maximal positive derivative (t_{MPD}) according to the previous ePAD technique to the time of peak systolic pressure (P_{sys}) plus a conservative time interval comprising three samples (see Discussion).

Second, a cardiac contractions signal (x(t)) is constructed from the ejection intervals of y(t) based on the impulse ejection model (46, 96). That is, x(t) is formed as an impulse train in which each impulse is located at t_{MPD} of each beat and has an area equal to the ensuing PP approximated as P_{sys} minus $y(t_{MPD})$ (i.e., ePAD). Note that x(t) represents a "complete" cardiac contractions signal, as the sample values between the impulses are defined to be zero.

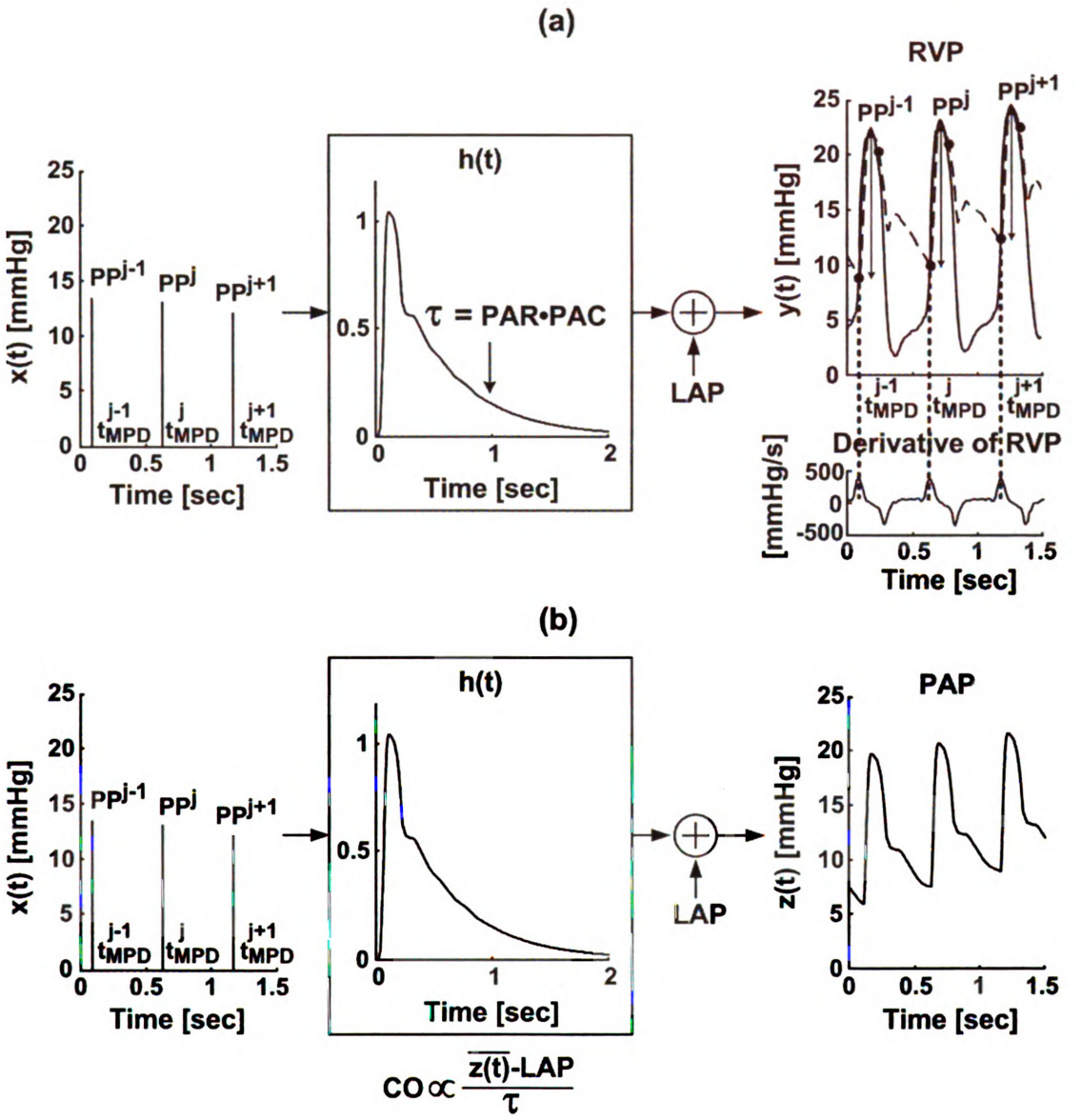

Figure 5.1 LTIA technique for monitoring relative CO change, LAP, and mean PAP from a right ventricular pressure (RVP) waveform. **(a)** First, the ejection intervals of the RVP waveform (y(t)) are identified to produce an incomplete PAP waveform. Specifically, as indicated with dots, the ejection interval of each beat (j) is detected from the time of the maximal positive derivative (t_{MPD}) to shortly after the peak systolic pressure. Second, a complete cardiac contractions signal (x(t)) is constructed from y(t). Third, average LAP and the impulse response (h(t)) are estimated so as to optimally couple x(t) to y(t) only over the ejection intervals. Fourth, the Windkessel time constant (τ) is determined by fitting an exponential to the tail end of h(t) once the faster wave reflections and inertial effects vanish. **(b)** Fifth, a complete PAP waveform (z(t)) is constructed from average LAP, h(t), and x(t) to establish mean PAP. Finally, proportional CO is computed similar to invoking Ohm's law.

Third, an impulse response (h(t)) and an additive constant term are estimated so as to optimally couple the complete "input" x(t) to the "output" y(t) over its ejection intervals only. The estimated constant term represents average LAP, while the estimated h(t) represents the PAP-LAP response to a single, solitary cardiac contraction. Since a large number of parameters cannot be reliably estimated from the limited information in the ejection intervals of y(t), h(t) is represented with a low order model capable of yielding a physiologic appearing single contraction PAP-LAP response. More specifically, h(t) and average LAP are estimated with the following third-order OE structure with constant term:

$$y(t) = \underbrace{\left(b_1 e^{-t/a_1} + b_2 e^{-t/a_2}\cos(a_3 t) + b_3 e^{-t/a_2}\sin(a_3 t)\right)u(t)}_{h(t)} \otimes x(t) + LAP + n(t) \quad (5.1)$$

where $\{a_k, b_k, k = 1\text{-}3\}$, which define h(t), are unknown parameters, u(t) is the unit step function, $\otimes$ is the convolution operation, and n(t) is the unmeasured residual error (89). (Note that Eq. 5.1 is an equivalent form of Eq. 2.9 in time-domain with model orders m = n = 3.) The seven unknown parameters including the constant term LAP are estimated from x(t) and y(t) via minimization of the mean square of n(t) over the ejection intervals. This optimization is achieved by numerically searching over a range of the nonlinear parameters $\{a_k, k = 1\text{-}3\}$ and estimating the linear parameters, $\{b_k, k = 1\text{-}3\}$ and LAP, for each $\{a_k, k = 1\text{-}3\}$ in closed-form with the linear least squares solution (89). If an average LAP greater than mean PAP (approximated as $P_{sys}/3+2ePAD/3$) or a negative h(t) results, then the parameter values providing the

next lowest mean square of n(t) over the ejection intervals are selected as the estimates.

Fourth, a single exponential is fitted to the tail end of the h(t) once the faster wave reflections and inertial effects have vanished in order to determine the Windkessel time constant (τ) of the pulmonary arterial tree, which is equal to the product of its total resistance (PAR) and compliance (PAC) (see Eq. 3.3). In principle, reliable determination of τ as well as average LAP is achieved by virtue of faithfully coupling x(t) to the inter-beat variations in the ejection intervals of y(t).

Fifth, the complete PAP waveform segment including its diastolic intervals (z(t)) is constructed by adding average LAP to the convolution between x(t) and h(t). In theory, z(t) will lack the high frequency detail in the actual PAP waveform segment due to the lower order of h(t) but will permit reliable estimation of mean PAP.

Finally, assuming constant PAC, proportional CO is determined by applying Ohm's law as follows:

$$CO \propto \frac{\overline{z(t)} - LAP}{\tau} \tag{5.2}$$

Note that, while PAC has been shown to be relatively constant over a wide hemodynamic range (see (156) and references therein), the relative CO change here is not expected to be valid over the course of years and an indefinite hemodynamic range. To account for significant PAC changes, the proportional CO could be calibrated every so often (e.g., annually and whenever mean PAP changes greatly) with absolute CO measurements (via, e.g., ultrasound).

5.3 Methods

5.3.1 Experimental procedures

Experiments were performed in four normal adult dogs (10-26 kg). The experiments were approved by the MSU All-University Committee on Animal Use and Care and are described in detail in Chapter 4. Briefly, each dog was studied on two separate days under general anesthesia. On the first day, chronic instrumentation was installed in the dog. An ultrasonic flow probe was placed around the ascending aorta for reference CO, and a fluid-filled catheter was inserted through the left atrial appendage for reference LAP. The dog was then allowed up to two weeks to recover from the open-chest surgery. On the second day, additional instrumentation was first placed in the dog. Micromanometer-tipped catheters were positioned for the RVP waveform for analysis, the reference PAP waveform, as well as the aortic pressure waveform (in two of the dogs). Surface electrodes were placed for standard ECGs. The measurements were then recorded at a sampling rate of 500-1000 Hz over the course of 100-230 minutes during a baseline period and three or four of the following interventions: various infusions of dobutamine, esmolol, phenylephrine, nitroglycerin, and volume. Generally speaking, dobutamine and volume increased CO and mean PAP with the latter intervention also enhancing LAP; esmolol and phenylephrine increased LAP and mean PAP; and nitroglycerin did not elicit a significant hemodynamic response. Overall, CO ranged from 0.9 to 6.5 L/min; LAP, from 4.5 to 31.5 mmHg; and mean PAP, from 10.2 to 36.3 mmHg. See Table 4.1 (dogs 1-4) for additional intervention details.

5.3.2 Data analysis

The technique was applied to 6-min disjoint segments of the RVP waveforms resampled to 90 Hz to estimate proportional CO and absolute LAP trends for each dog. Each estimated proportional CO trend was then normalized by its mean value so as to produce a trend in relative CO change expressed in percent (e.g., values of 60% and 140% would respectively indicate a 40% decrease and increase in CO from the mean value). (Note that the mean value was utilized here, because normalization with any single estimated proportional CO value would bias the subsequent evaluation results.) The estimated relative CO change and LAP trends were then evaluated against their corresponding reference trends derived from the aortic flow probe CO and LAP catheter measurements through 1) classic regression plots to illustrate the estimated values versus the reference values; 2) Bland-Altman plots to show the estimation errors versus the accurate reference values and indicate the constant bias μ and precision σ of the estimation errors; 3) the root-mean-square of the estimation errors (RMSE = $\sqrt{(\mu^2+\sigma^2)}$) to quantitatively indicate the overall error size; and 4) the slope and (y-)intercept of the Bland-Altman plots, including the statistical significance of the linear model, to quantitatively reveal any relationship between the estimation errors and reference values. Percent errors in the estimated relative CO change and absolute errors in the estimated LAP were specifically assessed to allow comparisons with many related studies in the past including our own (e.g., the calculation of the former errors here is identical to the computation of the percent errors in the estimated and once calibrated CO in Chapter 3 and Chapter 4). In

addition, the trends in mean PAP also estimated by the technique were evaluated against their corresponding reference trends derived from the measured PAP waveforms through the quantitative metrics only for the sake of brevity.

The previous, related techniques were also applied to the RVP waveforms. These techniques included the ePAD technique and the aforementioned technique for estimating proportional CO through a portion of the systolic RVP area of each beat ("PCCO") as well as a technique for estimating mean PAP from intra-beat RVP features and an ECG ("pmPAP"). These three intra-beat analysis techniques are described in detail elsewhere (28, 69-71, 107, 110, 124) and fully specified in Fig. 5.2. To have a fair comparison, the resulting estimates of proportional CO, LAP, and mean PAP for each beat were averaged over the same 6-min segments analyzed by the LTIA technique. The estimated trends were then likewise evaluated through the quantitative metrics.

5.4 Results

Table 5.1 lists the RMSEs of the relative CO change, absolute LAP, and mean PAP estimated by the LTIA technique for each dog. Table 5.2 shows the RMSEs, the slopes, and the intercepts of Bland-Altman plots of the relative CO change, LAP, and mean PAP estimated by the new technique as well as the previous intra-beat analysis techniques over all four dogs, while Fig. 5.3 illustrates regression and Bland-Altman plots of the relative CO change and LAP estimated by the LTIA technique pooled over all the dogs.

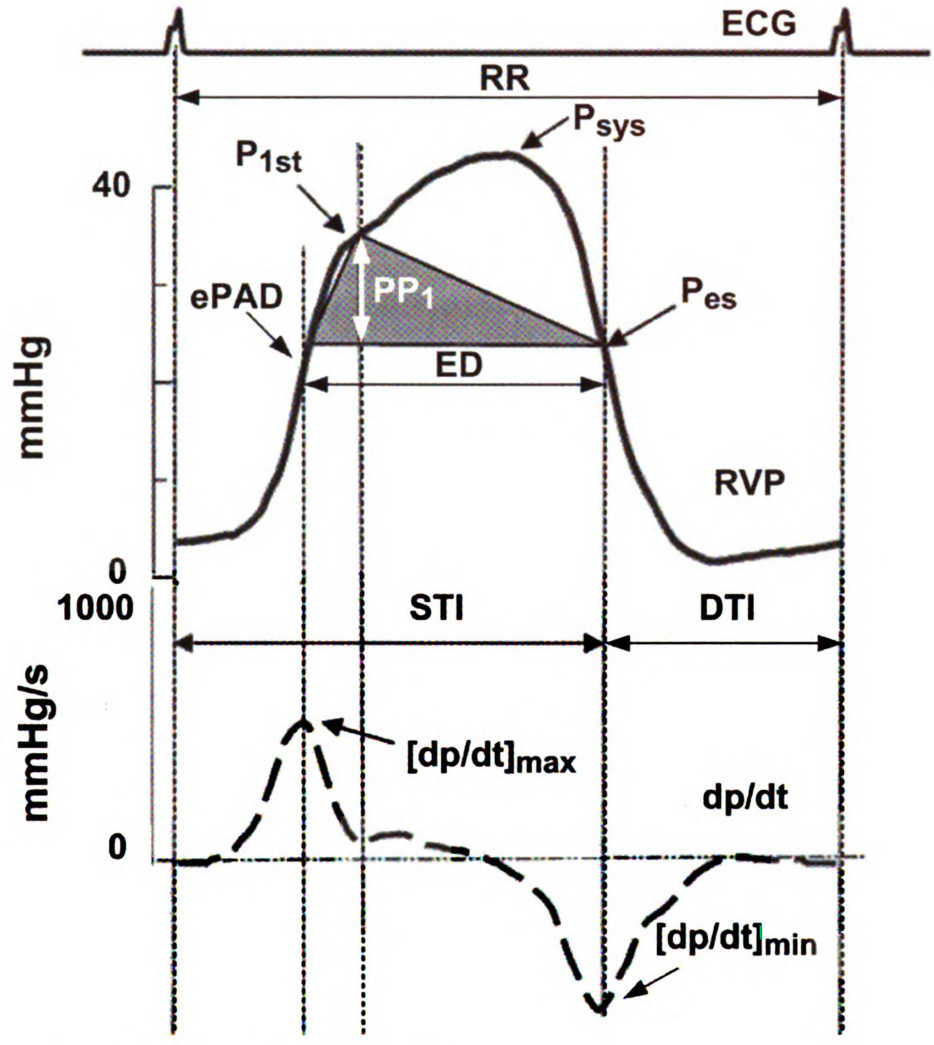

PCCO: CO $\propto$ $PP_1 \cdot ED/RR$

ePAD: LAP = ePAD

pmPAP: Mean PAP = (DTI/RR)·ePAD + (STI/RR)·P_{sys}

Figure 5.2 The three previous techniques for monitoring relative CO change, LAP, and mean PAP by intra-beat analysis of the RVP waveform (28, 69-71, 107, 110, 124). P_{1st} indicates the value of RVP at the time of the first zero crossing (from positive to negative) of the third derivative of the waveform following the time of its maximal positive first derivative. (Adapted from (71).)

Visually, the relative CO change and LAP estimates from the new technique showed a good overall correspondence with their accurate reference values.

Quantitatively, the RMSE of the relative CO change estimates was 16.0% over all the dogs (ranging from 11.7% to 24.2% for each dog), whereas the RMSE of the LAP estimates was 2.0 mmHg over all the dogs (spanning from 1.7 mmHg to 2.5 mmHg for each dog).

Table 5.1 RMSEs of the hemodynamic variables estimated by the LTIA technique of Fig. 5.1 for each dog.

Dog	CO RMSE [%]	LAP RMSE [mmHg]	Mean PAP RMSE [mmHg]
1	16.4	2.3	2.6
2	24.2	1.9	4.6
3	12.2	2.5	3.5
4	11.7	1.7	1.9
TOTAL	**16.0**	**2.0**	**3.1**

Table 5.2 RMSEs, slopes, and intercepts of Bland-Altman plots of the hemodynamic variables estimated by the LTIA technique of Fig. 5.1 and the previous techniques of Fig. 5.2 over all the dogs.

Technique	CO			LAP			Mean PAP		
	RMSE [%]	Slope [unitless]	Intercept [%]	RMSE [mmHg]	Slope [unitless]	Intercept [mmHg]	RMSE [mmHg]	Slope [unitless]	Intercept [mmHg]
New	16.0	NS		2.0	-0.33	2.2	3.1	-0.23	5.0
PCCO	19.4	-0.29	30.1	–	–	–	–	–	–
ePAD	–	–	–	5.2	NS		–	–	–
pmPAP	–	–	–	–	–	–	3.7	-0.27	7.1

NS indicates that the linear model is not statistically significant (i.e., $p > 0.05$).

However, for unclear reasons, the LAP estimation errors did possess an inverse relationship with the reference LAP values (not quantitatively indicated in Fig. 5.3). These errors also have a small constant bias of -0.8 mmHg presumably due to a similar bias in the estimated end-diastolic PAP (results not shown). The RMSE of the mean PAP estimates from the new technique was 3.1 mmHg over all the dogs (with a

low of 1.9 mmHg and a high of 4.6 mmHg for each dog). The mean PAP estimates were also inversely related to their reference values, which likely stemmed from the similar relationship for the LAP estimates.

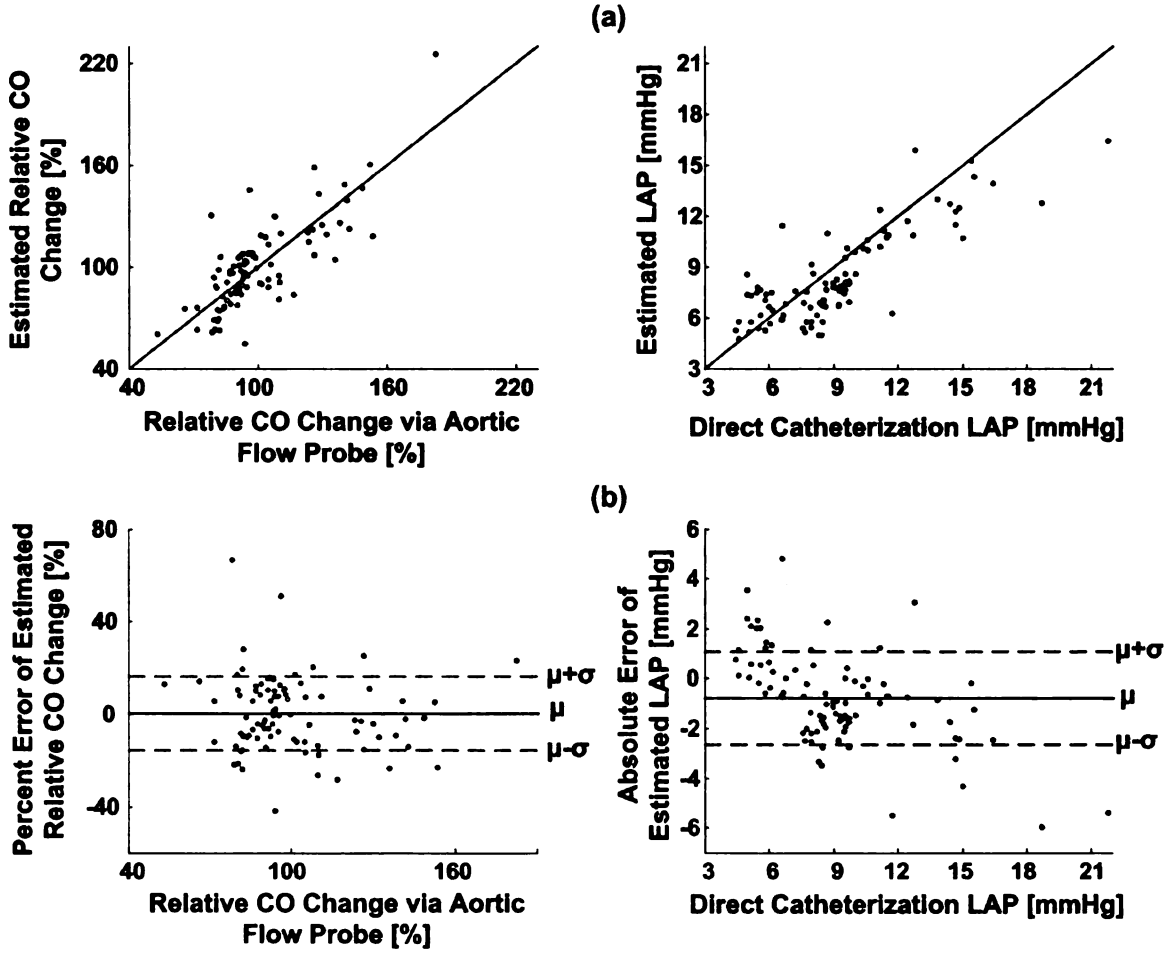

Figure 5.3 **(a)** Regression plots and **(b)** Bland-Altman plots of the relative CO change and LAP estimated by the new technique of Fig. 5.1 over all four dogs. μ and σ respectively indicate the constant bias and precision error.

For comparison, the corresponding overall RMSEs of the relative CO change, LAP, and mean PAP estimates from the previous intra-beat techniques were 21%, 160%, and 19% higher, respectively. Further, these relative CO change and mean PAP estimates have inverse relationships with their reference values. Note that the

above results exclude one RVP waveform segment (i.e., one data point) for which all techniques revealed gross estimation errors (see Discussion).

5.5 Discussion

We previously developed two impulse response based techniques to continuously monitor relative CO change from a minimally invasive or non-invasive peripheral ABP waveform (90, 106) and LAP in addition to absolute CO (after a single calibration) from the PAP waveform (156) (see Chapter 3 and Chapter 4). The major steps are to estimate an impulse response and, in the case of the latter technique, an additive constant term (representing LAP) that optimally couple(s) a cardiac contractions input to the BP waveform output and then determine the Windkessel time constant for computing proportional CO from the tail end of the impulse response once the faster wave reflections and inertial effects vanish. Here, we adapted these steps for application to the RVP waveform by invoking the fact that RVP is, in general, nearly equal to PAP during the ejection intervals. In particular, the ejection intervals of the RVP waveform are detected (see below), and then an impulse response and constant term are estimated that optimally couple the cardiac contractions input to effectively the ejection intervals of the PAP waveform output (see Fig. 5.1a). Significantly, the entire PAP waveform may be constructed thereafter to monitor mean PAP as well (see Fig. 5.1b). The impetus for the latest technique is to permit long-term monitoring of vital hemodynamic variables with an established implantable RVP measurement device. Such monitoring could also be achieved by way of passing the pressure sensor lead of the device from the right ventricle to the pulmonary artery

and then applying our PAP waveform analysis technique. However, lead instability and increased risk (e.g., arrhythmias) in the latter site render this alternative less practical (124).

We tested the new RVP waveform analysis technique against aortic flow probe CO and LAP and PAP catheter measurements from four dogs during common hemodynamic interventions. The estimated relative CO change, LAP, and mean PAP generally showed good agreement to the accurate reference measurements (see Table 5.1 and Fig. 5.3), with overall RMSEs of 16.0%, 2.0 mmHg, and 3.1 mmHg, respectively. For comparison, the corresponding RMSEs of the previous intra-beat analysis techniques (see Fig. 5.2) were all higher, especially for LAP (see Table 5.2). Thus, analysis of the subtle, inter-beat variations in the RVP waveform can indeed improve the estimation of average hemodynamic variables. (Of course, the trade-off of this type of analysis is that very rapid changes cannot be detected (see Discussion in Chapter 4).) For further comparison, the overall RMSEs of the relative CO change and LAP estimated from the same four dogs by our previous PAP waveform analysis technique were 15.6% and 1.6 mmHg (156). Thus, aside from one outlier (see below), the new technique was largely able to overcome the missing PAP information.

A key step of our technique is the identification of the ejection intervals of the RVP waveform. Specifically, reliable detection of the onset of each ejection interval (or, equivalently, pulmonary artery end-diastolic pressure) is considerably more important than the end of each ejection interval, as a faithful estimate of PP is most crucial (see, e.g., x(t) in Fig. 5.1a). The non-trivial detection of each ejection interval onset was accomplished here with the well-tested ePAD technique (28, 110, 124).

However, for one of the analyzed RVP waveform segments, this technique provided an estimate of pulmonary artery end-diastolic pressure that was much smaller than the reference LAP value. As a result, the new technique, the ePAD technique, and the PCCO and pmPAP techniques, which are also based on ePAD (see Fig. 5.2), all showed marked estimation errors for this segment. This single outlier was excluded to avoid misleading results. While the ePAD technique was otherwise able to provide satisfactory estimates of pulmonary artery end-diastolic pressure (but not LAP), future efforts to improve the detection are certainly warranted.

In summary, we have developed a new technique to monitor relative CO change and LAP by RVP waveform analysis and have demonstrated its feasibility based on four chronic canine experiments. With future successful testing, the technique may be employed for chronic hemodynamic monitoring of congestive heart failure patients with an implanted RVP measurement device. For example, after transferring the RVP waveform recorded from the established device to a personal computer using an external telemeter (112), the technique could be readily executed in near real-time on the personal computer. In addition, the technique may potentially be utilized for continuous hemodynamic monitoring of critically ill patients via a right ventricular catheterization rather than the more risky pulmonary artery catheterization.

CHAPTER 6

ROBUST PULSE WAVE VELOCITY ESTIMATION BY SYSTEM IDENTIFICATION

6.1 Introduction

Aortic stiffness has been shown to be an independent predictor of mortality in hypertensive patients. PWV is a marker of aortic stiffness and is convenient to measure compared to other indices of aortic stiffness (93). Moreover, PWV may permit continuous, non-invasive, and cuff-less monitoring of BP as they show strong, positive correlation (119). In the context of this dissertation, since AC is inversely related to arterial stiffness, PWV can be used to track the changes of AC $\left(AC \propto \frac{1}{PWV^2}\right)$ and hence eliminate the assumption of constant AC in the LTIA technique described in Chapter 3. Furthermore, the cuff-less BP estimated from PWV can be utilized for calibration in the LTIA technique based on PPG waveform (see Section 3.6).

PWV is conventionally determined through the foot-to-foot time delay between the onsets of upstroke of proximal and distal arterial waveforms (27, 48). Typically, the waveforms are obtained non-invasively using a handheld transducer that measures pressure via applanation tonometry from carotid and femoral artery. However, such measurements are particularly susceptible to motion artifact that may restrict the

value of the PWV marker of aortic stiffness. In the case of BP monitoring via PWV, BP variations induce relatively small changes in PWV (119). Thus, even seemingly small inaccuracies in PWV measurements can lead to large BP errors. Indeed, as exemplified in Fig. 6.1, plots of PWV versus BP often show a great deal of scatter about the line of best fit (97, 119). Such scatter obviously limits the utility of PWV in tracking BP changes.

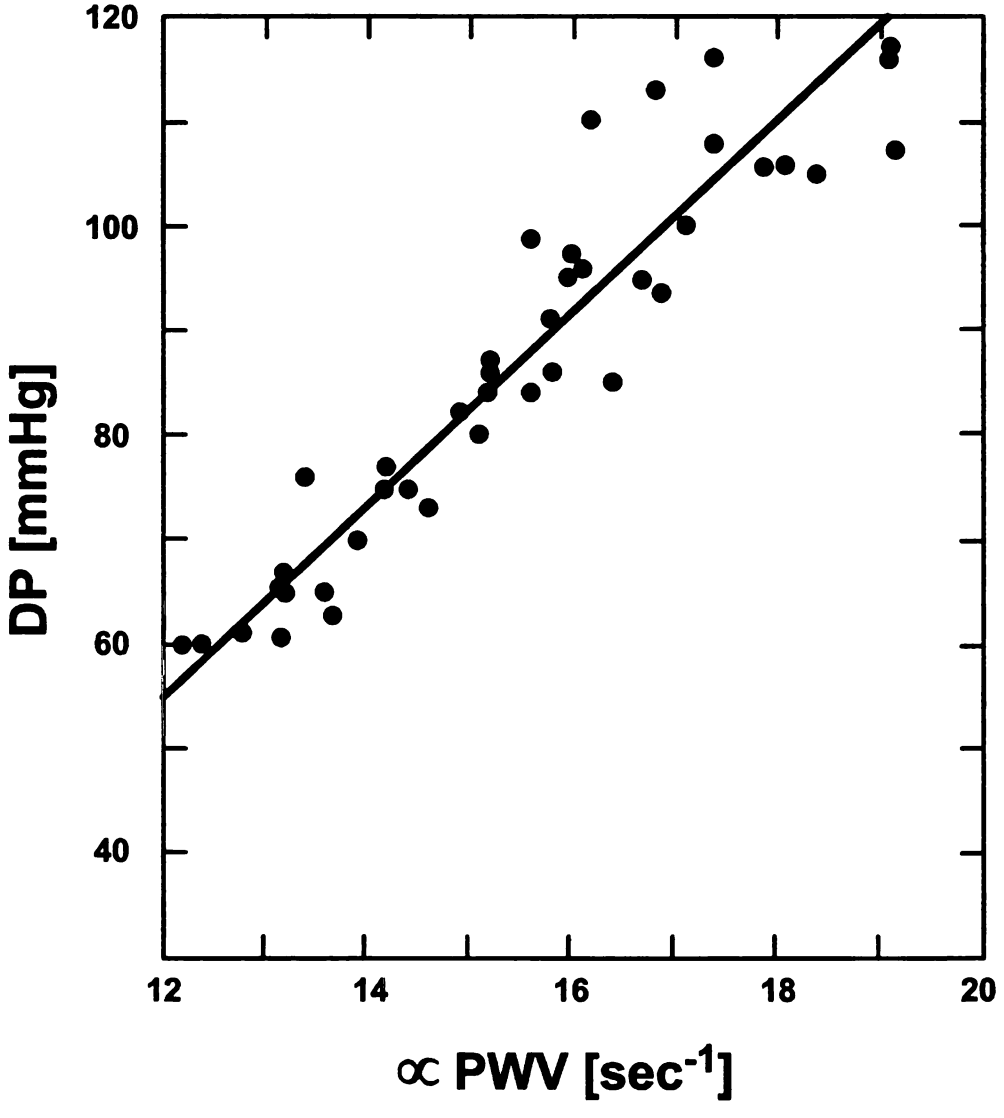

Figure 6.1 Typical plot of diastolic pressure (DP) versus proportional pulse wave velocity (PWV). (Adapted from (97).)

Previous investigators have sought to reduce the error in PWV measurements through signal processing. Sola et al. more accurately detected the foot of an arterial waveform via parametric modeling (135). Pruett et al. determined the time delay through measurement of multiple time delays taken from the early systolic portions (i.e., before return of the reflected wave) of two arterial pressure waveforms (119). This particular method is notable in that it seeks to extract the time delay from more than one pair of samples of the waveforms (i.e., additional waveform information). However, the drawback is that is may only be applicable to arterial pressure waveforms and not other, more readily available arterial waveforms such as those indicating pulsatile volume.

In this chapter, robust estimation of PWV was sought using the general approach of system identification through two types of modeling: physiologic-based (i.e., gray-box) model and black-box model.

In the first study, PWV is estimated based on the well-known tube model of arterial wave reflection (139, 151). First, the transfer function relating a measured central arterial pressure waveform to a peripheral arterial pressure waveform measured from the lower body is defined in terms of the parameters of the model, which include the time delay for wave travel between the two measurement sites. Then, all parameters are estimated by finding the transfer function that optimally couples the two waveforms. Finally, PWV is computed from the reciprocal of the time delay estimate. Thus, this arterial tube model-based technique effectively computes PWV from all pairs of samples of the waveforms after mathematically eliminating the reflected wave. The technique was applied to high fidelity canine

arterial pressure waveforms obtained over a wide pressure range before and after contamination with known amounts of noise.

In the second study, an arbitrary proximal arterial waveform is regarded as an input to a dynamic black-box system, while any distal arterial waveform is considered to be the resulting output. Then, the system, which optimally couples the input to output, is identified. Finally, the time delay of the identified system is used to calculate PWV. Similar to the first technique, PWV is effectively determined from all waveform information. The technique was applied to arterial waveforms collected from humans subjected to a LBNP protocol described in Chapter 3.

We quantitatively evaluated the resulting PWV estimates of both techniques in terms of their correspondence to arterial pressure, the principal acute determinant of aortic stiffness. For comparison, the conventional foot-to-foot detection techniques were likewise assessed.

6.2 The Techniques

6.2.1 Arterial tube model-based technique

The technique estimates PWV by tube model-based analysis of measured central and peripheral (lower body) arterial pressure waveforms ($p_c(t)$ and $p_p(t)$). The technique is shown in Fig. 6.2 and is implemented as follows.

First, the transfer function relating $p_c(t)$ to $p_p(t)$ is specified through a uniform tube terminated by a lumped parameter load (see Fig. 6.2a). More specifically, the tube represents the path for wave travel between the two measurement sites.

Consistent with Poiseuille's law, this tube is frictionless and therefore has constant characteristic impedance ($Z_c = \sqrt{(I/AC)}$, where I and AC are the arterial inertance and compliance) and allows waves to travel with constant delay time from one end of the tube to the other ($T_d = \sqrt{(I \cdot AC)}$).

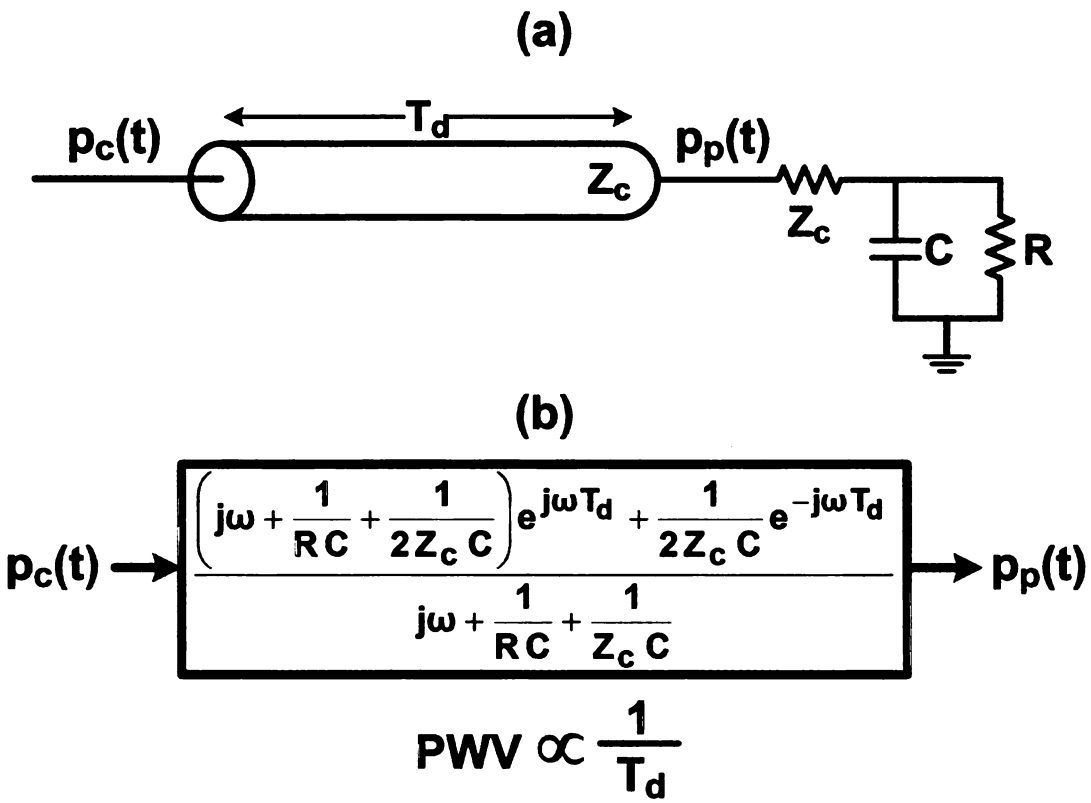

Figure 6.2 Technique for robust estimation of PWV from central and peripheral (lower limb) arterial pressure waveforms ($p_c(t)$ and $p_p(t)$) based on an arterial tube model.

The terminal load represents the arterial bed distal to the peripheral artery measurement site. This load is characterized by a three-element Windkessel accounting for peripheral resistance and compliance (R and C) while matching the tube impedance at infinite frequency. Waves traveling along the tube in the forward

(left-to-right) direction are reflected backwards at the terminal load in a frequency-dependent manner. By summing the forward and backward waves at each tube end (after appropriate time shifting to account for the wave travel time delay), the transfer function relating $p_c(t)$ to $p_p(t)$ is defined in terms of three unknown parameters, namely T_d, RC, and Z_cC (see Fig. 6.2b).

The three parameters are then estimated by finding the tube model-based transfer function, which when applied to $p_c(t)$, best fits $p_p(t)$ in the least squares sense. This nonlinear optimization is specifically achieved through a numerical search over a physiologic range of the parameters. Finally, proportional PWV is computed through the reciprocal of the estimated T_d. (Note that the proportionality constant, which may be determined by the physical distance between the proximal and distal waveform measurement sites, is irrelevant for both stiffness and BP monitoring.)

The conventional foot-to-foot detection technique is implemented by identifying each waveform foot through the maximal second derivative between the minimum (i.e., DP) and maximal first derivative of the beat. PWV is then computed from the average of the foot-to-foot time delay over the same data segment analyzed by the new technique.

6.2.2 Black-box system identification technique

Based on waveforms collected in this study, a differentiated ICG waveform, which is related to the central aortic flow rate, is regarded as the input (x(t)) to the black-box system. A peripheral ABP waveform is considered to be the corresponding

output (y(t)). Fig. 6.3 illustrates the technique implemented as follows.

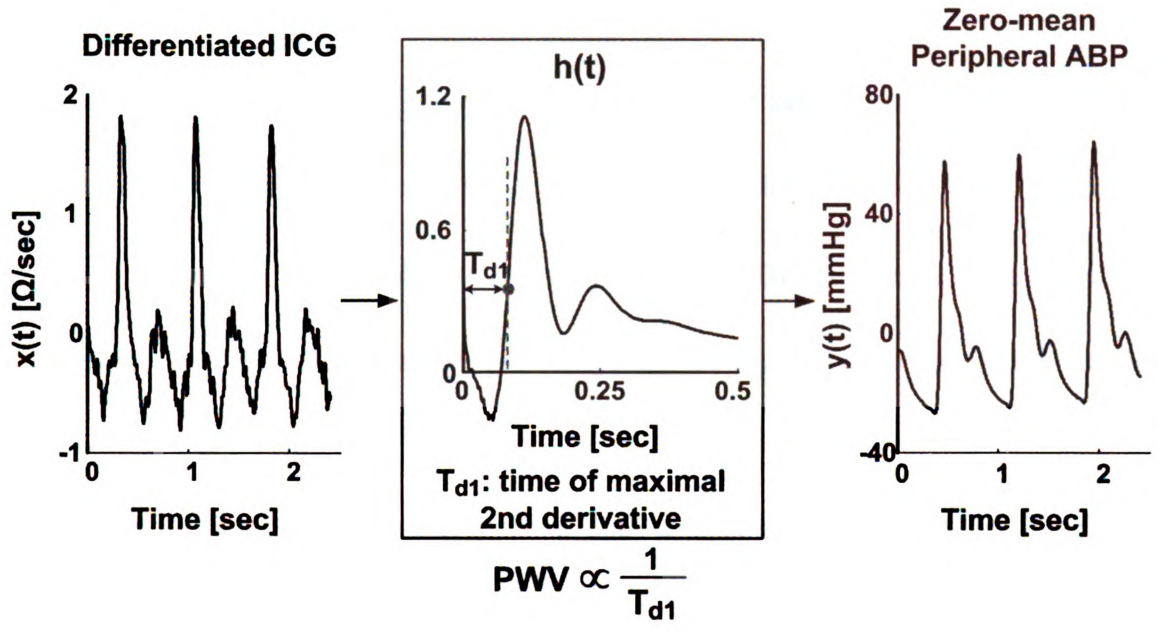

Figure 6.3 Black-box system identification technique for robust estimation of PWV from impedance cardiography (ICG) and peripheral ABP waveforms.

First, the system impulse response (h(t)) is identified, which when convolved with x(t), best fits y(t) in the least squares sense. More specifically, h(t) is estimated according to the following ARX equation:

$$y(t) = \sum_{k=1}^{m} a_k y(t-k) + \sum_{k=1}^{n} b_k x(t-k) + e(t) \qquad (6.1)$$

where e(t) is an unobserved residual error, $\{a_k, b_k\}$ are unknown parameters fully defining h(t), and m and n represent the model order (89). The term m is set to five, while n is set to the time delay estimated by the conventional foot-to-foot detection technique (i.e., T_{d2} (see below)). (Note that the results that follow were not very sensitive to the choice of m.) The parameters are estimated from x(t) and y(t) through

linear least squares minimization of e(t).

Next, the time delay of the impulse response h(t) (T_{d1}) is detected as the time at the maximum of the second derivative between the first zero-crossover with positive derivative and the peak value. The T_{d1} estimate may be viewed as the time delay between the entire differentiated ICG and peripheral ABP waveform segments after equalizing their shapes. Finally, the reciprocal of T_{d1} is taken to arrive at the proportional PWV estimate.

Fig. 6.4 illustrates the conventional foot-to-foot detection method for PWV estimation from the two waveforms.

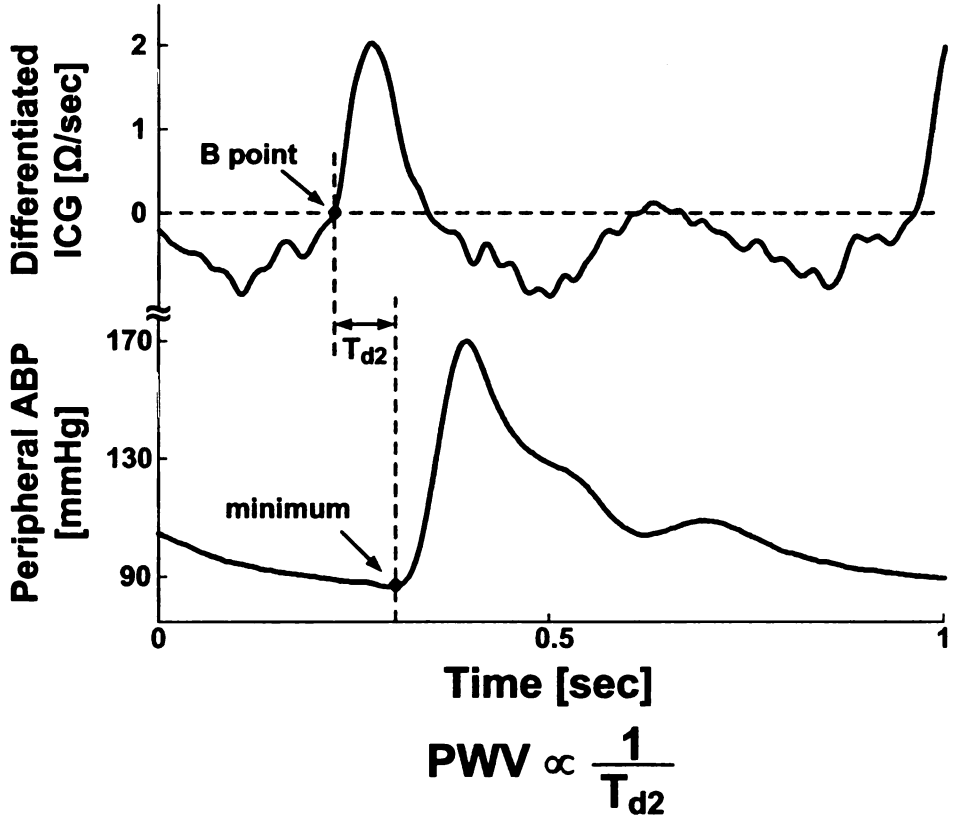

Figure 6.4 Conventional detection method for estimation of PWV from ICG and peripheral ABP waveforms.

First, the standard B points of the differentiated ICG waveform (41, 154) and the minima (i.e., DP) of the peripheral ABP waveform are detected to indicate their foots for each beat. (Note that other commonly used detection methods actually yielded inferior correspondence to BP here.) Then, the time delay between each B point and ensuing DP (T_{d2}) is determined. Finally, this time delay is averaged over the same data segment analyzed by the system identification technique, and the reciprocal is taken for the PWV estimate.

6.3 Methods

6.3.1 Arterial tube model-based technique

Experiments were performed in six healthy adult beagles (10-12 kg) under an experimental protocol approved by the MSU All-University Committee on Animal Use and Care. For each dog, general anesthesia was induced by an intravenous injection of propofol (2.2-6.6 mg/kg) and maintained with an inhaled mixture of oxygen and isoflurane (1.5-2.5%). A micromanometer-tipped catheter (Millar Instruments, Houston, TX) was placed in a femoral artery for the peripheral ABP waveform. A similar catheter was inserted in the opposite femoral artery or a carotid artery and positioned in the ascending aorta for the aortic pressure waveform. A catheter was also placed in a cephalic vein for drug and isotonic fluid administration, and electrodes were positioned for standard ECG measurements. In the fifth dog, a bipolar electrode catheter (EP Technologies, Boston Scientific, Sunnyvale, CA) was inserted into a jugular vein and advanced to the right atrium for high rate pacing with

an external pulse generator (Medtronic, Minneapolis, MN). In the sixth dog, a quadrapolar ablation catheter (EP Technologies) was inserted into a femoral vein and positioned to ablate the AV node and to then apply bipolar electrical stimulation to the His bundle as previously described (128) for low rate pacing with the external pulse generator. Placement of all central catheters was accomplished by guidance with a single-plane lateral projection fluoroscopic imaging unit (GE, Milwaukee, WI). The analog transducer outputs were interfaced to a personal computer via an A/D conversion system (DataQ Instruments, Akron, OH). The arterial pressure waveforms and ECG measurements were recorded at a sampling rate of 1000 Hz during a baseline period and following infusions of phenylephrine and nitroglycerin in the first dog; dobutamine and esmolol in the second dog; norepinephrine and xylazine in the third dog; saline and progressive hemorrhage in the fourth dog; verapamil and high rate pacing in the fifth dog; and vasopressin (prior to AV node ablation) and low rate pacing in the sixth dog. Several infusion and pacing rates were employed followed by recovery periods.

In absence of a noise model for handheld tonometer measurements, the model of Li et al. (84) of arterial pressure waveform artifact arising from patient movement was utilized. That is, different realizations of zero-mean brown noise between 1.5 and 18 Hz was added to each of the arterial pressure waveforms to attain signal-to-noise ratios (SNRs) of 10, 5, and 0 dB. The technique was then applied to estimate PWV from each 15 sec segment of the clean and noisy pairs of waveforms resampled at 500 Hz.

The conventional foot-to-foot detection technique was also applied to estimate

PWV from the same pairs of waveform segments. At the low SNRs, each beat could only be properly delineated from the R-wave of the ECG waveform. Thus, the conventional technique here assumes that the R-wave can be accurately detected despite the noise. (Note that identifying the waveform foot via DP or prefiltering the waveforms did not improve the results.)

Finally, the PWV estimates of each technique at each SNR were assessed in terms of their ability to predict DP and MAP of the noiseless waveforms. In particular, the arterial pressure was predicted by mapping the PWV estimates through the best-fit line between these estimates and the arterial pressure measurements for each animal. The RMSE of the predicted arterial pressure was then calculated over all the animals.

6.3.2 Black-box system identification technique

Previously collected physiologic data from humans subjected to a LBNP protocol to simulate hemorrhage and retransfusion were studied. The experimental procedures were approved by the Institutional Review Board of the Brooke Army Medical Center and are described in detail in Chapter 3.

Briefly, healthy human volunteers in the supine posture were secured in an LBNP chamber. Instruments were positioned for measurement of hemodynamic, neural, and metabolic variables. These measurements included a non-invasive ICG waveform for calculation of beat-to-beat stroke volume (HIC-2000 Bio-Electric Impedance Cardiograph, Bio-impedance Technology, Chapel Hill, NC) and a non-invasive finger ABP waveform (Finometer, Finapres Medical Systems, Amsterdam, The Netherlands). The physiologic variables were recorded during a 5-min baseline period and

following sequential exposure to -15, -30, -45, -60, -70, -80, -90, and -100 mmHg of LBNP for 5 minutes each. LBNP was terminated early, if signs and symptoms of hemodynamic decompensation appeared. Hemodynamic decompensation was identified in real time by the attending investigator as a precipitous fall in systolic pressure greater than 15 mmHg concurrent with the onset of pre-syncopal symptoms such as bradycardia, grey-out (loss of color vision), tunnel vision, sweating, nausea, or dizziness. After cessation of LBNP and a 5-min equilibration period, the physiologic variables were recorded for an additional 5-min recovery period.

Steady segments of the physiologic data during the baseline period, each available LBNP level, and the recovery period were analyzed. To obtain a reasonable evaluation of the ability of PWV estimates to track changes in the BP of a subject, physiologic data were included in this study only from those subjects whose DP varied by >20 mmHg. 15 subjects from a total of 66 available subjects met this inclusion criterion.

The conventional detection method was first employed to estimate PWV from the contemporaneous pairs of 15-sec segments of ICG and peripheral ABP waveforms. PWV was then estimated by applying the black-box system identification technique to the same pairs of waveform segments.

Each of the PWV estimates was evaluated in terms of its correspondence to DP through two quantitative metrics. First, the correlation coefficient (ρ) between the PWV estimates and corresponding DP measurements was calculated per subject. The ρ-values were then averaged over all the subjects. Second, DP was estimated by

mapping the PWV estimates from a subject through the line of best fit determined via the aforesaid correlation analysis for that subject. The RMSE of the estimated DP was then calculated over all the subjects.

6.4 Results

6.4.1 Arterial tube model-based technique

Arterial pressure varied widely over analyzed waveform segments. In particular, DP ranged from 30 to 142 mmHg, while MAP changed from 45 to 172 mmHg.

Fig. 6.5 illustrates sample segments of the arterial pressure waveforms before and after contamination with noise of varying amounts. Although the artifact in the waveforms particularly at the lowest SNR may appear excessive, this level of noise permitted assessment of the full capabilities and limitations of our arterial tube model-based technique. Fig. 6.6 shows the arterial pressure RMSEs of our technique and the conventional foot-to-foot detection technique versus SNR. Without noise, the DP and MAP RMSEs of our technique were 5.1 and 5.4 mmHg, respectively, whereas the corresponding RMSEs of the conventional technique were 6.2 and 6.0 mmHg. Thus, even when applied to high fidelity waveforms, our technique can yield some improvement in accuracy. But more significantly, as the SNR decreased, the DP and MAP RMSEs of our technique became progressively smaller relative to their conventional technique counterparts. In fact, our technique was roughly twice as accurate as the conventional technique at the lowest SNR and only mildly affected by artifact at higher SNRs.

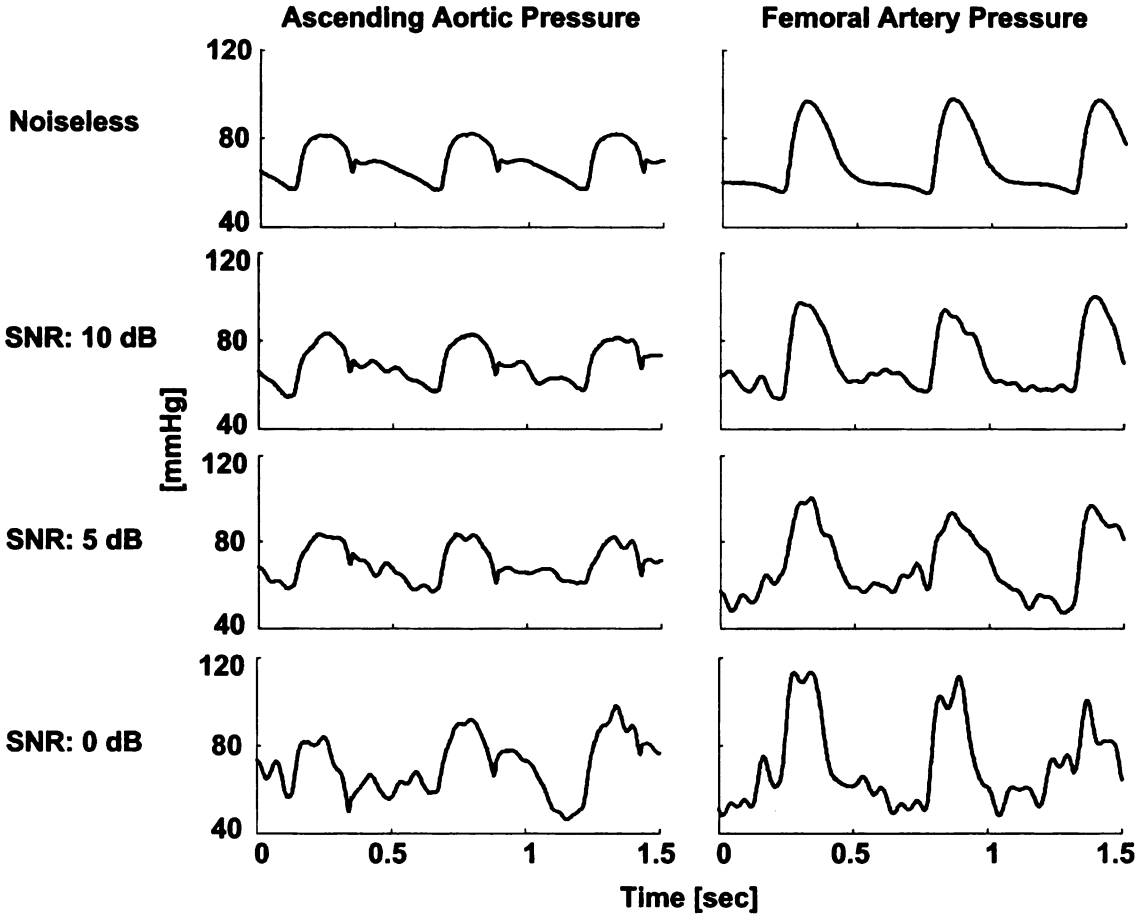

Figure 6.5 Sample segments of measured arterial pressure waveforms before and after contamination with noise of varying amounts. SNR is signal-to-noise ratio.

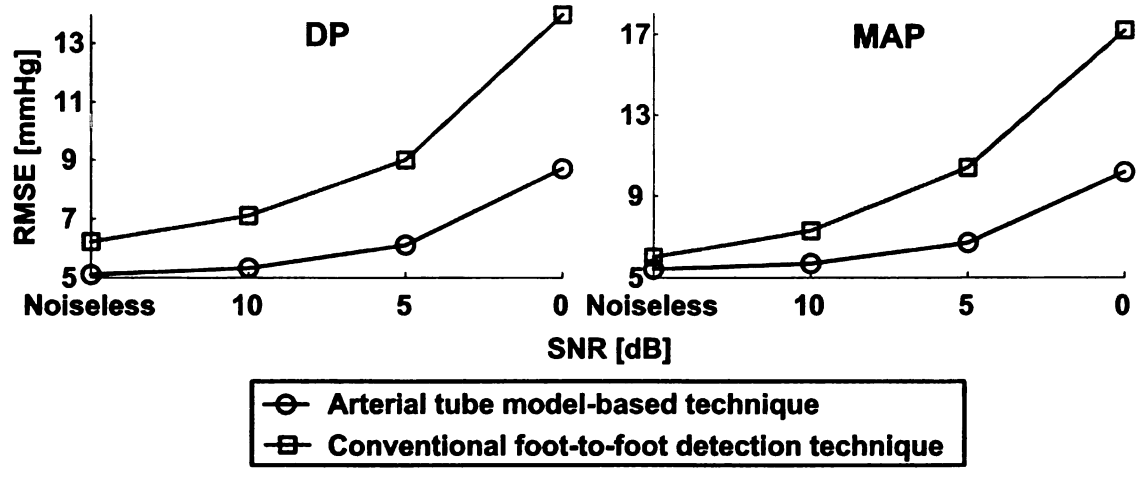

Figure 6.6 RMSE of the predicted DP and mean arterial pressure (MAP) as a function of SNR.

6.4.2 Black-box system identification technique

The average ρ-value (mean±SD) between the PWV estimates of the system identification technique and the DP measurements was 0.81±0.16, whereas the corresponding ρ-value for the conventional detection method was 0.59±0.37. Fig. 6.7 illustrates plots of the DP estimated via each of the PWV estimates versus reference DP over all of the subjects. The RMSE of the PWV estimates of the system identification technique was 4.5 mmHg. For comparison, the corresponding error of the conventional detection method was 6.5 mmHg.

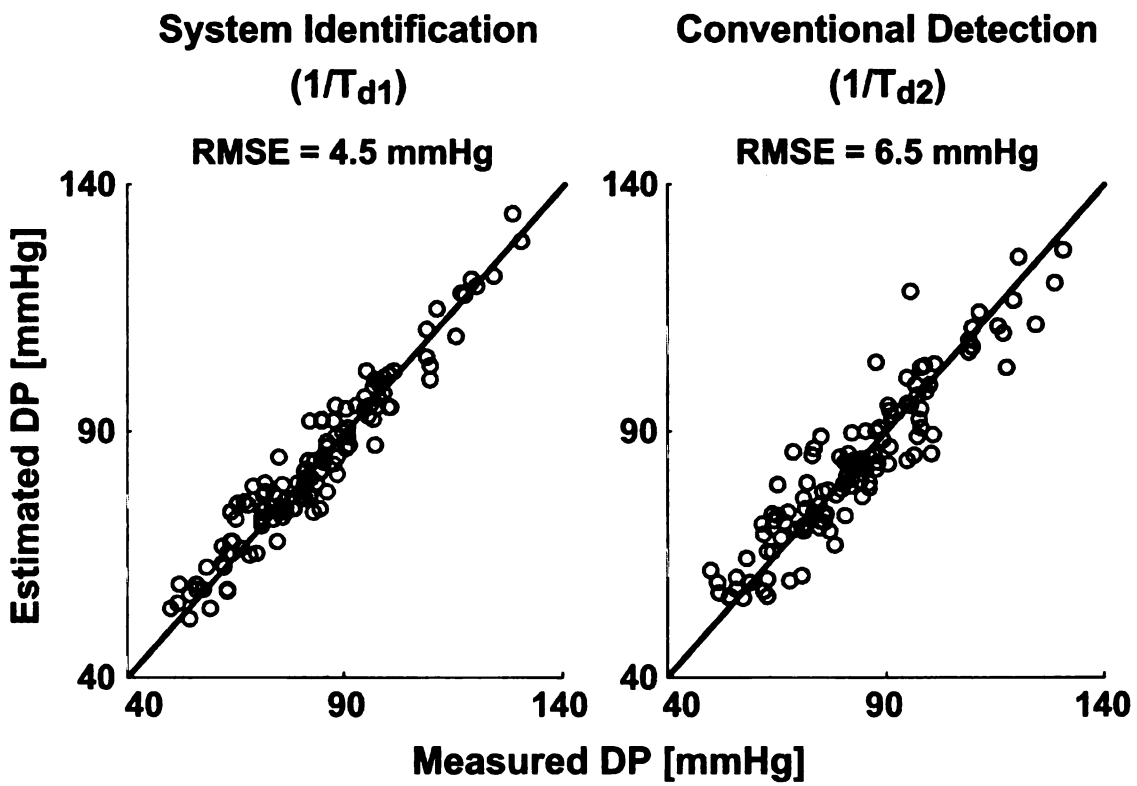

Figure 6.7 DP estimated via proportional PWV estimate versus measured DP over all the subjects.

6.5 Discussion

System identification techniques via both physiologic-based and black-box model were proposed to estimate PWV by analysis of proximal and distal arterial waveforms. Preliminary results showed that both techniques were superior to the conventional foot-to-foot detection technique in terms of predicting arterial pressure. However, in absence of reference aortic stiffness measurements and data recorded from clinical patients, to what extent the techniques can track the changes of arterial stiffness and improve the prediction of patient outcomes remains to be determined.

The arterial tube model-based technique is actually more general than what has been described above. Firstly, the technique as shown in Fig. 6.2 may be directly applied to any pair of proximal and distal arterial pressure waveforms to obtain the PWV between the two measurement sites. Secondly, this technique is also applicable to proximal and/or distal arterial waveforms that reflect flow rate after differencing (rather than summing) the forward and backward waves to define an appropriate transfer function in terms of the model parameters (see, e.g., (142)).

One disadvantage of the arterial tube model-based technique is that it can not be applied to arbitrary arterial waveforms other than pressure and flow rate waveforms. Another drawback of this technique as described above is that it is intended for application to simultaneously measured arterial waveforms. In practice, however, proximal and distal arterial waveform measurements for aortic stiffness monitoring are often made one at a time with a handheld transducer while an ECG waveform is being continuously recorded. One potential way for the technique to accommodate

this practice is as follows. First, the impulse response relating the ECG waveform to the proximal arterial waveform ($h_c(t)$) is estimated using standard black-box system identification (89). Then, the impulse response relating the ECG waveform to the distal arterial waveform ($h_p(t)$) is likewise estimated. Finally, the arterial tube model-based technique is applied to the impulse response estimates (i.e., for arterial pressure waveforms, $p_c(t) = h_c(t)$ and $p_p(t) = h_p(t)$ in Fig. 6.2).

The black-box system identification technique also improves PWV estimation accuracy. In addition, another advantage of the technique is that it is applicable to arbitrary pulsatile arterial waveforms including those indicating pressure, volume, flow rate, and even body weight measured with contact sensors (e.g., PPG, impedance pneumography without filtering out the "heart bump", and BCG) or non-contact systems (e.g., laser Doppler vibrometry, infrared thermal imaging). An ECG waveform may even be used as the proximal waveform. Therefore, the black-box system identification technique may be more applicable in practice than the arterial tube model-based technique. The disadvantage of the black-box system identification approach is that it may not be able to monitor beat-to-beat BP.

In conclusion, the two system identification techniques may be directly used to potentially improve the monitoring of arterial stiffness. Such capability could conceivably allow for meaningful aortic stiffness monitoring even by a less experienced operator of applanation tonometry or Doppler ultrasound. However, further evaluation should be performed on clinical data with reference arterial stiffness measurements to assess the ability of improving the prediction of patient

outcomes. For cuff-less BP monitoring, more challenges need to be resolved before it could be employed in practice. For example, a PWV-BP calibration curve must be constructed. Moreover, PWV estimated by regular methods (including the conventional foot-to-foot detection technique and the two system identification techniques) generally corresponds better to DP and MAP than SP. Thus, determining SP accurately is another large issue in cuff-less BP monitoring through PWV estimate. One potential improvement for the system identification techniques to resolve this problem is to set the system parameters to be pressure-dependent and obtain three PWV estimates corresponding to DP, MAP, and SP respectively.

CHAPTER 7

SUMMARY AND FUTURE WORK

7.1 Accomplishments and Summary

We have developed several techniques to monitor vital hemodynamic variables (i.e., CO, LAP, and PWV) by mathematical analysis of readily available physiologic measurements (e.g., BP, PPG, and ICG waveforms) in an attempt to achieve continuous and effective hemodynamic monitoring. The key step in all the techniques is to first identify an impulse response from available measurements and then estimate the hemodynamic variables based on the impulse response (i.e., impulse response estimation).

More specifically, a LTIA technique and two extensions of it were proposed to monitor CO and LAP (in the latter two techniques) by analyzing peripheral ABP, PAP, and RVP waveforms respectively. These three techniques were evaluated by experimental data from animal/human subjects and generally showed good agreements with reference measurements and superiorities to other competing techniques.

In addition, pilot studies were conducted to demonstrate the feasibility of extending the LTIA technique to the calibrated PPG waveform for CO monitoring and estimating PWV robustly to monitor arterial stiffness and cuff-less BP from proximal and distal arterial waveforms. Preliminary results derived from experimental

animal/human data have shown application potentiality of these techniques in clinical practices.

With further successful testing on clinical data over wide hemodynamic ranges, these impulse response estimation techniques may ultimately be applied in various clinical settings (e.g., ICU, combat casualty care, outpatient settings, and home healthcare) for continuous and effective hemodynamic monitoring.

7.2 Future Work

Although we have shown feasibilities of the impulse response estimation techniques for clinical application, further investigation and method improvement are required, which are summarized as follows.

1) Only pilot studies have been performed to assess the system identification techniques for estimating PWV and further the arterial stiffness and BP. The evaluations in the studies are based on the correspondence between the PWV estimates and BP measurements rather than the reference arterial stiffness. Therefore, the abilities of these techniques to accurately monitor the stiffness changes need to be validated with clinical data including reference arterial stiffness measurements. For cuff-less BP monitoring, as discussed in Chapter 6, challenges such as the PWV-BP calibration curve and the determination of SP via PWV estimate need to be settled as well. (Note that the PWV-BP calibration curve and separate estimation of DP, MAP, and SP via PWV are also necessary for the PPG calibration in the extended LTIA technique (see Section 3.6).) In terms of technical improvement, the arterial tube model-based technique can potentially be enhanced in several ways. For example, the

transfer function parameters may be estimated using total least squares to better account for measurement artifact in both arterial waveforms (17). As another example, a tapered tube and/or a higher order or even optimal order terminal load may be employed to more accurately represent the arterial system. However, these refinements come at the cost of substantially increased mathematical complexity. In the black-box system identification technique, while ARX linear least squares identification using implicit time delay estimation was applied (see Chapter 6), any of the available system identification techniques (e.g., OE equation, Laguerre basis functions, total least squares parameter estimation, explicit time delay estimation, nonlinear system representation) may be employed (18, 148).

2) The LTIA technique for peripheral ABP waveform analysis assumes constant AC through the period of analysis, which represents a source of error in CO estimates. To improve the technique, AC changes must be monitored as well. As mentioned in Chapter 6, PWV could be used for AC monitoring because AC is inversely related to PWV. In this case, to estimate PWV using system identification techniques, the peripheral ABP waveform is available as the distal arterial waveform. While a central pressure waveform is needed for the arterial tube model-based technique, the black-box system identification technique shows greater flexibility in practice and any pulsatile central arterial measurement can be used as the proximal arterial waveform. For example, the proximal waveform can be recorded by the BCG technique, which is a simple non-invasive measurement of the recoil of the body weight to cardiac ejection forces and only requires a weighing scale (64, 137). Of course, the PWV estimation by black-box system identification technique from BCG and peripheral

ABP waveform and the LTIA technique with AC compensation must be further investigated.

With aforesaid technique improvements and evaluations, a continuous and non-invasive system for CO and arterial stiffness monitoring, as illustrated in Fig. 7.1, may be employed in home healthcare, various inpatient and outpatient settings, and even combat casualty care with proper design of the scale for BCG measurement. Specifically, PWV is first estimated by the black-box system identification technique from BCG and peripheral ABP waveforms. Then, the LTIA technique accounting for the AC variations tracked by PWV estimate is applied to the peripheral ABP waveform for CO monitoring. Meanwhile, the PWV also provides a marker of the arterial stiffness.

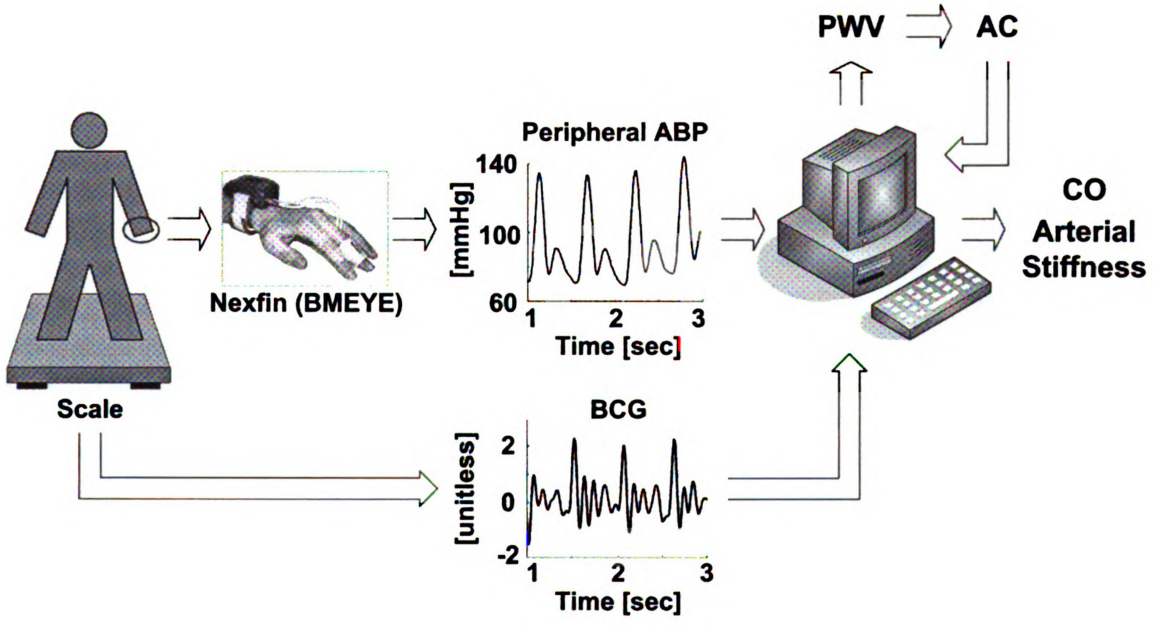

Figure 7.1 Continuous and non-invasive monitoring system for CO and arterial stiffness by mathematical analysis of ballistocardiography (BCG) and peripheral ABP waveforms. (Reproduced in part from (1).)

3) Demonstrated only by two canine experiments with undesired anesthesia procedures, the PPG-based LTIA technique (see Section 3.6) needs much more validation studies with different data sets. In addition, the AC compensation described above may likewise be used in this technique as well. Furthermore, the PPG waveform has to be calibrated to BP levels before applying the technique. The calibration can be achieved provided the two problems in cuff-less BP monitoring via PWV (i.e., the PWV-BP calibration curve and separate estimation of DP, MAP, and SP) are solved. Likewise, Fig. 7.2 shows a potential hemodynamic system upon the completion of the above work, which is similar to the one shown in Fig. 7.1 except that the peripheral ABP waveform is replaced by a PPG waveform. Therefore, this system is more economical and may have wider applications.

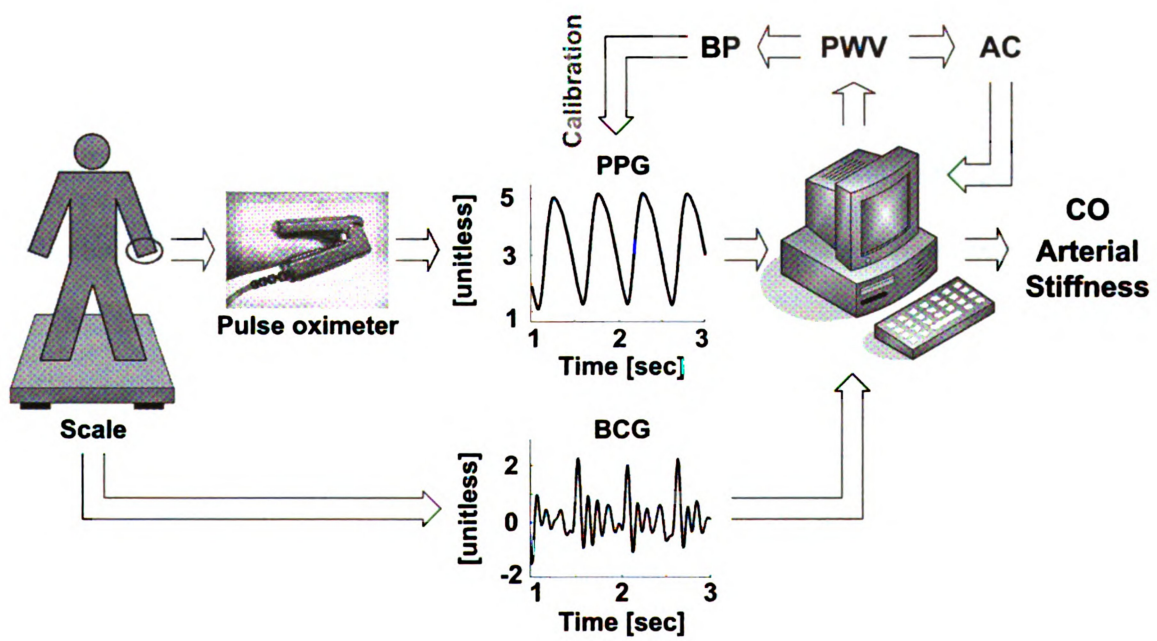

Figure 7.2 Continuous, non-invasive, and low-cost monitoring system for CO and arterial stiffness by mathematical analysis of BCG and PPG waveforms. (Reproduced in part from (9).)

In Fig. 7.2, to calibrate the PPG waveform, three PWV values are estimated and mapped to DP, MAP, and SP respectively through the PWV-BP curve. The resulting DP, MAP, and SP values are then used to calibrate the PPG waveform. The PPG can also be measured from lower limb (e.g. the toe) so that the PWV estimate would in principle have better correspondence to arterial compliance/stiffness.

4) The LTIA techniques based on PAP and RVP waveforms (see Chapter 4 and Chapter 5) need to be further validated by data collected from critically ill patients or congestive heart failure patients with implanted devices measuring RVP waveforms. In principle, the assumption of constant PAC could likewise be removed by estimate the PWV in the pulmonary circulation. However, pulmonary arterial waveforms are relatively difficult to measure, especially for non-invasive measurements. Thus, the PAC compensation is not considered here. Fig. 7.3 shows continuous CO and LAP monitoring systems based on the two LTIA techniques, which may be applied to ICU patients with pulmonary artery or right ventricular catheterization and patients with implanted RVP measurement devices for long-term hemodynamic monitoring.

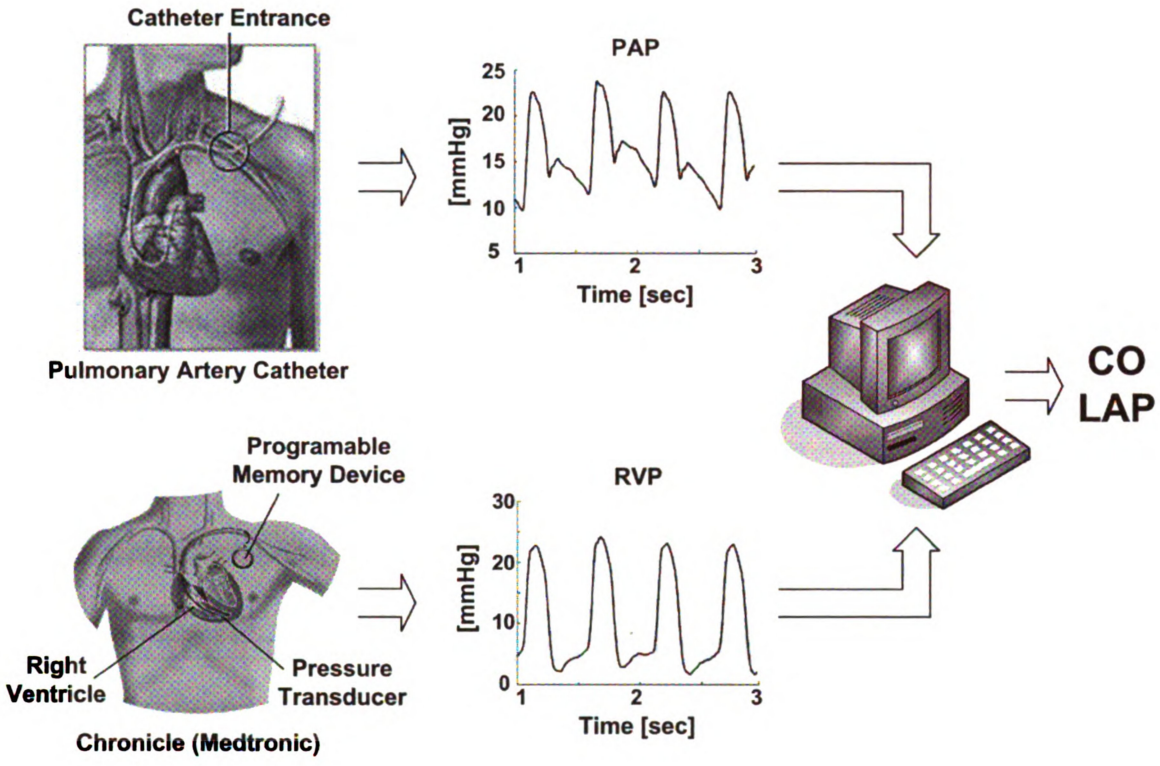

Figure 7.3 Continuous CO and LAP monitoring systems by mathematical analysis of PAP and RVP waveforms. (Reproduced in part from (7, 10).)

REFERENCES

1. BMEYE [Online]. BMEYE. http://www.bmeye.com. [2009].

2. Cardiovascular Monitoring [Online]. LiDCO Ltd. http://www.lidco.com/html/strategy/cardiovascular.asp. [2009].

3. CVP Diagnostics [Online]. CVP Diagnostics, Inc. http://cvpdiagnostics.com. [2009].

4. Edwards Lifesciences Edwards Lifesciences LLC. http://www.edwards.com/default.htm. [2010].

5. Finapres Medical Systems [Online]. Finapres Medical Systems. http://www.finapres.com. [2009].

6. Flowsensors [Online]. Transonic Systems Inc. http://www.transonic.com/HT107_Sec._C_Flowprobes.pdf. [2007].

7. Medtronic [Online]. Medtronic, Inc. http://www.medtronic.com. [2009].

8. The MIMIC II database [Online]. PhysioNet. http://www.physionet.org/physiobank/database/mimic2db/. [2006].

9. Pulse Oximeter [Online]. Pulse-Oximeter-Plus. http://pulse-oximeter-plus.com. [2008].

10. Swan Ganz Catheterization [Online]. MedlinePlus. http://www.nlm.nih.gov/medlineplus/ency/imagepages/18087.htm. [2009].

11. Transonic surgical flowsensors & flowmeters [Online]. Transonic Systems Inc. http://www.transonic.com/catalogs/Surgical/USA/USATofClinical04p12.pdf. [2008].

12. **Allen J**. Photoplethysmography and its application in clinical physiological measurement. *Physiol Meas* 28: R1-R39, 2007.

13. **Allen J, and Murray A**. Modelling the relationship between peripheral blood pressure and blood volume pulses using linear and neural network system identification techniques. *Physiol Meas* 20: 287-301, 1999.

14. **Aoyagi T, and Miyasaka K**. Pulse oximetry: its invention, contribution to medicine, and future tasks. *Anesth Analg* 94: 51-53, 2002.

15. **Asmar R**. *Arterial Stiffness and Pulse Wave Velocity. Clinical Applications*. St. Louis, MO: Elsevier, 1999.

16. **Barcroft H, Edholm OG, McMichael J, and Sharpey-Schafer EP.** Posthaemorrhagic fainting: study by cardiac output and forearm flow. *Lancet* 1: 489-491, 1944.

17. **Björck Å.** *Numerical Methods for Least Squares Problems*. Philadelphia: SIAM, 1996.

18. **Bjorklund S.** A survey and comparison of time-delay estimation methods in linear systems. In: *Electrical Engineering*. Linkoping, Sweden: Linkoping University, 2003.

19. **Bland JM, and Altman DG.** Statistical methods for assessing agreement between two methods of clinical measurement. *Lancet* i: 307-310, 1986.

20. **Bloch KE.** Impedance and inductance monitoring of cardiac output. In: *Principles and practice of intensive care monitoring*, edited by Tobin MJ. New York: McGraw-Hill, 1998, p. 915-930.

21. **Bourgeois MJ, Gilbert BK, Donald DE, and Wood EH.** Characteristics of aortic diastolic pressure decay with application to the continuous monitoring of changes in peripheral vascular resistance. *Circ Res* 35: 56-66, 1974.

22. **Bourgeois MJ, Gilbert BK, Von Bernuth G, and Wood EH.** Continuous determination of beat to beat stroke volume from aortic pressure pulses in the dog. *Circ Res* 39: 15-24, 1976.

23. **Burton AC.** Relation of structure to function of the tissues of the wall of blood vessels. *Physiol Rev* 34: 619-642, 1954.

24. **Challoner AV.** Photoelectric plethysmography for estimating cutaneous blood flow. In: *Non-Invasive Physiological Measurements*, edited by Polfe P. London: Academic, 1979, p. 125-151.

25. **Chang CM, Cassuto Y, Pendergast DR, and Farhi LE.** Cardiorespiratory response to lower body negative pressure. *Aviat Space Environ Med* 65: 615-620, 1994.

26. **Chittock DR.** The pulmonary artery catheter and critical care: the cart is before the horse. *Crit Care Med* 34: 1820-1822, 2006.

27. **Chiu YC, Arand PW, Shroff SG, Feldman T, and Carroll JD.** Determination of pulse wave velocities with computerized algorithms. *Am Heart J* 121: 1460-1470, 1991.

28. **Chuang PP, Wilson RF, Homans DC, Stone K, Bergman T, Bennett TD, and Kubo SH.** Measurement of pulmonary artery diastolic pressure from a right

ventricular pressure transducer in patients with heart failure. *J Card Fail* 2: 41-46, 1996.

29. **Cibulski AA, Lehan PH, and Hellems HK.** Pressure methods for estimating right and left ventricular stroke volumes. *Am J Physiol* 225: 1460-1466, 1973.

30. **Convertino VA.** Lower body negative pressure as a tool for research in aerospace physiology and military medicine. *J Gravit Physiol* 8: 1-14, 2001.

31. **Convertino VA, and Sather TM.** Effects of cholinergic and beta-adrenergic blockade on orthostatic tolerance in healthy subjects. *Clin Auton Res* 10: 327-336, 2000.

32. **Cooke WH, Ryan KL, and Convertino VA.** Lower body negative pressure as a model to study progression to acute hemorrhagic shock in humans. *J Appl Physiol* 96: 1249-1261, 2004.

33. **Cooper ES, and Muir WW.** Continuous cardiac output monitoring via arterial pressure waveform analysis following severe hemorrhagic shock in dogs. *Crit Care Med* 35: 1724-1729, 2007.

34. **Cournand A.** Some aspects of the pulmonary circulation in normal man and in chronic cardiopulmonary diseases. *Circulation* 2: 641-657, 1950.

35. **Critchley LA, and Critchley JA.** Lung fluid and impedance cardiography. *Anaesthesia* 53: 369-372, 1998.

36. **Critchley LAH.** Impedance cardiography. The impact of new technology. *Anaesthesia* 53: 677-684, 1998.

37. **Critchley LAH, and Critchley JAJH.** A meta-analysis of studies using bias and precision statistics to compare cardiac output measurement techniques. *J Clin Monit Comput* 15: 85-91, 1999.

38. **deBoisblanc BP, Pellett A, Johnson R, Champagne M, McClarty E, Dhillon G, and Levitzky M.** Estimation of pulmonary artery occlusion pressure by an artificial neural network. *Crit Care Med* 30: 261-266, 2003.

39. **Della Rocca G, Cecconi M, and Costa MG.** Mini invasive hemodynamic monitoring: from arterial pressure to cardiac output. *Signa Vitae* 3: S7-S9, 2008.

40. **DeLoskey AF, Nichols WW, Conti CR, and Pepine CJ.** Estimation of beat-to-beat stroke volume from the pulmonary arterial pressure contour in man. *Med & Biol Eng & Comput* 16: 707-714, 1978.

41. **DeMarzo AP, and Lang RM.** A new algorithm for improved detection of aortic

valve opening by impedance cardiography. *Computers in Cardiology* 23: 373-376, 1996.

42. **Derichard A, Robin E, Tavernier B, Costecalde M, Fleyfel M, Onimus J, Lebuffe G, Chambon JP, and Vallet B.** Automated pulse pressure and stroke volume variations from radial artery: evaluation during major abdominal surgery. *Br J Anaesth* 103: 678-684, 2009.

43. **Ehlers KC, Mylrea KC, Waterson CK, and Calkins JM.** Cardiac output measurements. a review of current techniques and research. *Ann Biomed Eng* 14: 219-239, 1986.

44. **Eleftheriadis S, Galatoudis Z, Didilis V, Bougioukas I, Schön J, Heinze H, Berger KU, and Heringlake M.** Variations in arterial blood pressure are associated with parallel changes in FlowTrac/Vigileo-derived cardiac output measurements: a prospective comparison study. *Crit Care* 13: R179, 2009.

45. **Engelberg J, and DuBois AB.** Mechanics of pulmonary circulation in isolated rabbit lungs. *Am J Physiol* 196: 401-414, 1959.

46. **Erlanger J, and Hooker DR.** An experimental study of blood-pressure and of pulse-pressure in man. *Bull Johns Hopkins Hosp* 12: 145-378, 1904.

47. **Frank O.** Die Grundform des arteriellen Pulses. Erste Abhandlung. Mathematische Analyse. *Z Biol* 37: 483-526, 1899.

48. **Geddes LA, Voelz MH, Babbs CF, Bourland JD, and Tacker WA.** Pulse transit time as an indicator of arterial blood pressure. *Psychophysiology* 18: 71-74, 1981.

49. **Gnaegi A, Feihl F, and Perret C.** Intensive care physicians' insufficient knowledge of right-heart catheterization at the bedside: time to act? *Crit Care Med* 25: 213-220, 1997.

50. **Gruen RL, Jurkovich GJ, McIntyre LK, Foy HM, and Maier RV.** Patterns of errors contributing to trauma mortality: lessons learned from 2,594 deaths. *Ann Surg* 244: 371-380, 2006.

51. **Guelen I, Westerhof BE, Van Der Sar GL, Van Montfrans GA, Kiemeneij F, Wesseling KH, and Bos WJ.** Finometer, finger pressure measurements with the possibility to reconstruct brachial pressure. *Blood Press Monit* 8: 27-30, 2003.

52. **Guyton AC, and Hall JE.** *Textbook of Medical Physiology*. Philadelphia: W.B. Saunders Company, 1996.

53. **Hallock P, and Benson IC.** Studies on the elastic properties of human isolated aorta. *J Clin Invest* 16: 595-602, 1937.

54. **Hanley JA, and McNeil BJ.** The meaning and use of the area under a receiver operating characteristic (ROC) curve. *Radiology* 143: 29-36, 1982.

55. **Hanley JA, and McNeil BJ.** A method of comparing the areas under receiver operating characteristic curves derived from the same cases. *Radiology* 148: 839-843, 1983.

56. **Harvey RM, and Ferrer MI.** Some effects of digoxin upon the heart and circulation in man; digoxin in left ventricular failure. *Am J Med* 7: 439-453, 1949.

57. **Heldt T.** Continuous blood pressure-derived cardiac output - should we be thinking long term? *J Appl Physiol* 101: 373-374, 2006.

58. **Henriquez AH, Schrijen FV, Redondo J, and Delorme N.** Local variations of pulmonary arterial wedge pressure and wedge angiograms in patients with chronic lung disease. *Chest* 94: 491-495, 1988.

59. **Herbert WH.** Limitations of pulmonary artery end-diastolic pressure as the reflection left ventricular end-diastolic pressure. *NY State J Med* 72: 229-232, 1972.

60. **Hopley L, and van Schalkwyk J.** Receiver operating characteristic curves: an introduction [Online]. Anaesthetist.com. http://www.anaesthetist.com/mnm/stats/roc/Findex.htm. [2007].

61. **Humphrey CB, Virgilio RW, Folkerth TL, and Fosburg RG.** An analysis of direct and indirect measurements of left atrial pressure. *J Thorac Cardiovasc Surg* 71: 643-647, 1976.

62. **Iberti TJ, Fischer EP, Leibowitz AB, Panacek EA, Silverstein JH, and Albertson TE.** A multicenter study of physicians' knowledge of the pulmonary artery catheter. *JAMA* 264: 2928-2932, 1990.

63. **Imholz BPM, Wieling W, van Montfrans GA, and Wesseling KH.** Fifteen years experience with finger arterial pressure monitoring: assessment of the technology. *Cardiovasc Res* 38: 605-616, 1998.

64. **Inan OT, Etemadi M, Wiard RM, Giovangrandi L, and Kovacs GT.** Robust ballistocardiogram acquisition for home monitoring. *Physiol Meas* 30: 169-185, 2009.

65. **Jansen JR, Schreuder JJ, Mulier JP, Smith NT, Settels JJ, and Wesseling KH.** A comparison of cardiac output derived from the arterial pressure wave against thermodilution in cardiac surgery patients. *Br J Anaesth* 87: 212-222, 2001.

66. **Jansen JRC, Schreuder JJ, Settels JJ, Kloek JJ, and Versprille A.** An adequate strategy for the thermodilution technique in patients during mechanical ventilation.

Intensive Care Med 16: 422-425, 1990.

67. **Jellema WT, Wesseling KH, Groeneveld AB, Stoutenbeek CP, Thijs LG, and van Lieshout JJ.** Continuous cardiac output in septic shock by simulating a model of the aortic input impedance: a comparison with bolus injection thermodilution. *Anesthesiology* 90: 1317-1328, 1999.

68. **Kane PB, Askanazi J, Neville JF, Mon RL, Hanson EL, and Webb WR.** Artifacts in the measurement of pulmonary artery wedge pressure. *Crit Care Med* 6: 36-38, 1978.

69. **Karamanoglu M.** A system for analysis of arterial blood pressure waveforms in humans. *Comput Biomed Res* 30: 244-255, 1997.

70. **Karamanoglu M, and Bennett TD.** A right ventricular pressure waveform based pulse contour cardiac output algorithm in canines. *Cardiovasc Eng* 6: 83-92, 2006.

71. **Karamanoglu M, McGoon M, Frantz RP, Benza RL, Bourge RC, Barst RJ, Kjellstrom B, and Bennett TD.** Right ventricular pressure waveform and wave reflection analysis in patients with pulmonary arterial hypertension. *Chest* 132: 37-43, 2007.

72. **Katz AM.** *Physiology of the Heart.* New York: Raven Press, 1992.

73. **Kearney TJ, and Shabot MM.** Pulmonary artery rupture associated with the Swan-Ganz catheter. *Chest* 108: 1349-1352, 1995.

74. **Kenner T.** Arterial blood pressure and its measurement. *Basic Res Cardiol* 83: 107-121, 1988.

75. **Kimmerly DS, and Shoemaker JK.** Hypovolemia and neurovascular control during orthostatic stress. *Am J Physiol* 282: H645-H655, 2002.

76. **Kobayashi K, Washizu M, Kondo M, Matsukura Y, Motoyoshi S, Miyasaka K, and Takata M.** Longitudinal distribution of pulmonary vascular compliance in dogs. *J Vet Med Sci* 58: 41-46, 1996.

77. **Kubicek WG, Karnegis JN, Patterson RP, Witsoe DA, and Mattson RH.** Development and evaluation of an impedance cardiac output system. *Aerosp Med* 37: 1208-1212, 1966.

78. **Kubicek WG, Patterson RP, and Witsoe DA.** Impedance cardiography as a noninvasive method of monitoring cardiac function and other parameters of the cardiovascular system. *Ann N Y Acad Sci* 170: 1970.

79. **Lankhaar JW, Westerhof N, Faes TJ, Gan CT, Marques KM, Boonstra A, van**

den Berg FG, Postmus PE, and Vonk-Noordegraaf A. Pulmonary vascular resistance and compliance stay inversely related during treatment of pulmonary hypertension. *Eur Heart J* 29: 1688-1695, 2008.

80. **Lapinsky SE, and Richards GA.** Pro/con clinical debate: pulmonary artery catheters increase the morbidity and mortality of intensive care unit patients. *Crit Care* 7: 101-103, 2003.

81. **Lappas D, Lell WA, Gabel JC, Civetta JM, and Lowenstein E.** Indirect measurement of left-atrial pressure in surgical patients. Pulmonary-capillary wedge and pulmonary-artery diastolic pressure compared with left-atrial pressure. *Anesthesiology* 38: 394-397, 1973.

82. **Leatherman JW, and Shapiro RS.** Overestimation of pulmonary artery occlusion pressure in pulmonary hypertension due to partial occlusion. *Crit Care Med* 31: 93-97, 2003.

83. **Levett JM, and Replogle RL.** Thermodilution cardiac output: a critical analysis and review of the literature. *J Surg Res* 27: 392-404, 1979.

84. **Li Q, Mark RG, and Clifford GD.** Artificial arterial blood pressure artifact models and an evaluation of a robust blood pressure and heart rate estimator. *Biomed Eng Online* 8: 2009.

85. **Liljestrand G, and Zander E.** Vergleichen die bestimmungen des minutenvolumens des herzens beim menschen mittels der stichoxydulmethode und durch blutdruckmessung. *Ztschr Ges Exper Med* 105-122, 1928.

86. **Linton DM, and Gilon D.** Advances in noninvasive cardiac output monitoring. *Ann Card Anaesth* 5: 141-148, 2002.

87. **Linton NW, and Linton RA.** Estimation of changes in cardiac output from the arterial blood pressure waveform in the upper limb. *Br J Anaesth* 86: 486-496, 2001.

88. **Liu C, and Webb CC.** Pulmonary artery rupture: serious complication associated with pulmonary artery catheters. *Int J Trauma Nurs* 6: 19-26, 2000.

89. **Ljung L.** *System Identification: Theory for the User.* Englewood Cliffs: Prentice Hall, 1987.

90. **Lu Z, and Mukkamala R.** Continuous cardiac output monitoring in humans by invasive and noninvasive peripheral blood pressure waveform analysis. *J Appl Physiol* 101: 598-608, 2006.

91. **Lundvall J, Bjerkhoel P, Edfeldt H, Ivarsson C, and Länne T.** Dynamics of transcapillary fluid transfer and plasma volume during lower body negative

pressure. *Acta Physiol Scand* 147: 163-172, 1993.

92. **Magalski A, Adamson P, Gadler F, Boehm M, Steinhaus D, Reynolds D, Vlach K, Linde C, Cremers B, Sparks B, and Bennett T.** Continuous ambulatory right heart pressure measurements with an implantable hemodynamic monitor: a multicenter, 12-month follow-up study of patients with chronic heart failure. *J Card Fail* 8: 63-70, 2002.

93. **Management of Arterial Hypertension of the European Society of Hypertension, and European Society of Cardiology.** 2007 Guidelines for the management of arterial hypertension: The Task Force for the management of arterial hypertension of the European Society of Hypertension (ESH) and of the European Society of Cardiology (ESC). *J Hypertens* 25: 1105-1187, 2007.

94. **Marik PE.** The systolic blood pressure variation as an indicator of pulmonary capillary wedge pressure in ventilated patients. *Anaesth Intensive Care* 21: 405-408, 1993.

95. **Marino PL, and Sutin KM.** *The ICU Book.* Baltimore: Lippincott Williams & Wilkins, 2006.

96. **Mark RG.** Cardiovascular Mechanics I, II, III [Online]. Harvard-MIT Division of Health Sciences and Technology. http://ocw.mit.edu/NR/rdonlyres/Health-Sciences-and-Technology/HST-542JSpring-2004/9BD6592A-2A98-4662-90B8-243E93A6C5EC/0/cardio_mech.pdf. [2008].

97. **Mark RG, and Keshner M.** Non-invasive blood pressure measurement using aortic pulse-wave velocity. In: *NEREM 74 Record (Proc IEEE Northeast Electronics Research and Engineering Meeting)*1974, p. 70-72.

98. **Martin JF, Volfson LB, Kirzon-Zolin VV, and Schukin VG.** Application of pattern recognition and image classification techniques to determine continuous cardiac output from the arterial pressure waveform. *IEEE Trans Biomed Eng* 41: 913-920, 1994.

99. **McDonald DA.** *Blood Flow in Arteries.* London: Edward Arnold, 1974.

100. **McDonald DA.** Regional pulse-wave velocity in the arterial tree. *J Appl Physiol* 24: 73-78, 1968.

101. **McIntyre KM, Vita JA, Lambrew CT, Freeman J, and Loscalzo J.** A noninvasive method of predicting pulmonary-capillary wedge pressure. *N Engl J Med* 327: 1715-1720, 1992.

102. **Medin DL, Brown DT, Wesley R, Cunnion RE, and Ognibene FP.** Validation of continuous thermodilution cardiac output in critically ill patients with analysis of

systematic errors. *J Crit Care* 13: 184-189, 1998.

103. **Metz CE**. Basic principles of ROC analysis. *Semin Nucl Med* 8: 283-298, 1978.

104. **Morris AH, Chapman RH, and Gardner RM**. Frequency of technical problems encountered in the measurement of pulmonary artery wedge pressure. *Crit Care Med* 12: 164-170, 1984.

105. **Mukkamala R, and Reisner AT**. Reply to van Lieshout and Jansen. *J Appl Physiol* 102: 827, 2007.

106. **Mukkamala R, Reisner AT, Hojman HM, Mark RG, and Cohen RJ**. Continuous cardiac output monitoring by peripheral blood pressure waveform analysis. *IEEE Trans Biomed Eng* 53: 459-467, 2006.

107. **Mulligan LJ, and Bennett TD**. Apparatus for measurement of mean pulmonary artery pressure from a ventricle in an ambulatory monitor. edited by Office EP. USA: 2004.

108. **Noordergraaf A**. *Circulatory System Dynamics*. New York: Academic Press, 1978.

109. **O' Rourke MF, and Yaginuma T**. Wave reflections and the arterial pulse. *Arch Intern Med* 144: 366-371, 1984.

110. **Ohlsson A, Bennett T, Nordlander R, Ryden J, Astrom H, and Ryden L**. Monitoring of pulmonary arterial diastolic pressure through a right ventricular pressure transducer. *J Card Fail* 1: 161-168, 1995.

111. **Ohlsson A, Kubo SH, Steinhaus D, Connelly DT, Adler S, Bitkover C, Nordlander R, Ryden L, and Bennett T**. Continuous ambulatory monitoring of absolute right ventricular pressure and mixed venous oxygen saturation in patients with heart failure using an implantable haemodynamic monitor: results of a 1 year multicentre feasibility study. *Eur Heart J* 22: 942-954, 2001.

112. **Ohlsson A, Nordlander R, Bennett T, Bitkover C, Kjellstrom B, Lee B, and Ryden L**. Continuous ambulatory haemodynamic monitoring with an implantable system. The feasibility of a new technique. *Eur Heart J* 19: 174-184, 1998.

113. **Payne RA, Symeonides CN, Webb DJ, and Maxwell SR**. Pulse transit time measured from the ECG: an unreliable marker of beat-to-beat blood pressure. *J Appl Physiol* 100: 136-141, 2006.

114. **Permutt S, Bromberger-Barnea B, and Bane HN**. Alveolar pressure, pulmonary venous pressure, and the vascular waterfall. *Med Thorac* 19: 239-260, 1962.

115. **Peters SG, Afessa B, Decker PA, Schroeder DR, Offord KP, and Scott JP**.

Increased risk associated with pulmonary artery catheterization in the medical intensive care unit. *J Crit Care* 18: 166-171, 2003.

116. **Philip JH, Long MC, Quinn MD, and Newbower RS**. Continuous thermal measurement of cardiac output. *IEEE Trans Biomed Eng* 31: 393-400, 1984.

117. **Piehl MD, Manning JE, McCurdy SL, Rhue TS, Kocis KC, Cairns CB, and Cairns BA**. Pulse contour cardiac output analysis in a piglet model of sever hemorrhagic shock. *Crit Care Med* 36: 1189-1195, 2008.

118. **Pinsky MR, and Vincent J**. Let us use the pulmonary artery catheter correctly and only when we need it. *Crit Care Med* 33: 1119-1122, 2005.

119. **Pruett JD, Bourland JD, and Geddes LA**. Measurement of pulse-wave velocity using a beat-sampling technique. *Ann Biomed Eng* 16: 341-347, 1988.

120. **Rapaport E, and Dexter L**. Pulmonary 'capillary' pressure. *Methods Med Res* 7: 85-93, 1958.

121. **Redling JD, and Akay M**. Noninvasive cardiac output estimation: a preliminary study. *Biol Cybern* 77: 111-122, 1997.

122. **Reisner AT, Xu D, Ryan KL, Convertino VA, Rickards CA, and Mukkamala R**. Monitoring non-invasive cardiac output and stroke volume during experimental human hypovolemia and resuscitation. Submitted.

123. **Reuben SR, Gersh BJ, Swadling JP, and Lee GdJ**. Measurement of pulmonary arterial distensibility in the dog. *Cardiovasc Res* 4: 473-481, 1970.

124. **Reynolds D, Bartelt N, Taepke R, and Bennett T**. Measurement of pulmonary artery diastolic pressure from the right ventricle. *J Am Coll Cardiol* 25: 1176-1182, 1995.

125. **Richard C, Warszawski J, Anguel N, Deye N, Combes A, Barnoud D, Boulain T, Lefort Y, Fartoukh M, Baud F, Boyer A, Brochard L, and Teboul JL**. Early use of the pulmonary artery catheter and outcomes in patients with shock and acute respiratory distress syndrome: a randomized controlled trial. *JAMA* 290: 2713-2720, 2003.

126. **Robin E, Costecalde M, Lebuffe G, and Vallet B**. Clinical relevance of data from the pulmonary artery catheter. *Crit Care* 10: S3, 2006.

127. **Rosenfeld BA, Dorman T, Breslow MJ, Pronovost P, Jenckes M, Zhang N, Anderson G, and Rubin H**. Intensive care unit telemedicine: alternate paradigm for providing continuous intensivist care. *Crit Care Med* 28: 3925-3931, 2000.

128. **Sanders R, Bailie M, and Olivier NB**. Stability of ventricular depolarization in conscious dogs with chronic atrioventricular dissociation and his-bundle pacing. *Pacing Clin Electrophysiol* 27: 1475-1483, 2004.

129. **Sarnoff SJ, and Berglund E**. Pressure-volume characteristics and stress relaxation in the pulmonary vascular bed of the dog. *Am J Physiol* 171: 238-244, 1952.

130. **Sather TM, Goldwater DJ, Montgomery LD, and Convertino VA**. Cardiovascular dynamics associated with tolerance to lower body negative pressure. *Aviat Space Environ Med* 57: 413-419, 1986.

131. **Saul JP, and Cohen RJ**. Respiratory sinus arrhythmia. In: *Vagal Control of the Heart: Experimental Basis and Clinical Implications*, edited by Levy MN, and Schwartz PJ. Armonk: Futura Publishing Co. Inc., 1994, p. 511-535.

132. **Segers P, Brimioulle S, Stergiopulos N, Westerhof N, Naeije R, Maggiorini M, and Verdonck P**. Pulmonary arterial compliance in dogs and pigs: the three-element windkessel model revisited. *Am J Physiol* 46: H725-H731, 1999.

133. **Sharma GV, Woods PA, Lambrew CT, Berg CM, Pietro DA, Rocco TP, Welt FW, Sacchetti P, and McIntyre KM**. Evaluation of a noninvasive system for determining left ventricular filling pressure. *Arch Intern Med* 162: 2084-2088, 2002.

134. **Shoukas AA**. Pressure-flow and pressure-volume relations in the entire pulmonary vascular bed of the dog determined by two-port analysis. *Circ Res* 37: 809-818, 1975.

135. **Sola J, Vetter R, Renevey P, Chetelat O, Sartori C, and Rimoldi SF**. Parametric estimation of pulse arrival time: a robust approach to pulse wave velocity. *Physiol Meas* 30: 603-615, 2009.

136. **Starmer CF, McHale PA, Cobb FR, and Greenfield JCJ**. Evaluation of several methods for computing stroke volume from central aortic pressure. *Circ Res* 33: 139-148, 1973.

137. **Starr I, Rawson AJ, Schroeder HA, and Joseph NR**. Studies on the estimation of cardiac output in man, and of abnormalities in cardiac function, from the heart's recoil and the blood's impacts; the ballistocardiogram. *Am J Physiol* 127: 1-28, 1939.

138. **Stetz CW, Miller RG, Kelly GE, and Raffin TA**. Reliability of the thermodilution method in the determination of cardiac output in clinical practice. *Am Rev Respirat Dis* 126: 1001-1004, 1982.

139. **Sugimachi M, Shishido T, Miyatake K, and Sunagawa K**. A new model-based method of reconstructing central aortic pressure from peripheral arterial pressure.

Jpn J Physiol 51: 217-222, 2001.

140. **Sun JX, Reisner AT, Saeed M, Heldt T, and Mark RG**. The cardiac output from blood pressure algorithms trial. *Crit Care Med* 37: 72-80, 2009.

141. **Swamy G, and Mukkamala R**. Estimation of the aortic pressure waveform and beat-to-beat relative cardiac output changes from multiple peripheral artery pressure waveforms. *IEEE Trans Biomed Eng* 55: 1521-1529, 2008.

142. **Swamy G, Xu D, Olivier NB, and Mukkamala R**. An adaptive transfer function for deriving the aortic pressure waveform from a peripheral artery pressure waveform. *Am J Physiol* 297: H1956-H1963, 2009.

143. **Swan HJ, Ganz W, Forrester J, Marcus H, Diamond G, and Chonette D**. Catheterization of the heart in man with the use of a flow-directed balloon-tipped catheter. *N Engl J Med* 283: 447-451, 1970.

144. **Tajimi T, Sunagawa K, Yamada A, Nose Y, Takeshita A, Kikuchi Y, and Nakamura M**. Evaluation of pulse contour methods in calculating stroke volume from pulmonary artery pressure curve (comparison with aortic pressure curve). *Eur Heart J* 4: 502-511, 1983.

145. **U.S. Department of Health and Human Services HRaSA, Bureau of Health Professions**. Projected Supply, Demand, and Shortages of Registered Nurses: 2000-2002. 2002.

146. **Vender JS**. Pulmonary artery catheter utilization: the use, misuse, or abuse. *J Cardiothorac Vasc Anesth* 20: 295-299, 2006.

147. **Verdouw PD, Beaune J, Roelandt J, and Hugenholtz PG**. Stroke volume from central aortic pressure? a critical assessment of the various formulae as to their clinical value. *Basic Res Cardiol* 70: 377-389, 1975.

148. **Wahlberg B**. System identification using Laguerre models. *IEEE Trans Autom Control* 36: 551-562, 1991.

149. **Welkowitz W, Cui Q, Qi Y, and Kostis JB**. Noninvasive estimation of cardiac output. *IEEE Trans Biomed Eng* 38: 1100-1105, 1991.

150. **Wesseling KH, Jansen JR, Settels JJ, and Schreuder JJ**. Computation of aortic flow from pressure in humans using a nonlinear, three-element model. *J Appl Physiol* 74: 2566-2573, 1993.

151. **Westerhof BE, Guelen I, Stok WJ, Wesseling KH, Spaan JA, Westerhof N, Bos WJ, and Stergiopulos N**. Arterial pressure transfer characteristics: effects of travel time. *Am J Physiol* 292: H800-807, 2007.

152. **Westerhof N, Sipkema P, Van Den Bos GC, and Elzinga G.** Forward and backward waves in the arterial system. *Cardiovasc Res* 6: 648-656, 1972.

153. **Wiesenack C, Fiegl C, Keyser A, Laule S, Prasser C, and Keyl C.** Continuously assessed right ventricular end-diastolic volume as a marker of cardiac preload and fluid responsiveness in mechanically ventilated cardiac surgical patients. *Crit Care* 9: R226-R233, 2005.

154. **Woltjer HH, Bogaard HJ, and de Vries PMJM.** The technique of impedance cardiography. *Eur Heart J* 18: 1396-1403, 1997.

155. **Xu D, Olivier NB, and Mukkamala R.** Cardiac output and left atrial pressure monitoring by right ventricular pressure waveform analysis for potential implantable device application. *IEEE Trans Biomed Eng* 56: 2335-2339, 2009.

156. **Xu D, Olivier NB, and Mukkamala R.** Continuous cardiac output and left atrial pressure monitoring by long time interval analysis of the pulmonary artery pressure waveform: proof of concept in dogs. *J Appl Physiol* 106: 651-661, 2009.

157. **Xu H, Zhou S, Ma W, and Yu B.** Prediction of pulmonary arterial wedge pressure from arterial pressure or pulse oximetry plethysmographic waveform. *Chin Med J* 115: 1372-1375, 2002.

158. **Yelderman ML.** Continuous measurement of cardiac output with the use of stochastic system identification techniques. *J Clin Monit* 6: 322-332, 1990.

159. **Yelderman ML, Quinn MD, McKown RC, Eberhart RC, and Dollar ML.** Continuous thermdilution cardiac output measurements in sheep. *J Thorac Cardiovasc Surg* 104: 315-320, 1992.

160. **Yelderman ML, Ramsay MA, Quinn MD, Paulsen AW, McKown RC, and Gillman PH.** Continuous thermodilution cardiac output measurement in intensive care patients. *J Cardiothorac Vasc Anesth* 6: 270-274, 1992.

161. **Zacharoulis AA, Evans TR, Ziady GM, Coltart DJ, and Shillingford JP.** Measurement of stroke volume from pulmonary artery pressure record in man. *Br Heart J* 37: 20-25, 1975.

162. **Zacharoulis AA, Mills CJ, Gabe IT, and Shillingford JP.** Estimation of stroke volume from the pulmonary artery pressure record. *Cardiovasc Res* 8: 506-516, 1974.

163. **Zink W, Nöll J, Rauch H, Bauer H, Desimone R, Martin E, and Böttiger BW.** Continuous assessment of right ventricular ejection fraction: new pulmonary artery catheter versus transoesophageal echocardiography. *Anaesthesia* 59: 1126-1132, 2004.

164. **Zollner C, Goetz AE, Weis M, Morstedt K, Pichler B, Lamm P, Kilger E, and Haller M.** Continuous cardiac output measurements do not agree with conventional bolus thermodilution cardiac output determination. *Can J Anaesth* 48: 1143-1147, 2001.